COLLOIDAL CRYSTALS OF MONODISPERSE SILICA IN POLYMER COMPOSITES

By

JAGDISH MAGHANMAL JETHMALANI

Bachelors of Science (Chemistry)
University of Bombay
Bombay, India
1986

Masters of Science (Organic Chemistry)
University of Bombay
Bombay, India
1988

Masters of Science (Chemistry)
University of Arkansas at Little Rock
Little Rock, Arkansas, USA
1992

Submitted to the Faculty of the
Graduate College of the
Oklahoma State University
in partial fulfillment for
the requirements for
the Degree of
DOCTOR OF PHILOSOPHY
July, 1996

COLLOIDAL CRYSTALS OF MONODISPERSE SILICA

IN POLYMER COMPOSITES

Thesis Approved:

Warren T Ford

Thesis Adviser

K D Berlin

Matt S. Hyl

Thomas C. Collins

Dean of the Graduate College

PREFACE

Monodisperse charged colloidal particles in aqueous and non-aqueous dispersions spontaneously form three dimensional crystal lattices known as colloidal crystals. Based on the concentration of the colloidal particles in the liquid dispersions, particle size and charges and the ionic impurities, homogeneous or heterogeneous nucleation initiates the crystallization process. In homogeneous nucleation, the particles order in a two dimensional hexagonal order on which the second and third layers of particles settle to form face-centered cubic (fcc), body-centered cubic (bcc) or hexagonal close-pack (hcp) lattices. Particles with low surface charge at high concentrations favor fcc lattices and particles with high surface charge at low concentrations favor bcc lattices.

Since the crystals have dimensions > 100 nm, the liquid dispersions are iridescent due to Bragg diffraction of visible light. Polystyrene latexes in aqueous dispersions form colloidal crystals which have potential applications in optical devices such as rejection filters, optical limiters and switches. A major drawback to these liquid dispersions containing colloidal crystals is that mechanical or thermal forces disrupt the crystal order, and hence, no diffraction is observed. To solve this instability problem, monodisperse colloidal silica particles were coated with 3-(trimethoxysilyl)propyl methacrylate (TPM), dispersed in monomers such as methyl methacrylate (MMA) and methyl acrylate (MA) to form colloidal crystals. Polymerization of MMA or MA dispersions traps the crystal order in the polymer composites, and thus, the colloidal crystals are stabilized. The diffraction wavelength as studied using a UV-visible spectrophotometer shifts to the blue by varying the particle concentration, by stretching the elastomeric poly(methyl acrylate) (PMA) film and by changing the angle of incident light, while the diffraction wavelength red shifts by swelling the PMA composite with more MA.

ACKNOWLEDGMENTS

I would like to express deep appreciation to my research adviser, Dr. Warren T. Ford for his guidance, instruction, valuable suggestions and his strong interest in the progress of my research. I wish to express my sincere gratitude to him for providing me with excellent research facilities, sharing knowledge and support. I am also grateful to Dr. Bruce Ackerson, Dr. Darrell Berlin, and Dr. Martin High for serving on my graduate committee.

I would like to thank Dr. Bruce Ackerson for helpful discussions during the progress of the project. I would also like to thank Dr. Hari Babu Sunkara for sharing knowledge, teaching various experimental techniques and moral support. I would like to thank Dr. Ackerson's group, especially Mr. Ulf Nobbmann, for particle size measurements by light scattering at all hours. I would like to thank Ms. Ginger Baker for the scanning electron microscopic (SEM) analysis of the composite films. I would like to thank Amanda, Sameer, Ken, and others in the group for their help and friendship.

Finally, I would like to acknowledge the Department of Chemistry for providing me an opportunity to continue my education and also the generous financial support in the form of teaching assistantship during the first year of my graduate study. I would like to thank Dr. Ford and National Science Foundation for the financial support in the form of research assistantship during the course of my graduate study at Oklahoma State University.

My special thanks to my mother Ms. Vimla M. Jethmalani, my sister Dr. Sunita M. Jethmalani, and my family for the love, understanding, motivation, support and encouragement. My special thanks to Dr. C. Bhuvaneswaran for the motivation and support.

TABLE OF CONTENTS

LIST OF TABLES

Chapter III

Chapter IV

Chapter V

Chapter VI

LIST OF FIGURES

Chapter III

Chapter IV

Chapter V

Chapter VI

LIST OF SCHEMES

Chapter I

Chapter II

Chapter III

Chapter IV

CHAPTER I

INTRODUCTION

A. COLLOIDAL CRYSTALS

Monodisperse charged colloidal particles have been known to self-assemble spontaneously into a three dimensional crystal lattice known as a colloidal crystal. As the colloidal crystalline lattice has large interplanar spacings of > 100 nm, Bragg diffraction of visible light occurs at specific wavelengths that correspond to the lattice spacings. Hence dispersions with ordered colloidal particles display beautiful iridescence.[1-13]

B. DISCOVERY OF COLLOIDAL CRYSTALS

Naturally occurring materials such as proteins, viruses and pigments exhibit colloidal crystalline behavior. In 1940's, Bernal and Fankuchen were the first scientists to observe the unusual behavior of rod-shaped particles of the Tobacco Mosaic Virus (TMV) which formed a two-dimensional triangular lattice.[14] Later in the 1950's, Williams and Smith observed another virus which also ordered into a crystalline lattice displaying iridescence, and hence it was later on known as Tipula Iridescent Virus (TIV).[15]

During the 1960's and 1970's, several researchers noticed that concentrated dispersions of polystyrene latexes in water showed iridescence which was due to the ordering of the colloidal particles into a crystal lattice.[1-13] Precious gemstones such as opals also display beautiful iridescence due to the diffraction of visible light. Using electron microscopy, Sanders found that the diffraction of light by opals is due to the refractive index mismatch between the silica particles and the silicic acid sol.[16] The diameter of the silica particles that form the crystal lattice was between 150-350 nm while the void spaces between them constitute the sol.

Using a light scattering technique, Clark, Hurd and Ackerson reported the diffraction from a single colloidal crystal of polystyrene latex in water.[10] Since, the discovery, researchers have been interested in optical diffraction from colloidal crystals. Review papers have been published that discuss colloidal crystals, polymeric colloidal crystals and polymer latex dispersions.[11-13]

C. FORMATION OF COLLOIDAL CRYSTALS

There are certain essential criteria involved in the formation of the colloidal crystals. For example, in the case of opals, there are three steps involved which lead to the formation of the colloidal crystal lattice.[11] These are:

(1) the formation of monodisperse colloidal silica particles,

(2) ordering and orientation of the particles into a crystalline lattice, and

(3) the cementing of the particles in the crystalline lattice.

There are many known examples of synthetic monodisperse systems available that form colloidal crystals. These systems are polymeric latex particles or colloidal silica particles. Examples of commercially available monodisperse latexes include polystyrene (PS), poly(methyl methacrylate) (PMMA), polyacrylate (PA), polyurethane (PU), silicone, and epoxys.[12] These latexes can be synthesized by emulsion, suspension or microemulsion polymerizations.[17,18] The particle sizes and particle monodispersities have been controlled by varying the concentration of the monomers and surfactants and by utilizing different polymerization techniques. The ordering and orientation of the particles from dispersions containing disordered colloidal particles occurs in several stages. Most of the research to date has been aimed at understanding the colloidal crystalline behavior in liquid dispersion.

D. FORMATION OF MONODISPERSE PARTICLES

In an emulsion polymerization, the monomer in an aqueous buffered phase, along with a water soluble initiator, a surfactant or an emulsifier forms monodisperse particles of 50 to 1000 nm diameters with polydispersity index of 4 %. Similarly, an emulsifier-free polymerizations, where an ionic monomer plays the role of an emulsifier or a surfactant, also produce monodisperse particles of similar diameters.[17,18] In microemulsions, the monomer-in-water or the water-in-monomer systems, along with surfactant and a initiator, form monodisperse particles in the range of 5 to 50 nm.[19] To date, vinyl monomers such as styrene, and acrylate monomers such as methyl methacrylate (MMA), have been used to form monodisperse particles. The initiator systems used are either potassium persulfate (KPS) ($K_2S_2O_8$) or azo compounds such as 2,2'-azobisisobutyronitrile (AIBN) which undergoes thermal dissociation to form free radicals. In case of AIBN, the initiation occurs in the monomer phase, while initiation by KPS occurs in the water phase. The propagation of the growing radical chain end occurs in the micelles containing more monomer, and further polymerization leads to the growth of the particles. Recently, a shot-growth technique has been used to form monodisperse particles with high surface charges.[20,21] In this technique, after 90 % consumption of the monomers, a second shot containing water-insoluble monomer, ionic monomer (which is in excess compared to the monomer) and an initiator, are added to form monodisperse latex particles with high surface charge.[20-22] The particles thus carry a charge due to the initiator end groups or due to the presence of ionic monomers incorporated in the latex particle.

Among the monodisperse inorganic systems, colloidal silica is the most widely used inorganic particle. In the 1960's, Stöber, Fink, and Bohn successfully synthesized monodisperse silica by basic hydrolysis and condensation of tetraethylorthosilicate (TEOS) in ethanol-water mixtures.[23] The particle monodispersity and the particle sizes

were controlled by varying the pH and the amounts of the TEOS, ammonia, and water in the reaction mixtures. This method was further modified by Bogush, Tracy, and Zukoski,[24] who subsequently added known quantities of TEOS to the seed particles induces formation of large particles of diameters between 100 to 1000 nm. Philipse and Vrij have perfected the method of coating different silane coupling agents on to the surface of colloidal silica particles.[25] Badley, Ford, McEnroe, Assink reported the synthesis of monodisperse particles by basic hydrolysis of TEOS which were coated with different silane coupling agents.[26]

E. MECHANISM OF CRYSTALLIZATION

There are at least two different mechanisms by which colloidal particles have been known to order into a crystal lattice.[11] These are as follows:

(1) steric repulsions and

(2) electrostatic repulsions.

In the case of sterically-stabilized colloidal particles, long carbon chains (C_8 to C_{18}) or polymer chains such as poly(ethylene glycol) have been either adsorbed or grafted onto the particle surfaces. Due to the steric interactions of the long chains, there is a net repulsion between the colloidal particles when they come close to one another. Thus, at very high particle concentrations, the sterically-stabilized particles order into crystal lattices which diffract UV light.

During the transition from fluid to the solid state, the colloidal particles have restricted Brownian motion and vibrate in all possible directions around their equilibrium positions in a crystal-like structure. The crystallization occurs as the particles exhibit long range electrostatic repulsions which is explained by Derjaguin-Landau-Verwey-Overbeek (DLVO) theory.[27] Similar to the DLVO theory, the Yukawa potential explains the interparticular repulsions.[13,28] Contrary to the DLVO theory, Sogami's theory not

only accounts for long range electrostatic repulsions but also the attractive forces between particles.[29] The driving force behind the liquid to crystal-like phase transition in aqueous or non-aqueous media is the interparticle interaction, mostly the repulsive force rather than the attractive force, which arise from the dissociation of surface ionic functional groups. The interparticle interaction between two particles of radius r at a distance x is best described by a screened Coulomb potential:[30,31]

$$U(r) = \frac{Z^2 e^2}{4\pi\varepsilon_0\varepsilon_r}\left(\frac{\exp(kr)}{1+kr}\right)\left(\frac{\exp(-kx)}{x}\right) \qquad (2)$$

where Z is the number of charges on a particle and e is the charge on an electron, ε_0, ε_r are the vacuum permittivity and dielectric constant of the suspending medium, and k is the inverse Debye screening length which depends on concentration of the counterions. As the dielectric constant of the medium increases, the dissociation of the surface ionic functional groups increases and the interparticle interaction decreases thus increasing the particle distance.

In the case of latex particles that are synthesized by emulsion polymerization,[19-22] typically a particle surface has ranged between 1,000 to 2,000 charges due to the initiators or surfactants. For colloidal silica, the dissociation of the surface hydroxyl groups provides a particle surface of 200 to 600 charges.[19-22] Due to the net surface charge, particles with similar charges show electrostatic repulsions, and, depending on the particle concentration (which is lower than that observed with sterically repelled particles), the particles order into different crystal lattices which are the most thermodynamically stable states.[16]

F. ORDERING OF COLLOIDAL PARTICLES

The monodisperse charged colloidal particles transform from a disordered to an ordered state in several stages. In dispersions, at low concentration of particles

undergoing Brownian motion or in a gas-like state undergo a transition to a liquid-like phase and at high particle concentration go to a solid-like phase which may be amorphous or crystalline in nature.[16,32-35] At particle concentrations above the liquid-solid phase boundary, homogenous nucleation initiates the crystallization where the particles order in two-dimensional (2D) arrays either on planar surfaces such as glass cells, vials and cuvets or in bulk. Heterogeneous nucleation occurs mostly on the planar surface of the glass cells at several sites. At low particle concentration, homogeneous nucleation occurs which leads to large crystallites, and, at high particle concentration, heterogeneous nucleation leads to small, polydisperse crystallites.[32-35] The subsequent settling of the next layer of particles on the nucleated 2D sites lead to a three dimensional crystal structures.

Based on the concentration of the particles, the order in which the second layer forms on top of the first layer and the subsequent settling of the particle layers lead to different structures which are as follows: two-dimensional structure → random layer structure → layer structure with one sliding degree of freedom → stacking disorder structure → face-centered-cubic (fcc) structure with (111) twin → normal fcc structure.[16,32] Thus, the three dimensional order of colloidal particles occurs in either ABA or ABC stacks, and fcc, body-centered cubic (bcc) and hexagonal close-packed (hcp) lattices have been observed. In an fcc lattice, the second layer of particles occupies the holes in the first layer, and the third particle layer occupies the holes in the second layer which do not have any particles in the previous two layers. The difference between a hcp and a fcc lattice is that in hcp the third layer of particles occupies the holes where there are particles in the first layer. Particles with low surface charge at high concentrations form fcc lattices, while particles with high surface charge at low particle concentrations form bcc lattices.[35-39] The dimensions of fcc or bcc colloidal crystal lattices usually are > 100 nm, causing Bragg diffraction of visible light.

G. CRYSTAL STRUCTURES OF COLLOIDAL PARTICLES IN AQUEOUS AND NON-AQUEOUS MEDIA

Several factors govern the formation and orientation of colloidal crystals, such as the particle size, the surface charge, the particle concentration, and the ionic strength of the medium. There are several examples of polystyrene latexes and colloidal silica in aqueous dispersions[37-40] and non-aqueous dispersions[36] that form three-dimensional crystalline lattices. Several methods have been used to understand the particle order and crystal structure in liquid dispersions. The crystal microstructures of colloidal particles in aqueous and non-aqueous dispersions have been studied under the stresses of shear, electrical fields, confinement between two plates, and elevated temperatures using light scattering,[10,37-41] metallurgical microscopy,[42-45] optical microscopy,[46,47] digital-imaging,[33-35] x-ray topography,[48] freeze fracture microscopy,[49] scanning and transmission electron microscopy,[50-52] and ultra small angle X-ray diffraction (USAXRD).[16,53,54] Using a light scattering technique, Clark, Hurd, and Ackerson have analyzed Kossel line patterns due to fcc and bcc lattices from colloidal crystals for polystyrene latex in water in thin glass cells.[10] They have also successfully shown that the d_{111} planes of fcc and the d_{110} planes of bcc lattices parallel to the plane of the glass cells and are responsible for Bragg diffraction of visible light. Highly charged particles such as polystyrene latexes in liquid dispersions at low concentrations (< 0.2 volume fraction) form bcc lattices, while lowly charged particles such as colloidal silica at high concentrations (> 0.2 volume fraction) form fcc lattices.[39] Colloidal silica between 0.2 and 0.25 volume fraction forms fcc or a mixture of fcc and hcp lattices in ethanol-toluene mixtures.[36]

H. MORPHOLOGY OF COLLOIDAL CRYSTALS

The morphologies of the colloidal crystallites have been studied by various researchers to understand the orientation of the crystal planes with respect to the planes of

the glass cells. Monovoukas and Gast studied the morphology and orientational behavior of aqueous dispersions of colloidal crystals of polystyrene latexes between crossed polarizers of an optical polarizing microscope.[46,47] They found that no light passed through the colloidal dispersion when the incident light was normal to the crystal planes, and the crystals were said to be at extinction. These results indicate that the d_{111} of fcc or d_{110} of bcc lattices orient parallel to the plane of the glass surface and therefore do not show birefringence. Rotating the cells away from the normal incident light, the dispersions showed beautiful iridescent crystals, which proved that the diffracting planes, d_{111} of fcc and d_{100} of bcc, were parallel to the plane of the glass.

I. THEORY OF BRAGG DIFFRACTION

The structures of colloidal crystals are similar to those of atomic and molecular crystals. The main difference is that the lattice dimensions of colloidal crystals are 3 orders of magnitude greater than the lattice dimensions of molecular crystals. Due to the large lattice dimensions of > 100 nm, Bragg diffraction of light comparable to the interplanar dimensions occurs from the colloidal dispersions.

Diffraction from colloidal crystals of monodisperse charged polystyrene particles in water has been successfully explained by the Bragg equation which was originally proposed for atomic crystals,[55,56] and is given as:

$$\lambda = 2dn\sin\theta \tag{2}$$

where λ is the wavelength of diffracted light, d is the interplanar spacing, n is the refractive index of the dispersion, and θ is the Bragg angle. The dynamical diffraction theory was proposed which modifies the Bragg equation and takes into account the interaction between incident and diffracted beams in the medium:[57]

$$\lambda_{corr} = \lambda\left(1 - \frac{\psi_0'}{2\sin^2\theta}\right) \tag{3}$$

where $\lambda = 2n_s d_{hkl} \sin\theta$ and $\psi_o' = 3\phi \frac{(m^2-1)}{(m^2+2)}$

ψ_o' is the real part of crystal polarizability, λ is the Bragg diffracted wavelength, λ_{corr} is the corrected diffraction wavelength (which in most cases does not differ from λ, d_{hkl} is the interplanar spacing), θ is the Bragg angle, m is the ratio of the refractive index of the particles to that of the surrounding medium, ϕ is the particle volume fraction, and n_s is the refractive index of the suspension calculated by

$$n_s = n_m (1-\phi) + n_p \phi \tag{4}$$

where n_m and n_p are the refractive indices of the medium and the particles, respectively.[38] The dense d spacings of most common lattices of colloidal crystals can be calculated theoretically from the volume fraction of the particles.[58]

For fcc (111)

$$\phi = \frac{2\pi}{3}\left(\frac{D_o}{a}\right)^3 \tag{5}$$

$$d = a/\sqrt{3} \tag{6}$$

For bcc (110)

$$\phi = \frac{\pi}{3}\left(\frac{D_o}{a}\right)^3 \tag{7}$$

$$d = a/\sqrt{2} \tag{8}$$

where a is lattice constant and D_o is particle diameter.

The bandwidths $(\Delta\lambda_o)'$ of Bragg diffracted peaks from the dispersions containing colloidal crystals can be calculated from the equation 9 given by Kosan and Spry.[58]

$$(\Delta\lambda_o)' = \frac{w_y |K\Psi_H| \lambda_o}{\sqrt{b}\sin\theta} \tag{9}$$

where $\Psi_H = \frac{2}{\pi^2 (3)^{3/2}} (m^2+1)\left(\frac{3}{m^2+2}\right)(\sin u - u\cos u)$

$u = \pi\sqrt{3/2}\left(\frac{D_o}{D}\right)$ and $D = \frac{a}{\sqrt{2}}$

w_y is a numerical factor = 1.155 from the Ewald theory, K is the polarization factor which is equal to unity for σ polarization and $|\cos 2\theta|$ for π polarization, b is the ratio of direction cosines of light rays (which is unity for Bragg diffraction), m is the ratio of the refractive index of the particles to that of the medium, and D is the center-to-center distance between two neighboring particles.

J. APPLICATIONS OF COLLOIDAL CRYSTALS

Since the 1980's, Asher and his research group have exploited the Bragg diffraction of light from polystyrene latexes in water.[31,37-39,55,56,59-61] Due to the diffraction of light from materials having colloidal crystals, it has been possible to make optical devices such as rejection filters.[38,47] Asher has patents on the formation of rejection filters where colloidal crystalline arrays of polystyrene latex in water Bragg diffract visible light.[58,59] They were able to tune the diffraction wavelength by varying the particle concentration and particle size and by changing the Bragg angle, θ.[37,57,58] Narrow bandwidth filters composed of monodisperse polystyrene latexes in water have been used to reject the Rayleigh scattering in a Raman spectrometer.[55,56] The colloidal crystals of latexes orient with the d_{hkl} planes parallel to the plane of the quartz cell. These systems are robust models for studies of atomic systems and for fundamental studies of crystal physics. The dispersions with an ordered array of particles have potential applications as rejection filters, optical limiters, and switches.[38,47] Another patent issued to Alvarez[62] for a similar approach lacks examples of diffraction from colloidal particles and provides no information about diffraction phenomenon from their materials.

Although there are many interesting properties and applications of colloidal crystals, there is a major problem with these systems. The colloidal crystalline arrays of latex particles in liquid dispersions have poor mechanical properties, and the crystal order is disrupted by the presence of any mechanical or thermal force that acts on the lattices.

The elastic modulus of these crystallites is small on the order of 10^2 to 10^3 Pa as compared to molecular or atomic crystals which have elastic modulus > 10^4 Pa. Haacke, Panzer, Magliocco, and Asher have overcome the mechanical instability by forming the colloidal crystalline arrays of polystyrene latexes in acrylamide solutions, which on polymerization, form hydrogels and thus traps the crystallites in them.[63-65]

K. OBJECTIVE OF THE RESEARCH

Due to the poor mechanical stabilities of colloidal crystals of polystyrene latexes in liquid dispersions, we propose to order colloidal silica modified with various silane coupling agents in monomer dispersions. These colloidal particles have low surface charge and, hence at particle concentrations > 0.2 volume fraction, will order into three dimensional crystal lattices. Once the crystal lattice has been established in monomer dispersions, polymerization of the monomers will form the silica-polymer composite which will in turn stabilize the colloidal crystals.

Inorganic filler materials in polymer composites often improve mechanical and thermal stabilities compared with the pure polymer matrix.[66-71] The majority of polymer composites known are blends of immiscible inorganic solids and organic polymers. The degree of mixing of these two phases influences the tensile strength and tensile modulus of the materials. Colloidal silica and silica fiber have been widely incorporated into organic polymer matrices to reinforce the polymeric materials. Polymers from vinyl monomers like styrene, MMA, N-vinylcarbazole and silane coupling agents functionalized on polymers, have been grafted or coated onto the surface of particles to enhance the compatibility of such particles with the polymer matrix to form composites.[72-77]

Colloidal silica in composites may be formed by the hydrolysis and condensation of TEOS or tetramethyl orthosilicate (TMOS).[67-69] Different types of materials have

emerged by changing the method of preparation.[70] Using the modified Stöber procedure of sol-gel process by Bogush, Tracy, and Zukoski and by Badley, Ford, McEnroe, and Assink,[23,24,26] colloidal silica particles of diameters 100-500 nm could be synthesized as shown in Scheme 1. Using the method of Philipse and Vrij,[25] the colloidal silica could be coated with silane coupling agent such as 3-(trimethoxysilyl)-propyl methacrylate (TPM) to form the TPM-silica particles as shown in Scheme 2.

Scheme 1. Synthesis of Colloidal Silica by Sol-Gel Process

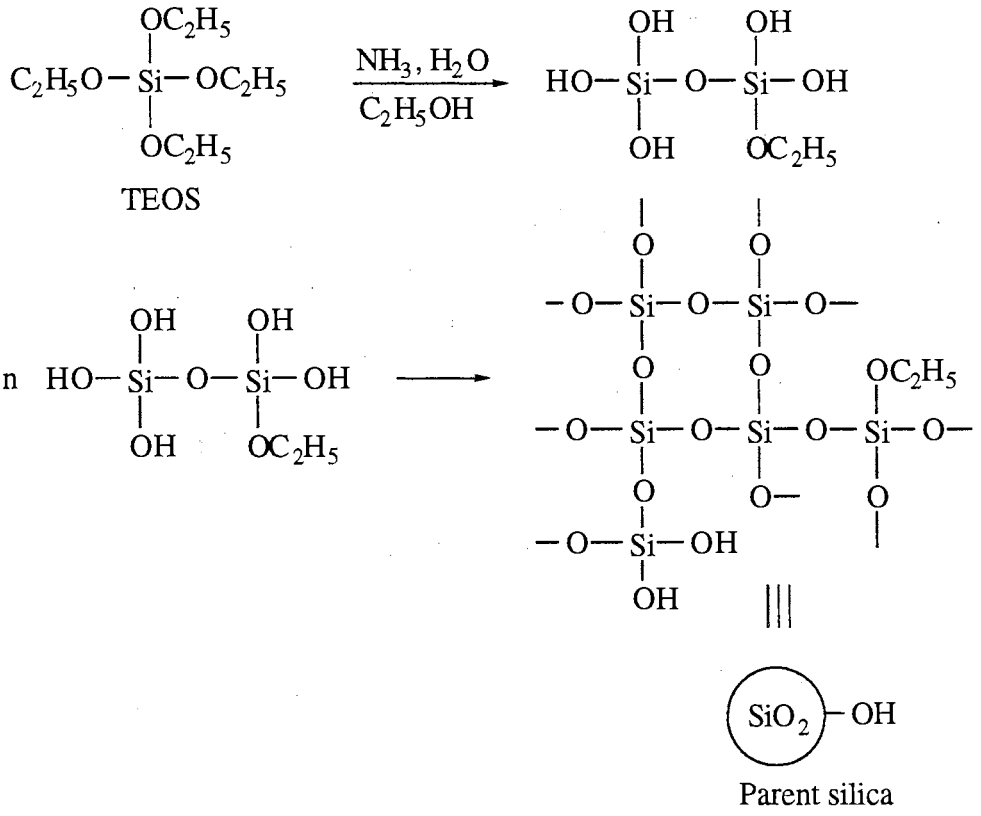

Scheme 2. Synthesis of TPM-silica Particles

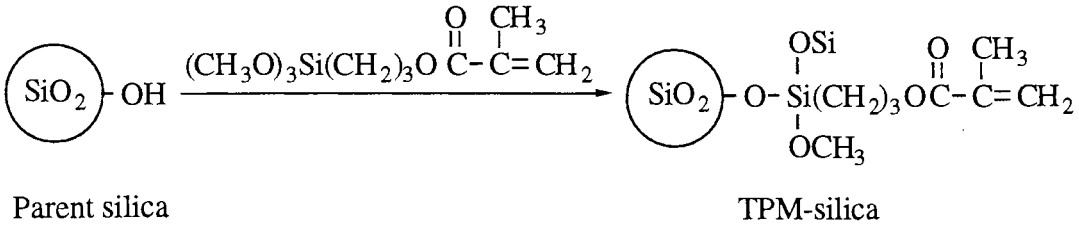

The particle can be transferred from ethanol to monomers such as MMA, methyl acrylate (MA), 2-hydroxyethyl methacrylate (HEMA) or 2,2,2-trifluoroethyl acrylate (TFEA) by dialysis or by centrifugation, decantation, and redispersion in different monomers. Once the particles are transferred in MMA or MA, the colloidal crystalline lattice can be established at certain particle concentrations. These monomer dispersions, along with a photoinitiator, can be filled in glass cells of 264 to 520 μm thickness to form the colloidal crystalline arrays. By using UV-visible spectrophotometry, the Bragg diffraction can be measured, and the crystal growth and morphology can be studied by polarizing microscopy. After good diffraction has been observed from the liquid dispersions, photopolymerization of these monomer dispersions will form thermoplastic silica-polymer composite films. During photopolymerization, the methacrylate group of TPM will be covalently linked to the methacrylate or acrylate groups of the monomers to form the silica-polymer composites as shown in Scheme 3.

Scheme 3. Synthesis of TPM-silica-Polymer Composite.

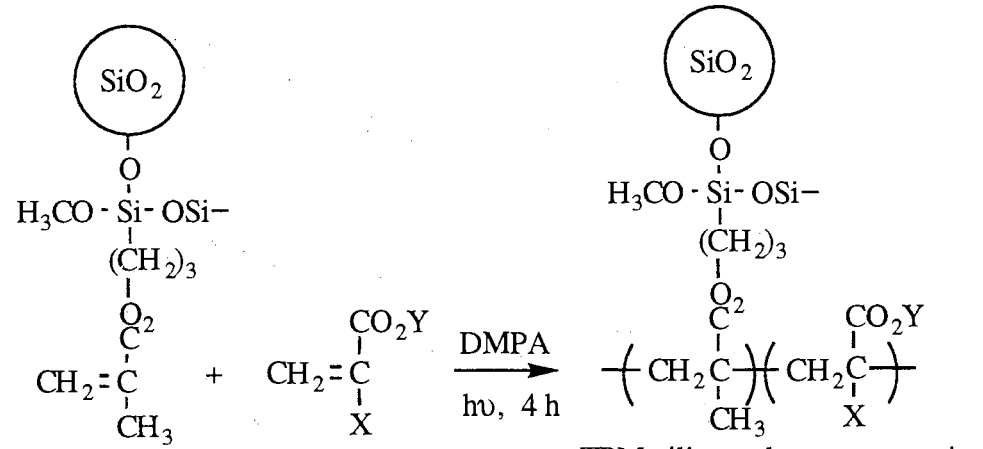

Covalent linkage between particles and polymer chains will enhance mechanical properties of our composite films. Obviously, the crystal structures and their orientations in the films are much more stable than in the dispersions. The rigid films will last longer

than the current optical rejection filters of aqueous colloidal crystalline dispersions. The tuning of the diffraction wavelength could theoretically be achieved by varying the particle size and particle concentration and by varying the Bragg angle. In the case of silica in elastomeric matrix, the diffraction wavelength can be tuned by altering the d-spacings of the crystallites by stretching and swelling the composite films.

REFERENCES

1. Alfrey, T. Jr.; Bradford, E. B.; Vanderhoff, J. W.; Oster, G. *J. Opt. Soc. Am.* **1954**, *44*, 603.
2. Luck, W.; Klier, M.; Wesslau, H. *Ber. Bunsenges. Phys. Chem.* **1963**, *67*, 75.
3. Luck, W.; Klier, M.; Wesslau, H. *Ber. Bunsenges. Phys. Chem.* **1963**, *67*, 84.
4. Luck, W.; Klier, M.; Wesslau, H. *Naturwissenschaften* **1963**, *67*, 75.
5. Hiltner, P. A.; Krieger, I. M. *J. Phys. Chem.* **1969**, *73*, 2386.
6. Hiltner, P. A.; Papir, Y. S.; Krieger, I. M. *J. Phys. Chem.* **1971**, *75*, 1881.
7. Krieger, I. M.; Hiltner, P. A. *Polymer Colloids Proceedings*, ACS Symposium on Polymer Colloids, Fitch, R., Ed. Plenum Press; New York, 1971, 63.
8. Williams, R.; Crandall, R. S. *Phys. Lett.* **1974**, *48*, 225.
9. Hoffman, R. L. *Trans. Soc. Rheol.* **1972**, *16*, 155.
10. Clark, N. A.; Hurd, A. J.; Ackerson, B. J. *Nature* **1979**, *281*, 57.
11. Pieranski, P. *Contemp. Phys.* **1983**, *24*, 25.
12. Okubo, T. *Prog. Polym. Sci.* **1993**, *18*, 481.
13. Dosho, S.; Ise, N.; Ito, K.; Iwai, S.; Kitano, H.; Matsuoka, H.; Nakamura, H.; Okumura, H.; Ono, T.; Sogami, I. S.; Ueno, Y.; Yoshida, H.; Yoshiyama, T. *Langmuir* **1993**, *9*, 394.
14. Bernal, J. D.; Fankuchen, I. *J. Gen. Physiol.* **1941**, *25*, 111.
15. Williams, R. C.; Smith, K. *Nature* **1957**, *4551*, 119.
16. Sanders, J. V. *Acta.Cryst.* **1968**, *A24*, 427.
17. Juang, M.S.; Krieger, I. M. *J. Polym. Sci. Polym. Chem. Ed.* **1976**, *14*, 2089.
18. Tamai, H.; Niino, K.; Suzawa, T. *J. Coll. Interface Sci.* **1989**, *131*, 1.
19. Antonietti, M.; Basten, R.; Lohmann, S. *Macromol. Chem. Phys.* **1995**, *196*, 441.
20. Kim, J. H.; Chainey, M.; El-Aasser, M. S.; Vanderhoff, J. W. *J. Polym. Sci. Part A: Polym. Chem.*, **1989**, *27*, 3187.

21. Kim, J. H.; Chainey, M.; El-Aasser, M. S.; Vanderhoff, J. W. *J. Polym. Sci. Part A: Polym. Chem.*, **1992**, *30*, 171

22. Sunkara, H. B.; Jethmalani, J. M.; Ford, W. T. *J. Polym. Sci. Polym. Chem. Ed.* **1992**, *30*, 1917.

23. Stöber, W.; Fink, A.; Bohn, E. *J. Colloid Interface Sci*. **1968**, *26*, 62.

24. Bogush, G. H.; Tracy, M. A.; Zukoski, C. F. *J. Non-Cryst. Solids* **1988**, *104*, 95.

25. Philipse, A. P.; Vrij, A. *J. Coll. Interface Sci*. **1988**, *128*, 121.

26. Badley, R. D.; Ford, W. T.; McEnroe, F. J.; Assink, R. A. *Langmuir*, **1990**, *6*, 792.

27. (a) Derjagiun, B. V.; Landau, L. *Acta Physiochim.* **1941**, *14*, 633. (b) Verwey, E. J. W.; Overbeek, J. Th. *Theory of the Stability of Lyophobic Colloids*; Elsevier; Amsterdam, 1948.

28. Ise, N.; Yoshida, H. *Acc. Chem. Res.* **1996**, *29*, 3.

29. Sogami, I.; Ise, N. *J. Chem. Phys.* **1984**, *81*, 6320.

30. Thirumalai, D. *J. Chem. Phys.* **1989**, *93*, 5637.

31. Rundquist, P. A.; Jagannathan, S.; Kesavamoorthy, R.; Brnardic, C.; Xu, S.; Asher, S. A. *J. Chem. Phys.* **1994**, *94*, 711.

32. Yoshiyama, T. *Polymer* **1986**, *27*, 827.

33. Van Winkle, D. H.; Murray, C. A. *Phys. Rev.A.*, **1986**, *34*, 562.

34. Murray, C. A.; Van Winkle, D. H. *Phys. Rev. Lett.* **1987**, *58*, 1200.

35. Murray, C. A.; Wenk, R. A. *Phys. Rev. Lett.* **1989**, *62*, 1643.

36. Dhont, J. K. G.; Smits, C.; Lekkerkerker, H. N. W. *J. Coll. Interface Sci.* **1992**, *152*, 386.

37. Carlson, R. J.; Asher, S. A. *Appl. Spectrosc.* **1984**, *38*, 297.

38. Rundquist, P. A.; Photinos, P.; Jagannathan, S.; Asher, S. A. *J. Chem. Phys.* **1989**, *91*, 4932.

39. Kesavamoorthy, R. Tandon, S.; Xu, S.; Jagannathan, S.; Asher, S. A. *J. Coll. Interface Sci.* **1992**, *153*, 188.

40. Okubo, T. *Langmuir* **1994**, *10*, 1695.

41. Monovoukas, Y.; Gast, A. P. *J. Coll. Interface Sci.* **1989**, *128*, 533.

42. Kose, A.; Ozaki, M.; Takano, K.; Kobayashi, Y.; Hachisu, S. *J. Coll. Interface Sci.* **1973**, *44*, 330.

43. Hachisu, S.; Yoshimura, S. *Nature*, **1980**, *283*, 188.

44. Ise, N.; Okubo, T.; Sugimura, M.; Ito, K.; Nolte, H. J. *J. Chem. Phys.*, **1983**, *78*, 536.

45. Okubo, T. *J. Chem. Phys.* **1987**, *86*, 2394.

46. Monovoukas, Y.; Gast, A. P. *Phase Transitions* **1990**, *21*, 183.

47. Monovoukas, Y.; Gast, A. P. *Langmuir* **1991**, *7*, 460.

48. Yoshimura, T.; Sogami, I. S. *Langmuir*, **1987**, *3*, 851.

49. Cohen, J. A.; Scales, D. J.; Ou-Yang, H. D.; Chaikin, P. M. *J. Coll. Interface Sci.* **1993**, *156*, 137.

50. Goodwin, J. W.; Ottewill, R. H.; Parentich, A. *J. Phys. Chem.* **1986**, *84*, 1580.

51. Kamenetzky, E. A.; Magliocco, L. G.; Panzer, H. P. *Science*, **1994**, *264*, 207.

52. Ishizu, K.; Sugita, M.; Kotsubo, H.; Saito, R. *J. Colloid Interface Sci*. **1995**, *169*, 456.

53. Matsuoka, H.; Ise, N. *Chemtracts Macromol. Chem.* **1993**, *4*, 59.

54. Konishi, T.; Ise, N. *J. Am. Chem. Soc.* **1995**, *117*, 8422.

55. Flaugh, P. L.; O'Donnell, S. E.; Asher, S. A. *Appl. Spectrosc*. **1984**, *38*, 848.

56. Asher, S. A.; Flaugh, P. L.; Washinger, G.; *Spectroscopy* **1986**, *1*, 26.

57. Zachariasen, W. H. "Theory of X-ray Diffraction in Crystals" John Wiley, New York, 1945.

58. Spry, R. J.; Kosan, D. J. *Appl. Spectrosc*. **1986**, *40*, 782.

59. Asher, S. A., U.S. Patent 4,627,689, 1986.

60. Asher, S. A., U.S. Patent 4,632,517, 1986.

61. Asher, S. A.; Kesavamoorthy, R.; Jagannathan, S.; Rundquist, P. A. *Nonlinear Optics III* **1992**, *SPIE Vol. 1626*, 238.

62. Alvarez, J. L. U.S. Patent 5,131,736, 1992.

63. Asher, S. A.; Jagannathan S. U.S. Patent 5,281,370, 1994.

64. Haacke, G.; Panzer, H. P.; Magliocco, L. G.; Asher, S. A. US Patent 5,266,238, 1993.

65. Panzer, H. P.; Giovanni, L.; Cohen, M. L.; Yen, W. S. US Patent 5,338,492, 1994.

66. Asher, S. A.; Holtz, J.; Liu, L.; Wu, Z. *J. Am. Chem. Soc.* **1994**, *116*, 4997.

67. Iler, R. K. *The Chemistry of Silica*; Wiley; New York, 1979; pp 582-588.

68. Sanchez, C.; Ribot, F. *New J. Chem.* **1994**, *18*, 1007.

69. Mark, J. E.; Lee, C. Y.-C.; Biancone, P. A., Eds. *Hybrid Organic-Inorganic Composites*; ACS Symposium Series 585; American Chemical Society; Washington, DC, 1995.

70. Landry, C. J. T.; Coltrain, B. K.; Brady, B. K. *Polymer* **1992**, *33*, 1486.

71. Ellsworth, M. W.; Novak, B. M. *Chem. Mater.* **1993**, *5*, 839.

72. Nishiyama, N.; Horie, K.; Schick, R.; Ishida, H. *Polym. Commun.* **1990**, *31*, 380.

73. Nishiyama, N.; Ishizaki, T.; Horie, K.; Tomari, M.; Someya, M. *J. Biomed. Mater. Res.*, **1991**, *25*, 213.

74. Morikawa, A.; Yamaguchi, H.; Kakimoto, M.; Imai, Y. *Chem. Mater.* **1994**, *6*, 913.

75. Wang, S.; Ahmad, Z.; Mark, J. E. *Chem. Mater.* **1994**, *6*, 943.

76. Nishiyama, N.; Komatsu, K.; Fukai, K.; Nemoto, K.; Kumagai, M. *Composites*, **1995**, *26*, 309.

77. Coltrain, B. K.; Landry, C. J. T.; O'Reilly, J. M.; Chamberlain, A. M.; Rakes, G. A.; Sedita, J. S.; Kelts, L. W.; Landry, M. R.; Long, V. K. *Chem. Mater.* **1993**, *5*, 1445.

CHAPTER II

SYNTHESIS OF SILICA POLYMER COMPOSITES

The formation of polymer composites containing colloidal crystals of silica was achieved in several steps by

i. the synthesis of silica particles by basic hydrolysis of tetraethylorthosilicate (TEOS),
ii. surface modification of colloidal silica particles with a silane coupling agent, 3-(trimethoxysilyl)propyl methacrylate (TPM), to form TPM-silica particles,
iii. transfer of TPM-silica particles from ethanol to methanol,
iv. transfer of modified particles from methanol to various monomers by dialysis,
v. formation of colloidal crystals in monomer dispersions in glass cells, and
vi. photopolymerization of the monomer dispersions to trap the colloidal crystalline arrays in to polymer composite films,

The morphology and Bragg diffraction from colloidal crystals in monomer dispersions were studied by UV-visible spectrophotometry and polarizing microscopy. In the case of TPM-silica-PMA composites, stretching and swelling experiments were performed, and the parent silica and TPM-silica particles were characterized.

A. MATERIALS AND INSTRUMENTATION.

Water was deionized twice with active carbon, and distilled in glass. TEOS, absolute ethanol, and TPM were distilled prior to use. Ammonium hydroxide (NH_4OH), MMA, MA, HEMA, TFEA, 2,2-dimethoxy-2-phenylacetophenone (DMPA), styrene, potassium hydrogen phthalate (KHP), and sodium hydroxide (NaOH) were used as received. The dialysis was achieved by using Spectra-Por® (Spectrum cat. # 132130) regenerated cellulose ester dialysis membrane tubing of 22 mm diameter with a molecular weight cut-off of 50,000.

The particle diameters were measured using a Joel 100 CXII transmission electron microscope (TEM) and dynamic light scattering (DLS). The structural and orientational details of the colloidal crystallites of TPM-silica particles in both the dispersion and thin polymeric films were studied by observing the orthoscopic images of the crystals between crossed polarizers on a Nikon Polarizing Microscope (OPTIPHOT-POL) and the images were photographed with a Nikon N 2000 camera. The transmission spectra of the samples were recorded with the incident light normal to the plane of the glass cell of a single beam Hewlett Packard 8452A UV-visible spectrophotometer equipped with diode array detector having a resolution of 2 nm. The photopolymerization of the dispersions was carried out using a medium pressure mercury vapor lamp (450 watts, Ace glass) surrounded by a vycor sleeve. The infrared spectroscopic analysis was done on a Nicolet model Impact 400 FTIR instrument. The conductometric titrations were done on YSI Model 31 Conductivity Bridge with an electrode with cell constant of 1.0. The cell was mounted on a stage that rotates around axes parallel and normal to the light. Tuning of the Bragg angle was achieved on a graduated 360° rotatory stage equipped with clamps and attached perpendicular to another graduated 360° rotatory stage, both having a least count of 2°.

B. FORMATION OF COLLOIDAL SILICA.

The colloidal silica was synthesized according to the modified Stöber method by Zukoski et. al.[1-3] The concentrations of TEOS, NH_3 and water in ethanol were based on the equations (1) and (2) discussed therein.

A typical synthesis of parent silica particles is as follows,

A 5000-mL, round-bottomed flask was placed in a water bath maintained at room temperature, and 1435 mL of freshly distilled ethanol, 13 mL of deionized double distilled water (2.2M), 96 mL of freshly distilled TEOS (0.264 M), and 84 mL of NH_4OH

(0.78 M) were added and magnetically stirred. During the initial twenty to thirty minutes of stirring, the clear solution turned cloudy and TEOS underwent hydrolysis and condensation to form silica particles as shown in Scheme 1 in Chapter I.

The solution was continuously stirred for 8 h. After this period, an aliquot of the dispersion was removed from the flask and placed in a culture tube and was further diluted with ethanol. The particle size in the diluted dispersion was analyzed by light scattering experiments done in Dr. Ackerson's laboratory. Based on the particle size and the calculations, more TEOS was added. The second portion of TEOS added was usually about 120 mL. The dispersion was then stirred for a period of 8 h. After this period, another aliquot was removed and analyzed for particle size measurements. A third portion of TEOS (96 mL) was added, and the whole dispersion was stirred for 8 h. Finally, the desired particle size of 160 nm was achieved for the parent silica by DLS measurements.

Scheme 1. Synthesis of TPM-Silica Particles

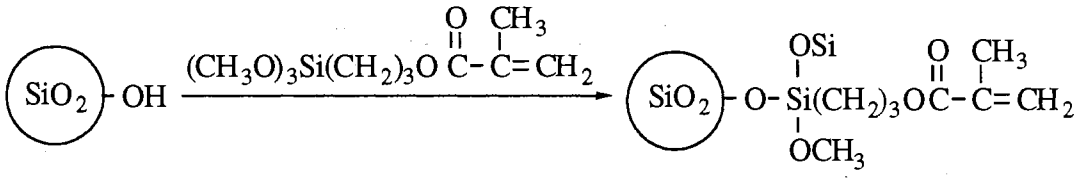

Parent silica TPM-silica

TPM was grafted onto the parent silica particles as described by the procedure of Philipse and Vrij[4] as shown in Scheme 1. Based on the concentration of particles in ethanol, surface area of particles, and the radius of the particles, the amount of TPM to be added was calculated based on the volume of the particles. Thus, to a 1700 mL sample of the parent silica dispersion, 80 mL of TPM was added, and the dispersion was stirred for 2 h. After this stirring period, 400 mL of ethanol was distilled off under atmospheric

pressure for 2-3 h period. Finally, the dispersion was concentrated by distilling off 600 mL of ethanol under vacuum at 25 °C until 500 mL of dispersion remained.

The concentrated dispersion of TPM-silica in ethanol was dialyzed against methanol using regenerated cellulose dialysis membrane tubing with molecular weight cutoff of 50000 (Spectra/Por 7, Spectrum) to remove any unreacted silane, water and ammonia as discussed by Hiltner et. al.[5] The particle concentration in methanol was increased to 56 wt % by distilling the methanol out under reduced pressure. The particles were thus stored in methanol dispersion. The TPM-silica particle sizes were also analyzed by DLS. The number average particle diameter was found to be 153 nm by TEM, with a polydispersity (standard deviation/mean) of 0.07, and 171 nm by DLS.[6-9] The density of the 152 nm diameter TPM-silica was measured using a 2 mL specific-gravity bottle. The volume of the specific-gravity bottle was calibrated using solvents acetonitrile, toluene, and water. The volume of a known amount of dried TPM-silica particles in acetonitrile was measured and the density of the TPM-silica particles was calculated.

C. PARTICLE CHARACTERIZATION

The surface characterization of parent and TPM-silica particles was done by conductometric titration. In two capped polyethylene bottles, 1.29 g of dried parent silica and 1.45 g of TPM-silica particles were redispersed in 75 mL deionized water each using a mechanical shaker and sonication for a period of two days. The conductometric titrations were accomplished by titrating the parent silica and TPM-silica dispersions with a standardized 0.004545 N NaOH solution. The NaOH solutions were standardized with known amounts of dried solid potassium hydrogen phthalate (KHP) using phenolphthalein indicator. Similarly, conductometric titrations have been done for commercially available silica particles as discussed by Okubo.[10]

For elemental analysis both parent and TPM-silica particles were air-dried at room temperature for several hours, oven-dried overnight at 90 °C, and vacuum dried overnight at 60 °C. For FT-IR analysis, KBr pellets of the dried parent silica, TPM-silica, and the TPM-silica-PMMA composite were made.

For the ^{29}Si solid state NMR analysis, 300-500 mg of the parent silica and TPM-silica particles in alcoholic solutions were dried in air, in an oven at 90 °C and finally under vacuum at 60 °C. The solid state NMR analyses of the parent silica and TPM-silica particles were carried out on a 300 MHz Chemagnetics NMR spectrometer. The composition of silica in different environments has been previously discussed.[12]

D. TRANSFER OF TPM-SILICA TO MONOMERS

A 10-15 cm long dialysis tube was washed several times with deionized water followed by closing one end of the tube with a string. The tube was then rinsed with methanol a couple of times and filled with methanol. The methanol inside the tube was then dialyzed with more methanol in a measuring cylinder for a period of 1-2 h. In the meanwhile, the methanolic dispersion of TPM-silica particles were mechanically shaken and ultrasonicated to completely redisperse the particles in methanol. Small portions of 5-7 mL of this concentrated dispersion were dialyzed against monomers such as MMA and MA. During a period of 24 h, the monomers in the measuring cylinder were replaced at least 4-5 times. The TPM-silica in the monomer dispersions were analyzed by ^{1}H-NMR which showed presence of <1 % methanol. Silica contents were analyzed by measuring 250 μL of the concentrated dispersion into a tared aluminum pan, air drying, oven-drying at 90 °C, and weighing the dried particles.

E. FORMATION OF COLLOIDAL CRYSTALS

i. Cell Preparation. The glass cells containing the colloidal crystal dispersions were specially designed for the photopolymerization experiments. Microscope slides (3"

x 1" x 1mm) were silylated overnight by immersion in a solution of 10% dichlorodimethylsilane in cyclohexane, washed with cyclohexane and water, and dried at 110 °C. To make a cell, one plain slide and one with two holes of 2 mm diameter drilled at one end were wiped clean with Kimwipes and a lint-free brush, sandwiched and clamped around one, two or three teflon spacers of 132 μm thickness, and sealed on two sides and one end using Devcon 5-Minute® epoxy and cured at room temperature. After the epoxy dried, the teflon spacers were removed, and the remaining end was sealed with the epoxy, leaving the holes open for filling the dispersions.

ii. Concentration Studies. For the ordering and orientation studies, the desired particle concentrations of 35, 37.5, 40, 42.5 and 45 wt % were made by diluting the 48 wt % dispersion with more MMA. For example, a MMA dispersion of 40 wt % particles and volume 0.6 mL was prepared from 0.5 mL of 48 wt % dispersion and 0.1 mL of MMA in a vial which contained 43.0 mg (1.0 wt % to the monomer) of photoinitiator, DMPA. Similarly, in case of TPM-silica in a MA dispersion, 9.0 mg (~0.2 wt% to the monomer) of DMPA was used. The DMPA was dissolved by vortex mixing for a minute, and syringed into the cell through the holes. A cover-slip with Duro™ Quick-Gel™ glue was used to seal the holes quickly, followed by sealing with 5-minute epoxy. The cell was kept horizontal at 25 ± 1 °C for crystallization and growth. Similarly, TPM-silica particles in a concentrated MA dispersion was diluted by adding more MA to make 35, 40 and 45 wt % particles dispersions. Visible spectra were obtained with the cells vertical.

E. MORPHOLOGY AND BRAGG DIFFRACTION

Bragg diffraction was measured by transmission spectrophotometry using a UV-visible spectrophotometer by holding the cells containing the monomer dispersions vertical with incident light normal to the plane of the glass cell. The transmission spectra were obtained by first running a background run through an empty glass cell. The

orthoscopic images between crossed polarizers were observed with the plane of the cell at an angle of 40-55° to the light beam of a polarizing microscope as discussed by Monovaukas and Gast[10,11] After filling the MMA dispersions in the cells, the crystallization occurred in several hours and during this period the cloudy dispersion became iridescent. The Bragg diffraction observed 18-24 hour after filling the cells show that the complete crystallization occurs in 24 h. In case of MA dispersion, the crystallization occurs in 1-2 minutes after filling the cells. In 6-8 h, the entire cell becomes completely iridescent and shows diffraction of light. The half-height bandwidths of the diffracted wavelengths were measured from the absorbance spectra using a ruler and correlating with the spectral width.

F. PHOTOPOLYMERIZATION

The cell containing the colloidal silica dispersion and the initiator, DMPA (wt % with respect to the MMA or MA), was placed horizontally in a water bath at 27 ± 1 °C, and irradiated for 3.5-4 h using a medium pressure 450 W Hg lamp surrounded by a vycor sleeve. The photochemical reactor has a medium pressure mercury vapor lamp (450 watts, Ace glass), which is surrounded by a vycor sleeve, 1 cm from the sample. The lamp and the sleeve are immersed in a water circulated quartz immersion jacket.

G. STRETCHING AND SWELLING OF TPM-SILICA-PMA FILMS

i. Stretching of PMA Composite Films. The films were stretched with a homemade device having clamps attached to a micrometer with a least count of 0.001 inch. The initial distance between the clamps holding the film was 1.0 cm. The transmission spectra before, during and after stretching were observed with the film normal to the incident light beam. The spectrum and the length of the film were measured after each stretch until only a weak peak remained in the spectrum. After release of stress, the films returned to their original dimensions in 2-4 h.

ii. Swelling of PMA Composite Films. To a 35 wt % TPM-silica-PMA composite film between glass slides held apart by two 132 μm pieces of teflon at each end, a solution of 1 wt % DMPA in MA monomer was transferred by capillary action. The sample was kept horizontally above MA monomer in a closed glass dish while MA diffused into the composite. During swelling the sample was removed from the dish periodically, and the visible spectrum was measured. More MA with 1 wt % initiator was added between the slides, and after further swelling, the excess MA was removed by wiping with Kimwipes, and the film was irradiated for 3-4 h. The swollen and repolymerized film was slightly thicker than the two teflon spacers.

I. SCANNING ELECTRON MICROSCOPY

Composite films were microtomed normal to the surface using a Sorvall RMC-MT 6000, followed by coating the surfaces with Au-Pd under vacuum in a Hummer II sputter coater. The samples were examined on a JEOL JSM-35U Scanning Electron Microscope at 25 kV and 20,000 magnification.

J. COMPUTER MODELING

ChemDraw v. 2.0 on a Macintosh computer was used to model the fcc and rhombohedral structures. The data was written in the form of a text document and then transformed into a fcc unit cell. The fcc unit cell was compressed normal to the d_{111} planes by 15 % to give a rhombohedral lattice.

REFERENCES

1. Stöber, W.; Fink, A.; Bohn, E. *J. Colloid Interface Sci*. **1968**, *26*, 62.
2. Bogush, G. H.; Tracy, M. A.; Zukoski, C. F. *J. Non-Cryst. Solids* **1988**, *104*, 95.
3. Badley, R. D.; Ford, W. T.; McEnroe, F. J.; Assink, R. A. *Langmuir*, **1990**, *6*, 792.
4. Philipse, A. P.; Vrij, A. *J. Coll. Interface Sci*. **1988**, *128*, 121.
5. Hiltner, P. A.; Papir, Y. S.; Krieger, I. M. *J. Phys. Chem.* **1971**, *75*, 1881.
6. Ackerson, B. J.; Clark, N. A. *J. Phys*. (Paris) **1981**, *42*, 929.
7. Pusey, P. N.; van Megen, W. *J. Chem. Phys.* **1984**, *80*, 3513.
8. Pecora, R., Ed. *Dynamic Light Scattering-Applications of Photon Correlation Spectroscopy*, Plenum Press, New York, 1985.
9. Nobbmann, U. M.S. thesis, Oklahoma State University, 1991.
10. Monovoukas, Y.; Gast, A. P. *Phase Transitions* **1990**, *21*, 183.
11. Monovoukas, Y.; Gast, A. P. *Langmuir* **1991**, *7*, 460.
12. Okubo, T. *J. Chem. Phys.* **1987**, *87*, 6733.
13. Joseph, R. M. S. thesis, Oklahoma State University, 1995.

CHAPTER III

COLLOIDAL CRYSTALS OF MONODISPERSE SILICA IN POLY(METHYL METHACRYLATE) FILMS

ABSTRACT

Monodisperse 152 nm colloidal silica particles in monomer dispersion form a three dimensional crystal lattice, and Bragg diffract visible light, and polymerization of monomer dispersion traps the crystal order into a robust silica-polymer composite. UV-visible spectrophotometric analyses show Bragg diffraction as low % transmittance (%T) peaks of 4 nm bandwidth at wavelengths (λ_{min}) between 556 and 508 nm for 35 to 45 wt % amorphous colloidal 3-(trimethoxysilyl)propyl methacrylate (TPM) coated silica (TPM-silica) in methyl methacrylate (MMA) dispersions. Nucleation, growth and morphology of crystallites are studied by polarizing microscopy. On photopolymerization of the MMA dispersion, the diffraction wavelength blue shifts to 490 nm. The colloidal silica and TPM-silica particles are characterized by TEM, DLS, elemental analysis, FTIR and conductometric titrations.

INTRODUCTION

Monodisperse charged colloidal particles in aqueous and non-aqueous media spontaneously self assemble to form three-dimensional lattices known as colloidal crystals.[1-4] High surface charge of particles, high dielectric constant of medium, low concentration of ionic impurities, and particles at < 0.2 volume fractions favor crystal-like structures. Though formation of crystal-like structures of charged colloidal particles has also been observed in nonaqueous solvents,[5-11] not much work has been done in these systems. The dissociation of surface ionic groups is much smaller in low dielectric constant media compared with water and thus a high particle concentration is required to form colloidal crystals.

Colloidal crystals of charged colloidal particles in aqueous and nonaqueous media efficiently Bragg diffract visible light as the lattice spacings have dimensions > 100 nm, and thus the dispersions display brilliant iridescent colors. The dispersions with ordered arrays of colloidal particles have potential applications as rejection filters[12,13] and optical limiters.[14,15] Narrow bandwidth filters composed of monodisperse polystyrene latexes in water have been used to reject the Rayleigh scattering in a Raman spectrometer.[16] Here the colloidal crystals of latexes orient with the most dense d_{hkl} planes parallel to the plane of a quartz cell. The diffraction of light can be calculated using the Bragg equation (1),

$$\lambda = 2dn \sin\theta \tag{1}$$

where λ is the wavelength of diffracted light, d is the interplanar spacing, n is the refractive index of the dispersion and θ is the Bragg angle.

A major drawback to these liquid dispersions is that weak shear, gravitational, electrical, or thermal forces disturb the crystalline order due to the low elastic modulus (10^{-2} to 10^{-3} Pa) of colloidal crystals.[3,17] Thus, sturdier colloidal crystals may have wider use as selective filters and other optical devices. Our approach in stabilizing the

colloidal crystals involves trapping the crystalline order in a solid matrix by photopolymerizing the dispersions of ordered amorphous silica in acrylic and methacrylic esters.[10,11] Colloidal crystalline arrays of polystyrene latexes have been stabilized in polyacrylamide gels.[18-21]

Polymer composites often have greater tensile modulus and strength than the parent polymer. The degree of mixing of filler materials such as carbon black, silica and silicates affects the tensile strength and abrasion resistance of rubber.[22] After carbon black, 1-30 nm diameter fumed silica has been one of the most widely incorporated filler materials.[23] Apart from commercially available silica, colloidal particles have been formed by basic or acidic hydrolysis of tetraethyl orthosilicate (TEOS) or tetramethyl orthosilicate (TMOS).[23-26] By using silica particles of diameters much smaller than the wavelength of visible light or by carefully matching the refractive index of fibers, optically clear composites of silica-PMMA have been prepared.[27,28] Due to segregation of incompatible particles, poor optical properties also have been observed from silica-PMMA composites.[29] To increase the compatibility between silica and acrylic, methacrylic, and vinyl polymer matrices, silane coupling agents have been grafted on colloidal silica.[30-34] Recently, we have reported blue and red shifts of diffraction wavelengths from TPM-silica in methyl acrylate (MA) dispersions and poly(methyl acrylate) (PMA) composite films.[35] We now report preparation and characterization of a novel class of composites constituted of regularly ordered compatible silica particles trapped in PMMA matrix. We have made composite films that are iridescent and transparent even though they contain up to 45 wt % 152 nm diameter silica particles. Covalent linkage between the TPM-silica particles and the PMMA matrix enhances the tensile strength, stabilizes the crystal order and orientations as compared to the other ordered colloidal crystals in aqueous or non-aqueous dispersions. The rigid films are highly selective filters of visible light, and are more robust and thermally stable than the current filters made of aqueous dispersions.

RESULTS

COLLOIDAL TPM-SILICA PARTICLES

Monodisperse amorphous colloidal parent silica, and TPM-silica in ethanol were prepared according to the published procedures.[6,7,36,37]

Scheme 1. Synthesis of TPM-silica Particles

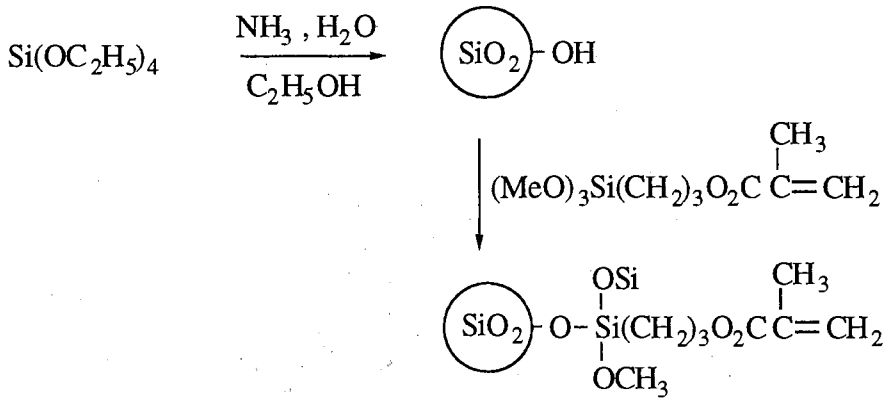

TPM-silica

Scheme 1 gives the chemical structure of parent and TPM-silica particles, while Table I gives particle diameters obtained from TEM and DLS and calculated polydispersity indices (mean/standard deviation), and Table II gives the elemental compositions, number of TPM groups, and number of ionizable groups measured by conductometric titrations.

Table I. Particle Diameters (nm) Measured by TEM and DLS

	TEM				DLS
sample	D_n	D_w	D_z	PDI[a]	D_z
parent silica	332	333	335	0.04	410
parent silica	152	152	153	0.04	159
TPM-silica	151	153	155	0.04	---

[a] Standard deviation/mean.

Colloidal silica usually has a polydispersity index between 4 and 7 %. However, we have prepared reasonably monodisperse silica particles by seed growth technique. The higher percents C and H for TPM-silica particles as compared to the parent silica is due to the TPM coated on the particles.[6,7,37] The TPM-silica particles are electrosterically stabilized and are colloidally stable in ethanol or in ethanol-toluene mixtures.[8] We have transferred the silica particles from ethanol to the desired monomer by the dialysis technique described by Hiltner[5] to transfer latex particles from aqueous to nonaqueous solvents. The TPM-silica particles are stable in a variety of monomers such as MMA, MA and 2-hydroxyethyl methacrylate (HEMA).

Table II. Elemental Composition and Surface Titration

	elemental analysis				
sample	%C	%H	%N	TPM/nm^2	σ (μC/cm^2)
parent silica	4.44	1.57	0.36	---	2.62
TPM-silica	7.76	1.92	0	~11	1.17

CHARACTERIZATION OF PARTICLES

Figure 1 shows a graph of conductance versus volume of NaOH added for parent silica particles redispersed in water. The σ-value calculated from the equivalence point was 2.62 μC/cm^2 for the strongly acidic groups. Similar results of conductometric titrations for commercially available silica have been reported where two equivalence points for the strongly and weakly acidic groups were observed.[38,39] Figure 2 shows a graph of conductance versus volume of NaOH added for TPM-silica particles redispersed in water. There is only one equivalence point observed in the graph. The σ-value calculated from the equivalence point is 1.17 μC/cm^2 for the strongly acidic group.

Figures 3, 4 and 5 show the FTIR spectra of parent silica, TPM-silica and TPM-silica-PMMA composite, respectively. The IR spectrum of the parent silica shows a

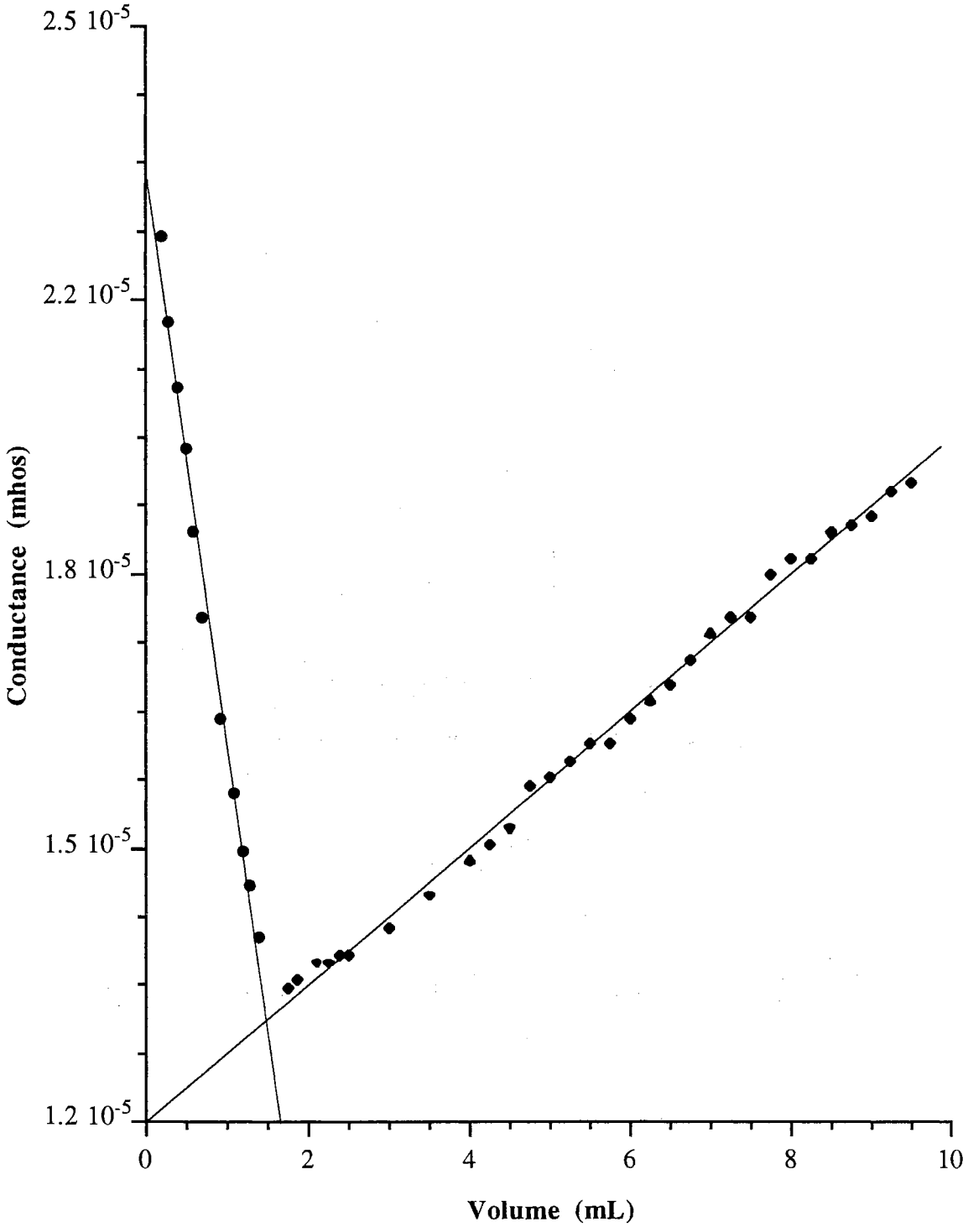

Figure 1. Conductometric titration of redispersed parent silica particles in water with a standardized 0.004545 N NaOH solution.

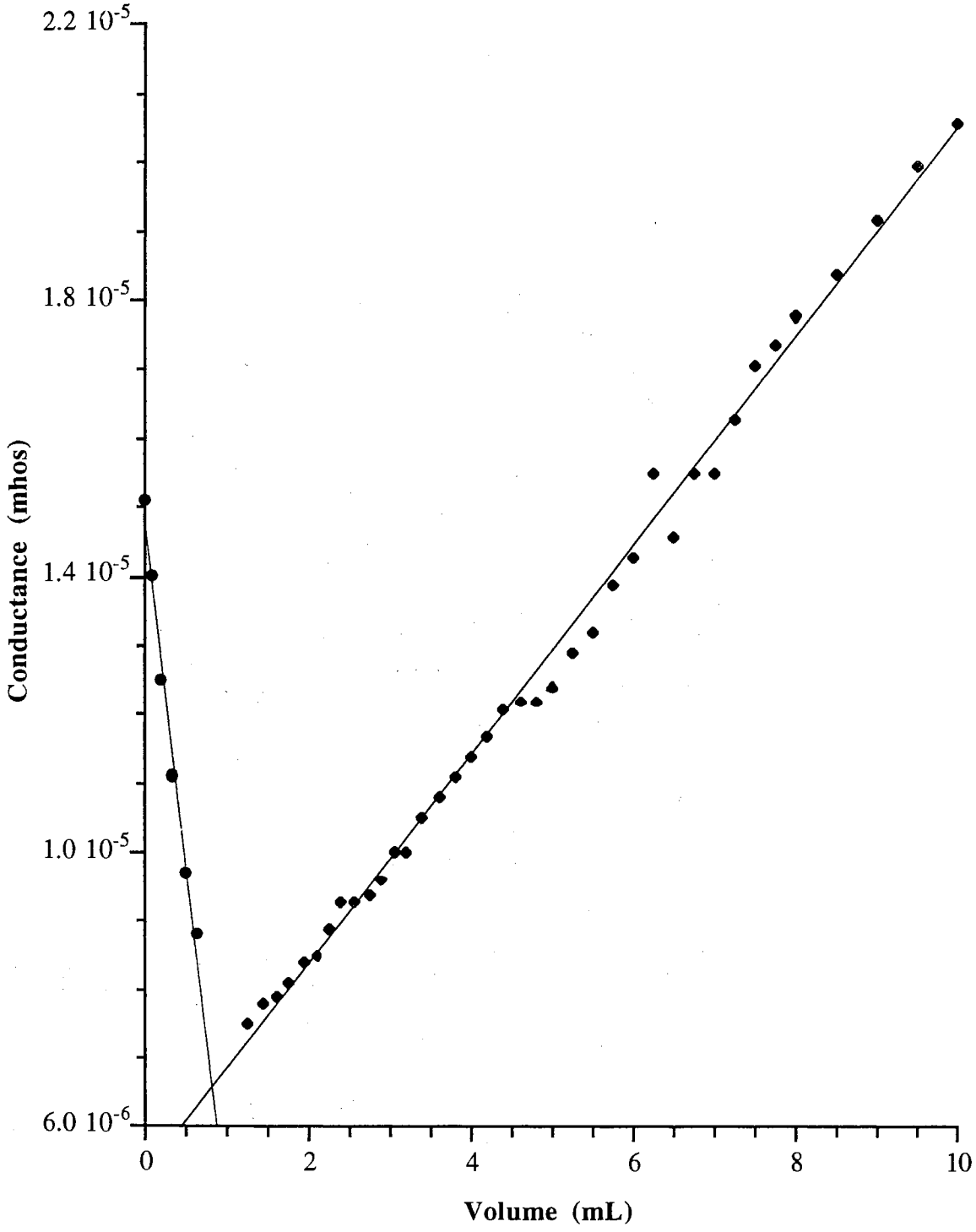

Figure 2. Conductometric titration of redispersed TPM-silica particles in water with a standardized 0.004545 N NaOH solution.

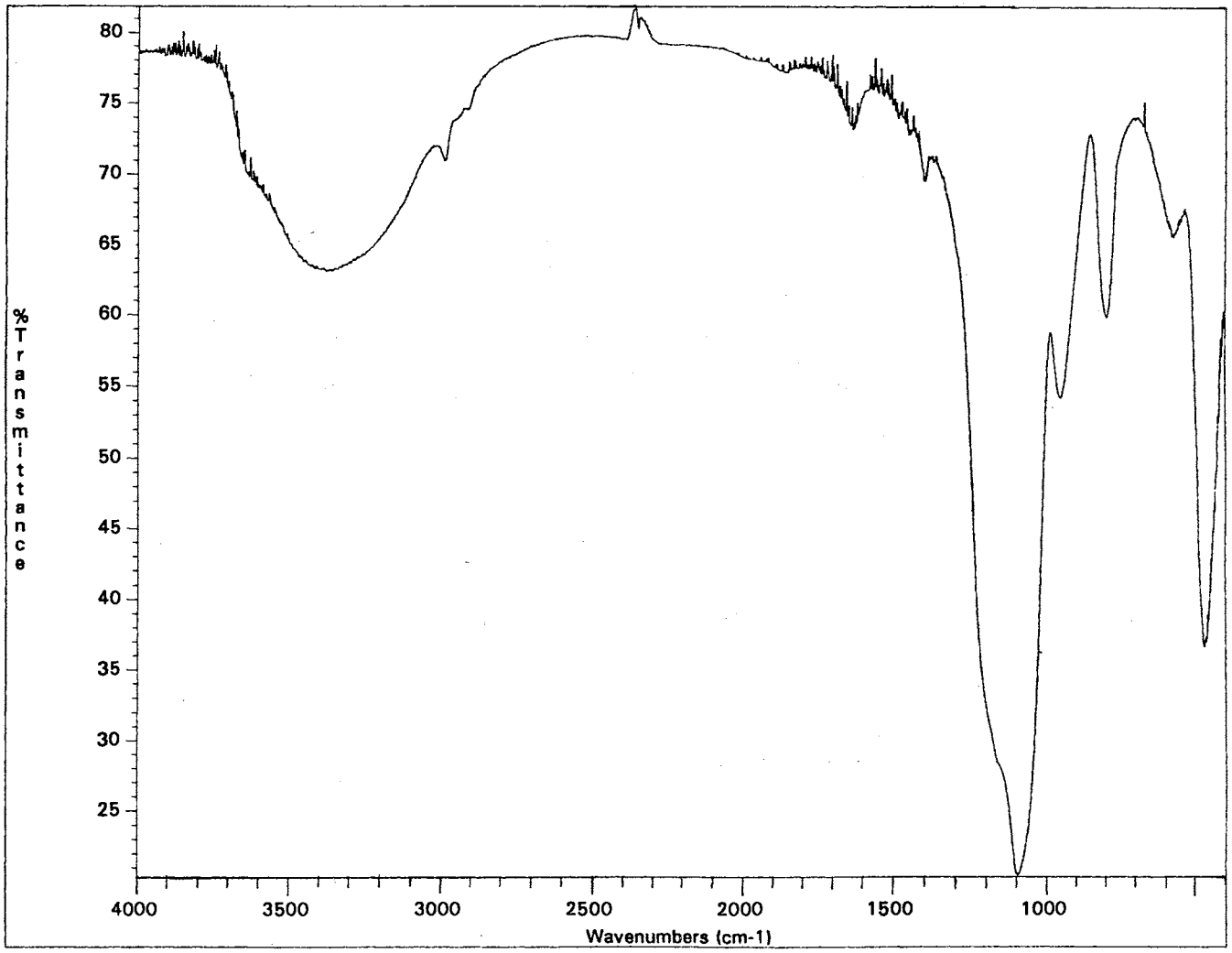

Figure 3. FTIR Spectrum of KBr Pellet of Parent Silica.

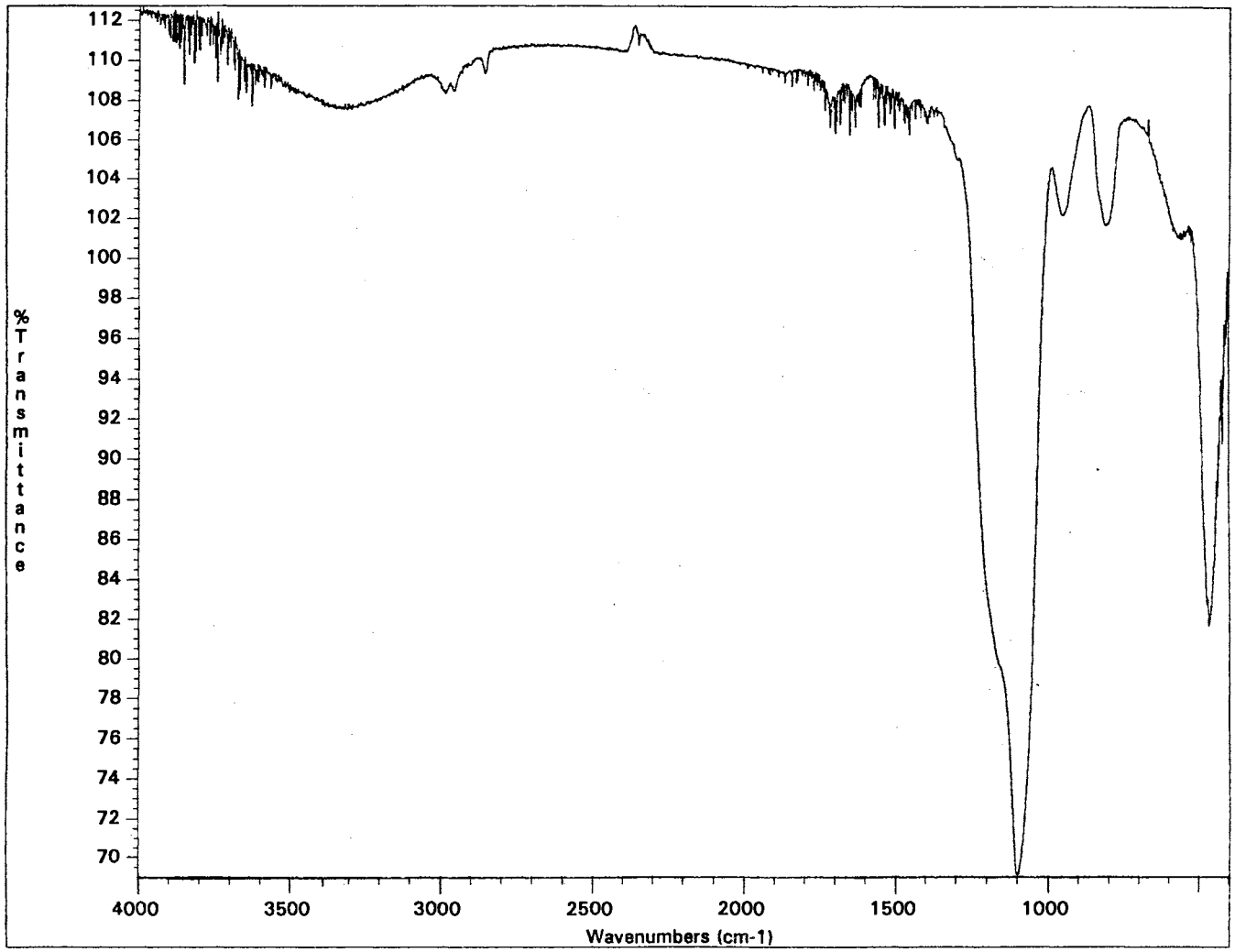

Figure 4. FTIR Spectrum of KBr Pellet of TPM-silica.

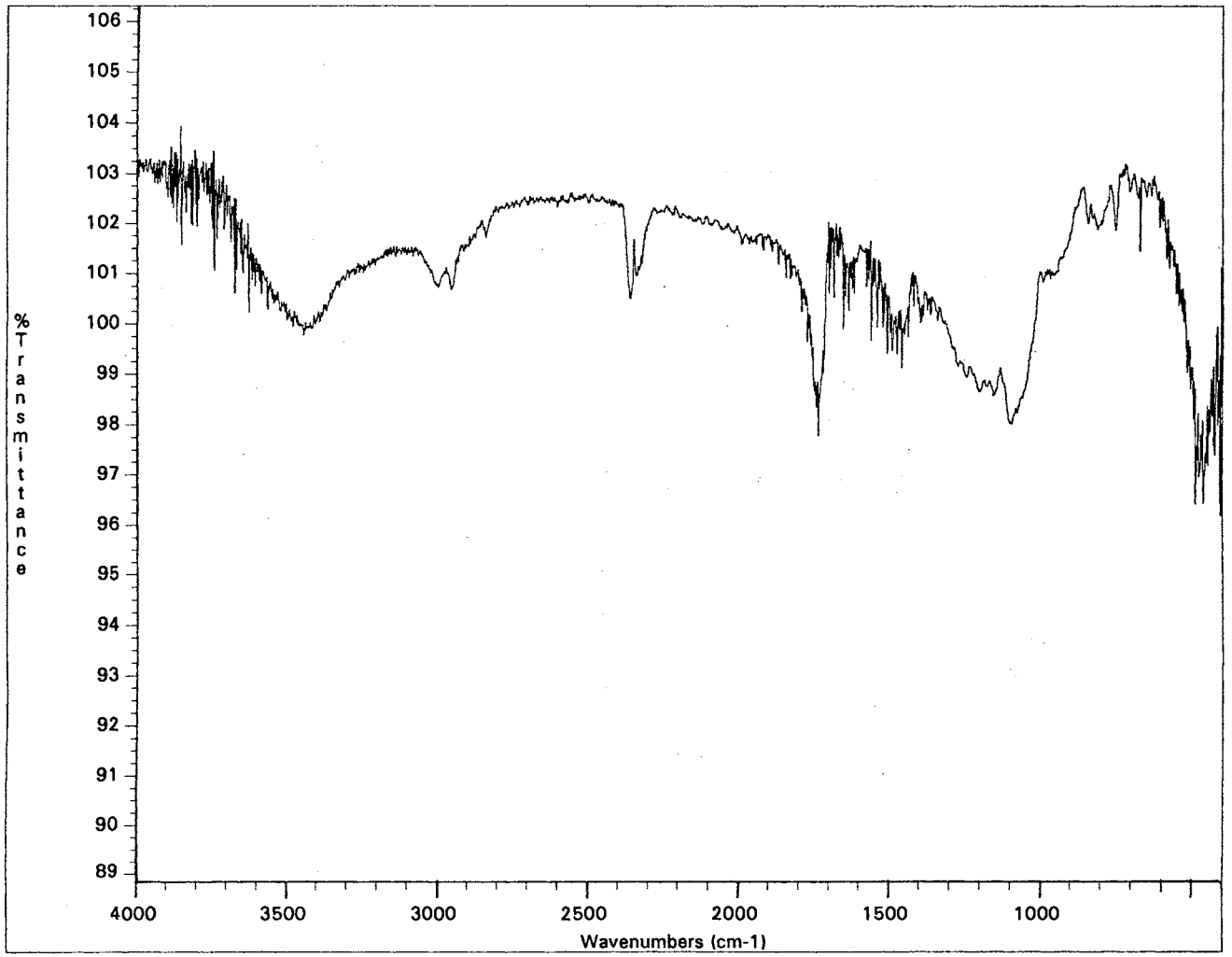

Figure 5. FTIR Spectrum of KBr Pellet of TPM-silica-PMMA Composite.

strong band for the strongly acidic -OH groups between 2700-3700 cm^{-1}, a very weak band for weakly acidic -OH groups at 3740 cm^{-1} and a strong band for the Si-O-Si linkages at 1100 cm^{-1}.[40] The appearance of weak band at 2700-3700 cm^{-1} for the surface -OH group in the case of TPM-silica particles suggests that the TPM groups are coated on the surface of the parent silica particles. The IR spectrum for the silica-PMMA composite shows appearance of weak bands at 1750 cm^{-1} for the carbonyl group of PMMA matrix and at 1100 cm^{-1} for Si-O-Si linkages at the TPM-silica particles.

MMA DISPERSIONS

Figure 6 shows the transmission spectra of MMA dispersions of colloidal crystals at 35 to 45 wt % 152 nm TPM-silica, while Table III gives the diffraction wavelengths. The ~9 mm diameter circular beam of incident light of a UV-visible spectrophotometer is normal to the plane of the cell. Initially, no diffraction was observed from the 35 and 37.5 wt % dispersions, whereas only weak diffraction was observed from the 40, 42.5 and 45 wt % dispersions. The wavelength of minimum transmission (λ_{min}) decreases from 550 to 508 nm as the particle concentration increases from 35 to 45 wt %. At the same time, the bandwidths of the peak at half-height were 3-4 nm. By changing positions of the cells in the spectrophotometer, the diffraction wavelength of the 37.5 and 40 wt % dispersions was found to be the same at top, center and bottom of the cell. Table IV reports the compositions and the spectral data from 35 and 40 wt % silica in MMA dispersions filled in thin glass cells.

Figure 7 shows the transmission spectra from a 40 wt % 152 nm TPM-silica in MMA and the effect of changing the angle of incident light. The first order diffraction wavelength shifts to the blue, and after 8.6° a diffraction peak at shorter wavelength shifts to the red. The photon energy (eV) at half-height of the diffraction wavelength versus the angle of the incident light is plotted in Figure 8.

Table III. Diffraction from Dispersions of 152 nm TPM-silica in MMA

% wt	ϕ[a]	time[b] (h)	obsd. λ_{min} (nm)	calcd. λ_{min}[c] (nm)
35.0[d]	0.195	67	550	550
37.5[e]	0.209	24	536	537
40.0[e]	0.223	18	528	526
42.5[d]	0.237	2	518	516
45.0[d]	0.251	2	508	512

[a] Based on the density of TPM-silica particles of 1.795 g cm^{-3}. [b] Time between filling the cells and measurement of the spectra. [c] Calculated from Bragg's Law (eq.1) assuming diffraction from d_{111} planes of fcc lattice (eq. # 2, ref. 45). [d] The MMA contained 2 wt % DMPA, and the temperature was maintained between 25 and 29 °C. [e] The MMA contained 1 wt % DMPA, and the temperature was maintained at 25 °C.

Table IV. Diffraction from Dispersions of TPM-Silica in MMA[a]

ϕ	n_D	time[b] (h)	λ_{min} (nm)	d_{111}[c] (nm)	obsd. bandwidth (nm)	calcd. bandwidth[d] (nm)
0.195	1.4192	72	552	195.2	3.4	3.1
0.223[e]	1.4203	8	532	187.3	3.6	3.1

[a] ϕ = volume fraction of the particles; λ_{min} = diffracted wavelength maximum of the dispersions. Particle diameter 152 nm with a polydispersity (standard deviation/mean) 0.04. The thickness of the cell is 264 μm. [b] Time between filling of the cells and measurement of the spectra. [c] Calculated from eq (1) in the text. The refractive index of the TPM-silica particles is 1.449.[8] [d] Bandwidths are full width at half maximum. [e] Particle diameter 153 nm with a polydispersity 0.08.

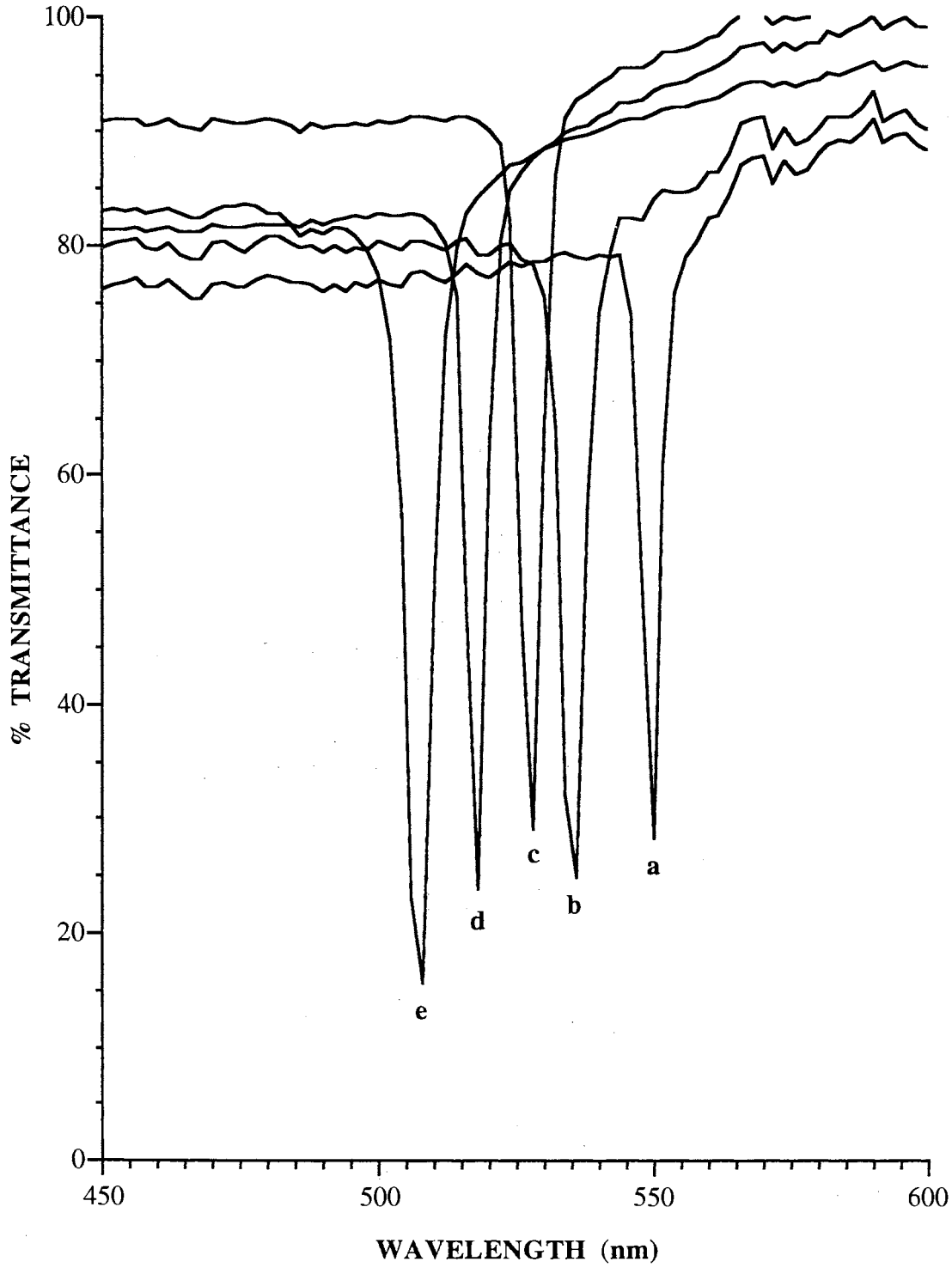

Figure 6. UV-visible transmission spectra of 152 nm TPM-silica in MMA dispersions (a) 35, (b) 37.5, (c) 40, (d) 42.5, and (e) 45 wt % particle concentrations.

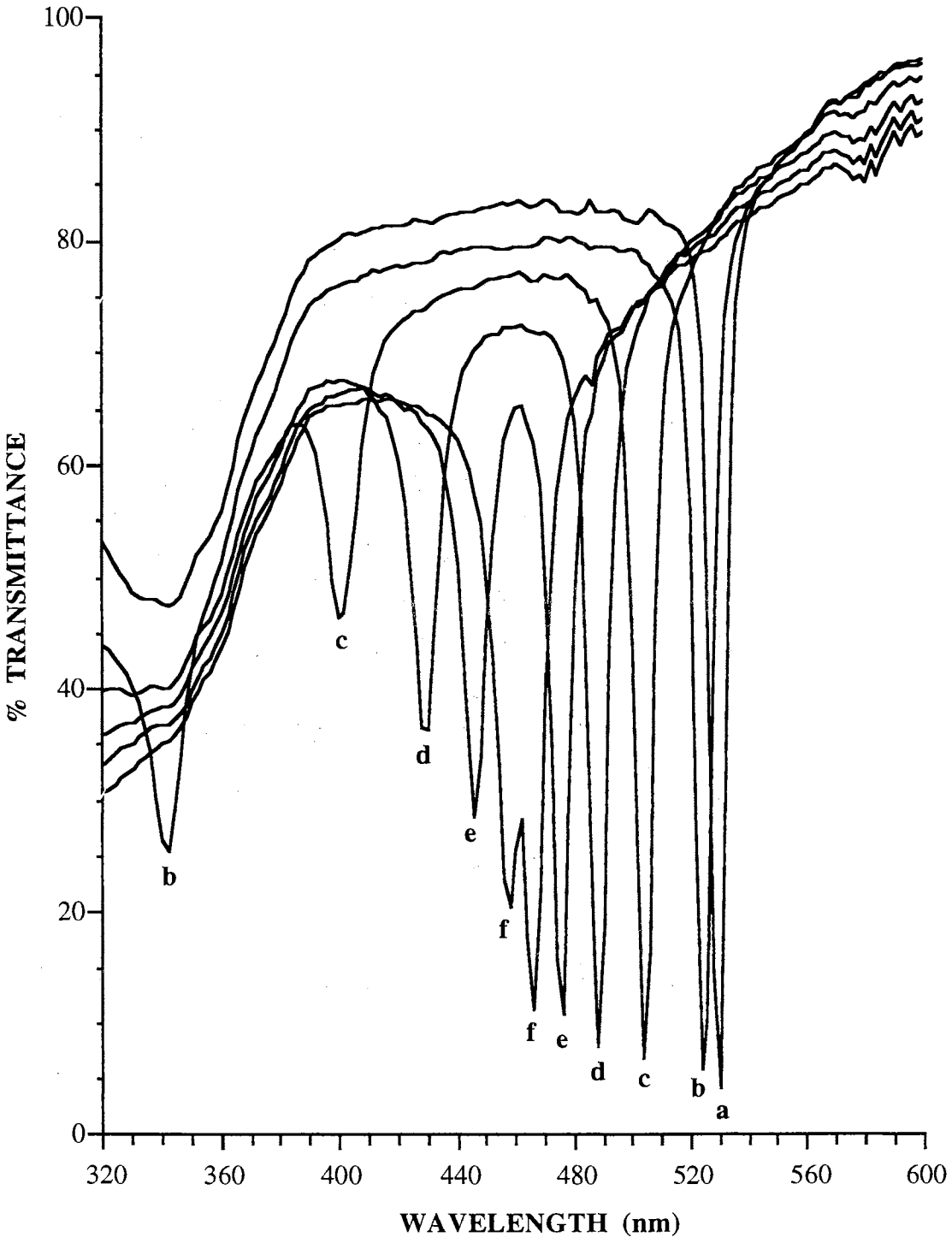

Figure 7. UV-visible transmission spectra of 40 wt % 152 nm TPM-silica in MMA as a function of angle of incident light, θ (°), (a) 0, (b) 8.6, (c) 18.0, (d) 23.0, (e) 26.1 and (f) 28.5°. $\theta = 90 - \theta_1$, where θ_1 is the glancing angle.

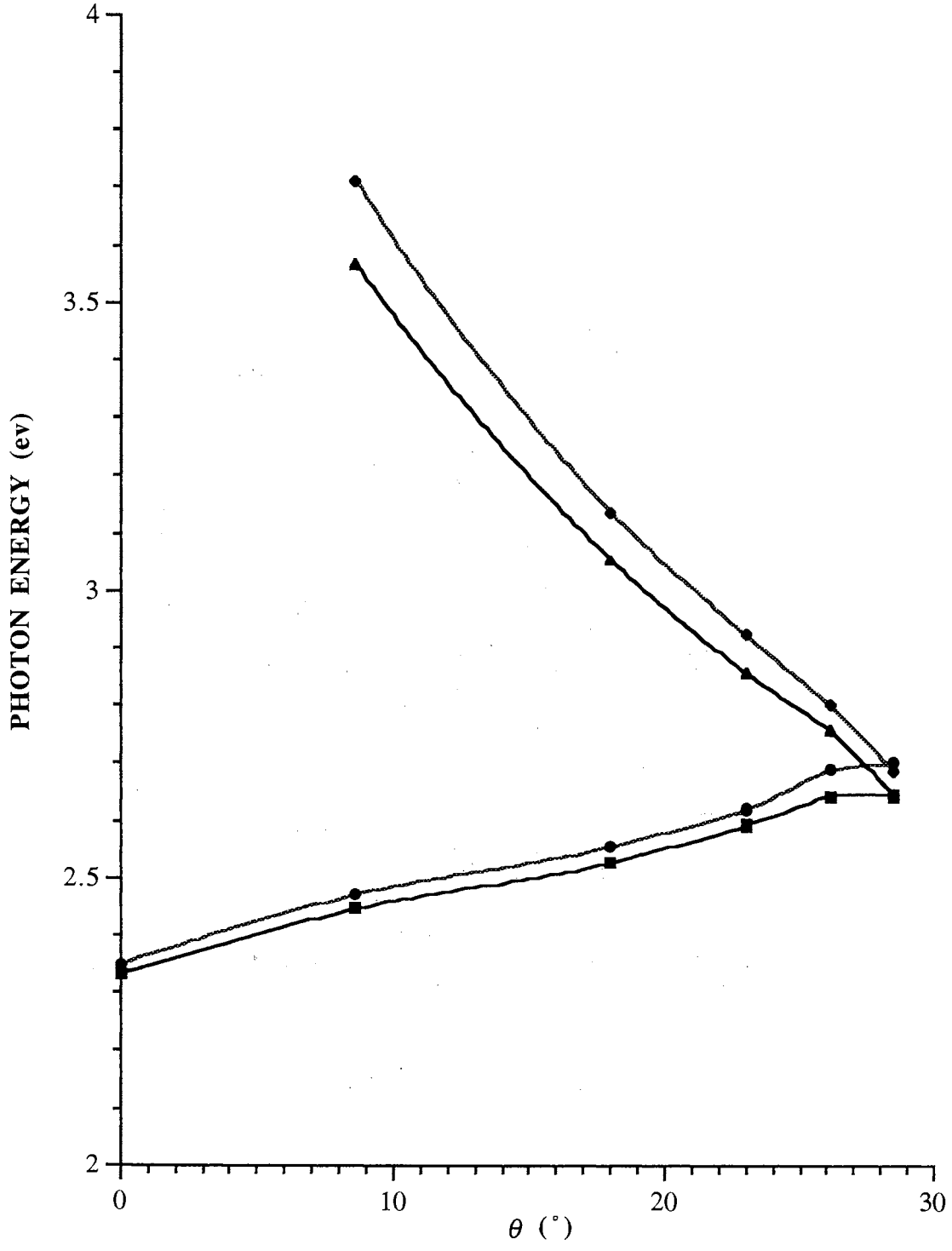

Figure 8. Plot of bandwidth photon energy (eV) at λ_{min} versus angle of the incident light θ (°) as shown in Figure 7. The parallel lines show the bandwidths of the photonic crystallites.

As the angle of the incident light is varied, the bandwidth for the first order diffraction increases while the bandwidth of the other diffraction peak decreases. These results have been previously observed with polystyrene latex in water.[41]

We have also ordered 332 nm TPM-silica in MMA, and Figure 9 shows the transmission spectrum of a 35 wt % silica in MMA dispersion. For the 35 wt % 332 nm TPM-silica, a 33 nm bandwidth of diffraction wavelength at 600 nm was observed.

PMMA COMPOSITE FILMS

When the MMA dispersions turned from cloudy to iridescent, indicating formation of colloidal crystals throughout the sample, we polymerized the 35 and 37.5 wt % TPM-silica particles in MMA dispersions containing 1 weight percent DMPA. The TPM groups on the silica copolymerize with monomer or comonomers as shown in Scheme 2. In order to achieve uniform irradiation in the entire thickness of the sample, we calculated the optimum amount of initiator concentration based on its extinction coefficient and the thickness of the sample by using the equation given by Bush et al:[42]

$$P = \frac{17.1\ M}{\varepsilon\ \rho\ m}$$

where P is the concentration of the initiator in weight percent, M is the molecular weight of the initiator, ρ is the density of the mixture in g mL^{-1} and m is the thickness of the dispersion in mils. (3.947×10^4 mils = 1 meter)

Figures 10 and 11 show transmission spectra of 35 and 37.5 wt % 152 nm TPM-silica in both MMA dispersions and PMMA composites. Table V shows comparison between the diffraction properties of the PMMA film and the 35 wt % 152 nm TPM-silica particles in MMA. The PMMA films show diffraction peaks between 490 and 486 nm with bandwidths ranging from 12 to 19 nm. The silica-PMMA film transmits 98, 88

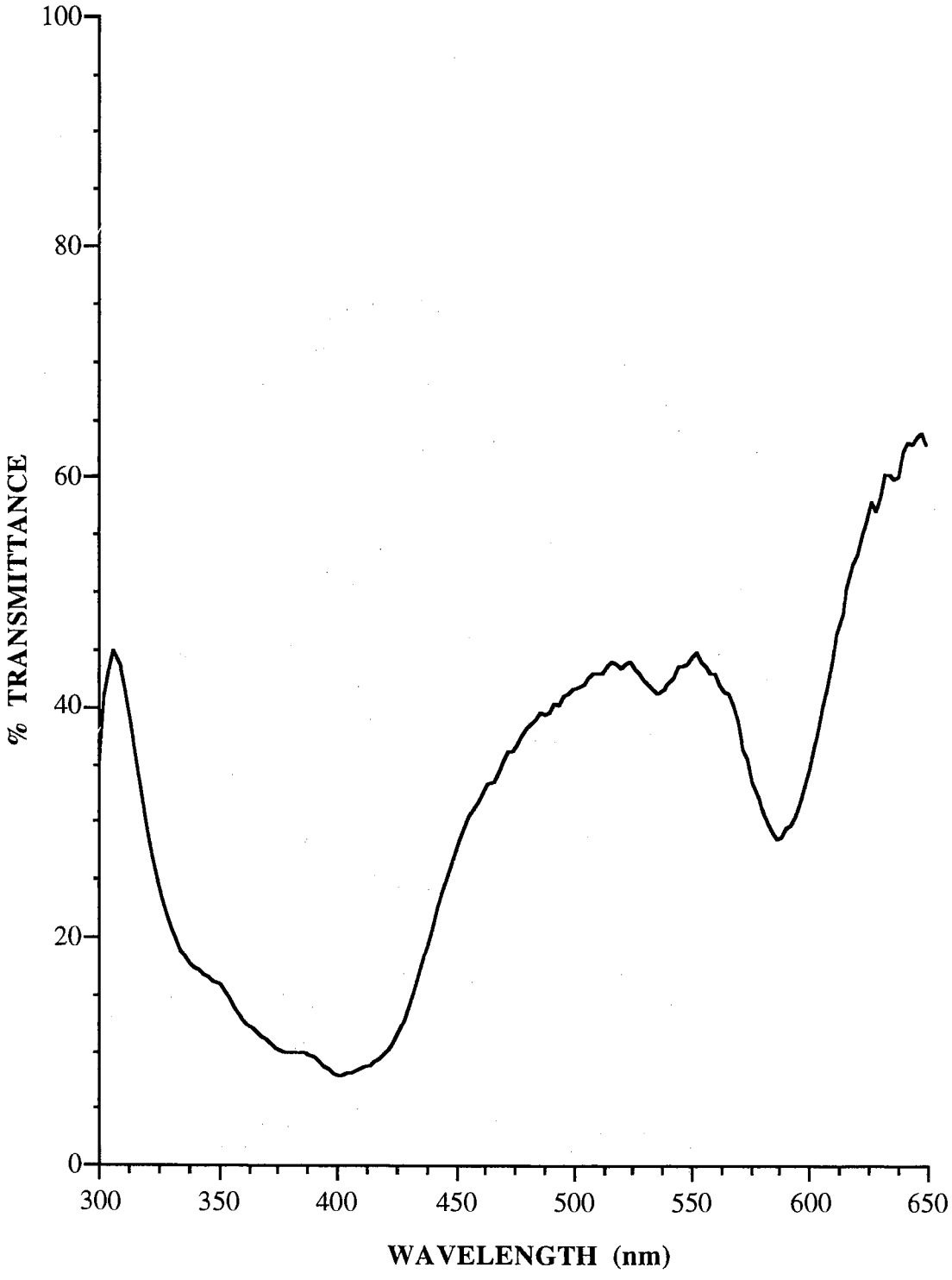

Figure 9. UV-visible transmission spectra of 35 wt % 332 nm TPM-silica in MMA.

and 65% of the incident light at 600, 520 and 400 nm, respectively. At Bragg's wavelength, which is at 490 nm, the film transmits only 45 % of the incident light.

Scheme 2. Synthesis of TPM-silica-PMMA Composite.

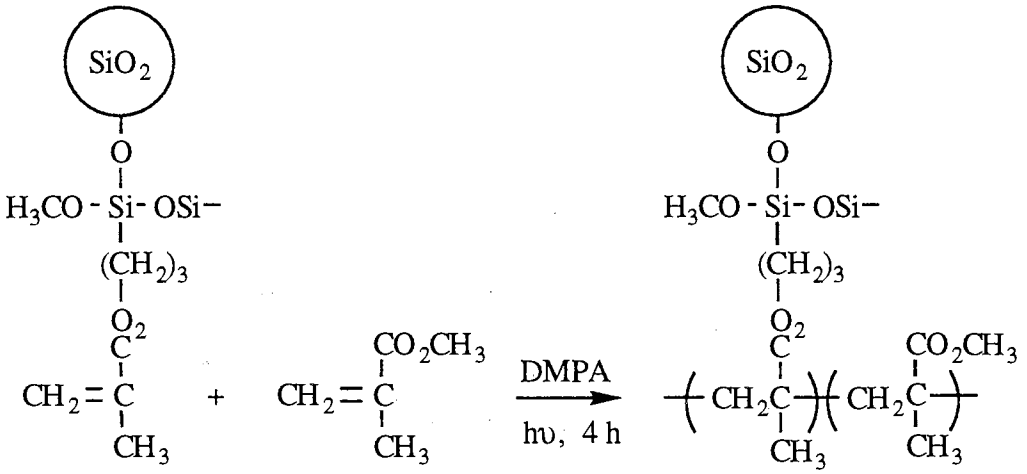

TPM-silica MMA TPM-silica-PMMA composite

Table V. Diffraction Properties of MMA Dispersions with PMMA films

	before polymerization		after polymerization		
wt %	λ_{min} (nm)	bandwidth (nm)	λ_{min} (nm)	bandwidth (nm)	decrease in d_{111} (%)[a]
0.195	554	4	490	12	15.2
0.209	536	4	486	19	13.0

[a] Calculated using Bragg equation (1).

No phase separation of the particles from the polymer was observed in the composites upon completion of the polymerization. The composite films thus formed are transparent and iridescent indicating that the particles are uniformly distributed in the polymer matrices. During photopolymerization, the order of the lattice planes of the crystals in the horizontal films was slightly disturbed as seen by the increase in the diffraction bandwidth from the composite film as compared to the liquid dispersion of same particle concentration.

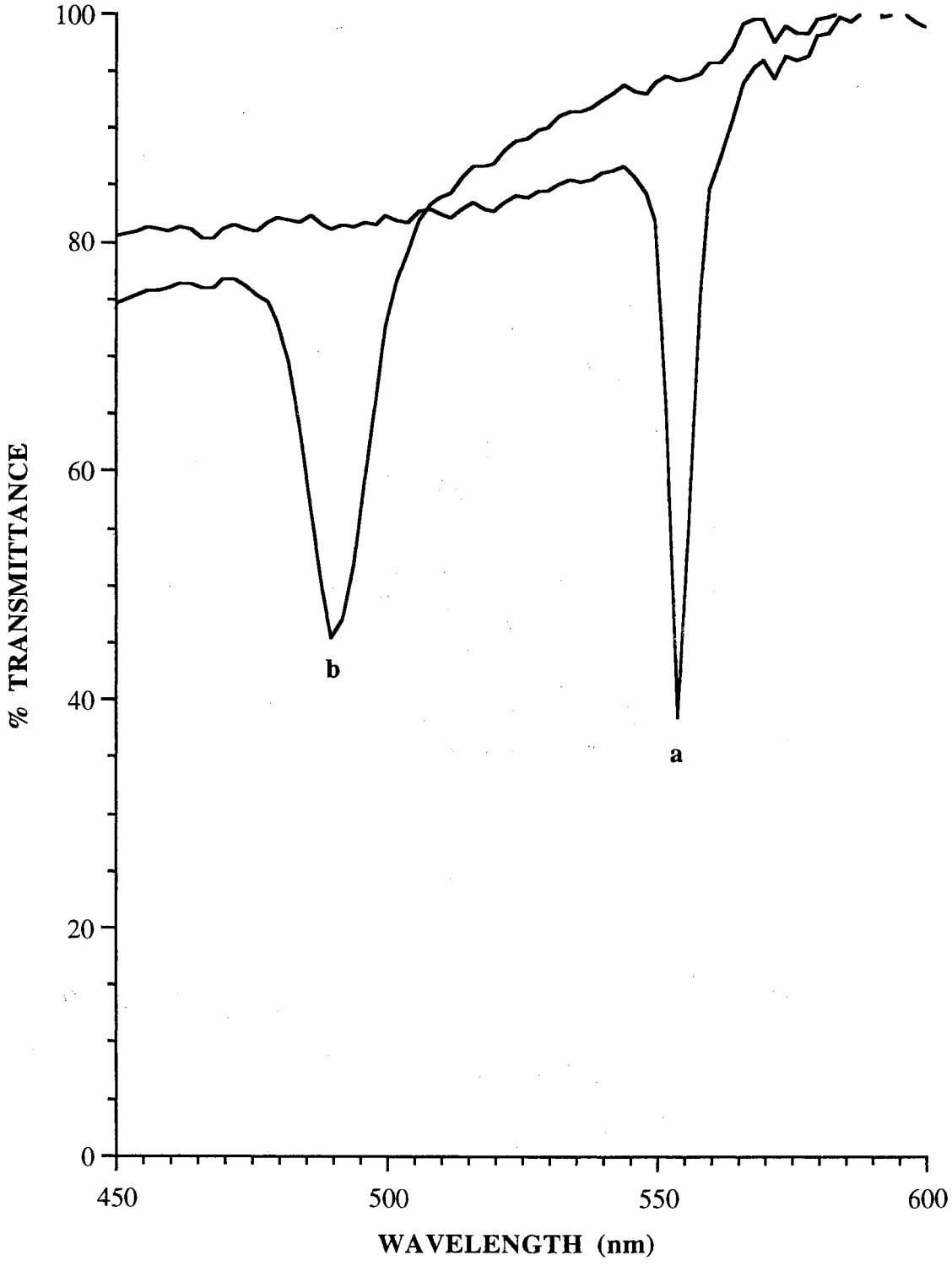

Figure 10. UV-visible transmission spectra of 35 wt % 152 nm TPM-silica (a) in MMA (b) in PMMA.

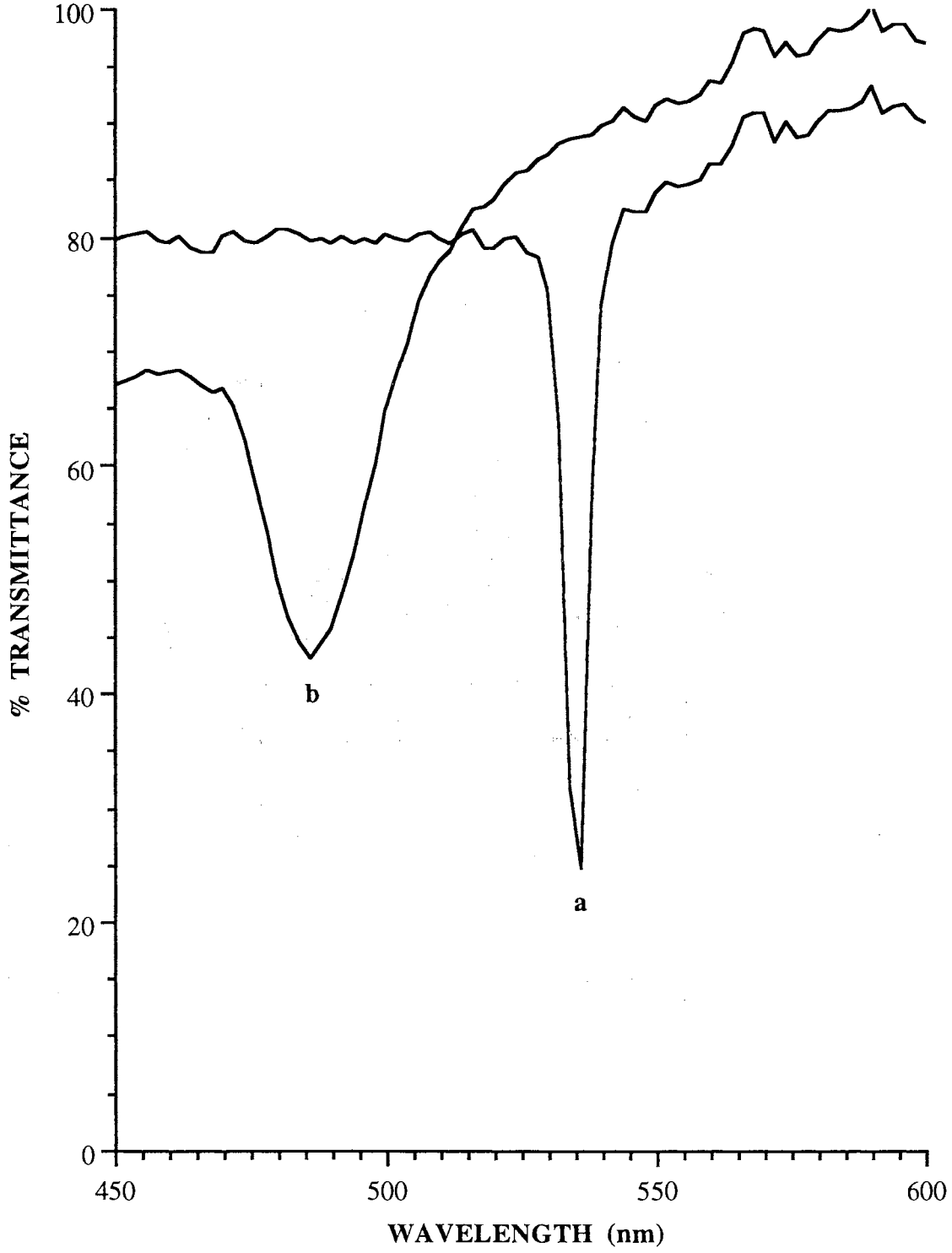

Figure 11. UV-visible transmission spectra of 37.5 wt % 152 nm TPM-silica (a) in MMA (b) in PMMA.

MORPHOLOGY OF THE CRYSTALLITES

The crystal growth and crystal orientation in MMA dispersions was observed via orthoscopic images between two crossed polarizers of a polarizing microscope. The 35-45 wt % solids dispersions of TPM-silica in MMA show a multi-colored mosaic of crystalline domains of dimensions 100 to 500 μm. In general, nucleation of colloidal crystals occurs both in bulk and on the surface of the glass cell. Heterogeneous nucleation occurs on glass surfaces and at cell edges where the dispersion is in contact with cured epoxy used to seal the cell while homogeneous nucleation occurs in the bulk of the dispersion. Heterogeneous nucleation leads to faster crystal growth at cell edges where large pillar shaped blue and green colored crystallites are observed as compared to the crystallites formed by homogeneous nucleation. The sizes of the crystallites in 264 μm thick cells vary with the particle concentrations in the MMA dispersions, and the crystals in the bulk grow large with progress of time. The orthoscopic images reveal crystallites having planes parallel to the plane of the glass throughout the bulk and at the cell edges filled with dispersions made of 37.5 and 40 wt % particle concentrations. The size of crystals decreases and the number of crystals increases with increasing wt % silica. Over a period of 1-7 days at 25 °C with the film plane horizontal, all dispersions in the cells fill with crystallites, and the dispersions turn from cloudy to iridescent. The crystals in bulk appear black (at extinction) when viewed under crossed polarizers as the lattice planes orient normal to the incident light. Upon tilting the cell to an angle of 40-55° between the film plane and the light,[43,44] crystals at extinction in bulk appear purple in color. Figures 12a and 12b show orthoscopic images of a 35 wt % TPM-silica in MMA dispersion at cell edge and in bulk at an angle between 40-55° to the incident light. Figure 13 shows a similar image in PMMA film at an angle between 40-55° to the incident light. In case of 332 nm TPM-silica particles, the crystallites are large and appear red colored with a few small crystallites that are yellow and green in color when the cells are rotated vertically between 40-55° to the incident light as shown in Figure 14.

Figure 12. Polarizing microscope images of a 35 wt % 152 nm TPM-silica at an angle between 40-55° to the incident light in MMA at (a) bulk and (b) cell edge.

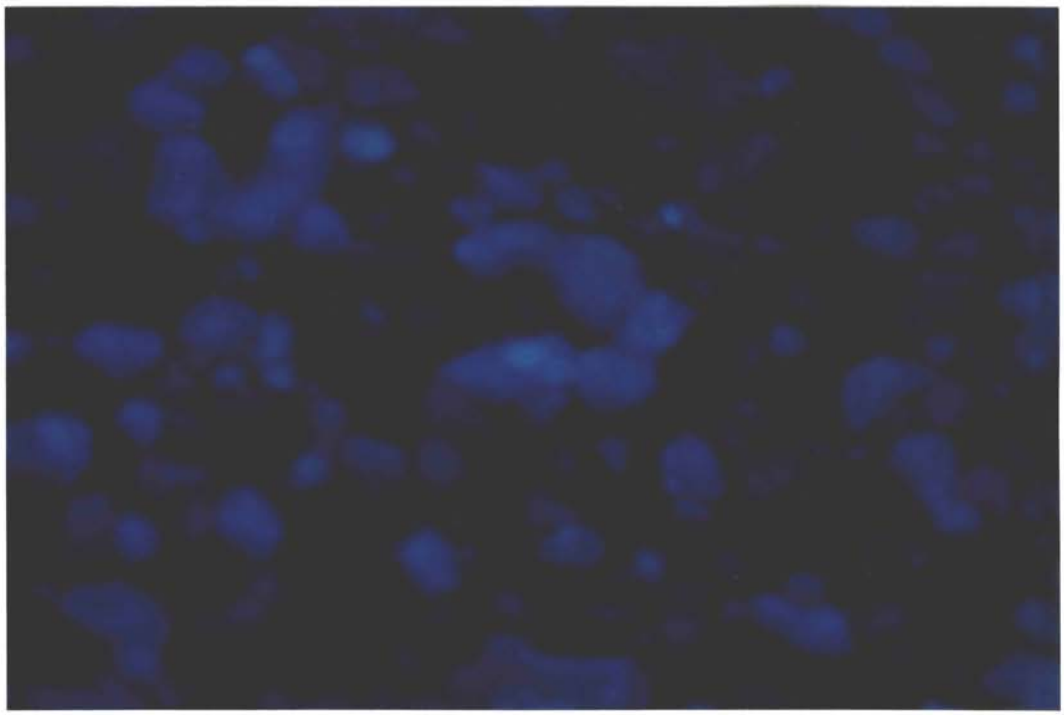

Figure 13. Polarizing microscope image of a 35 wt % 152 nm TPM-silica at an angle between 40-55° to the incident light in PMMA film.

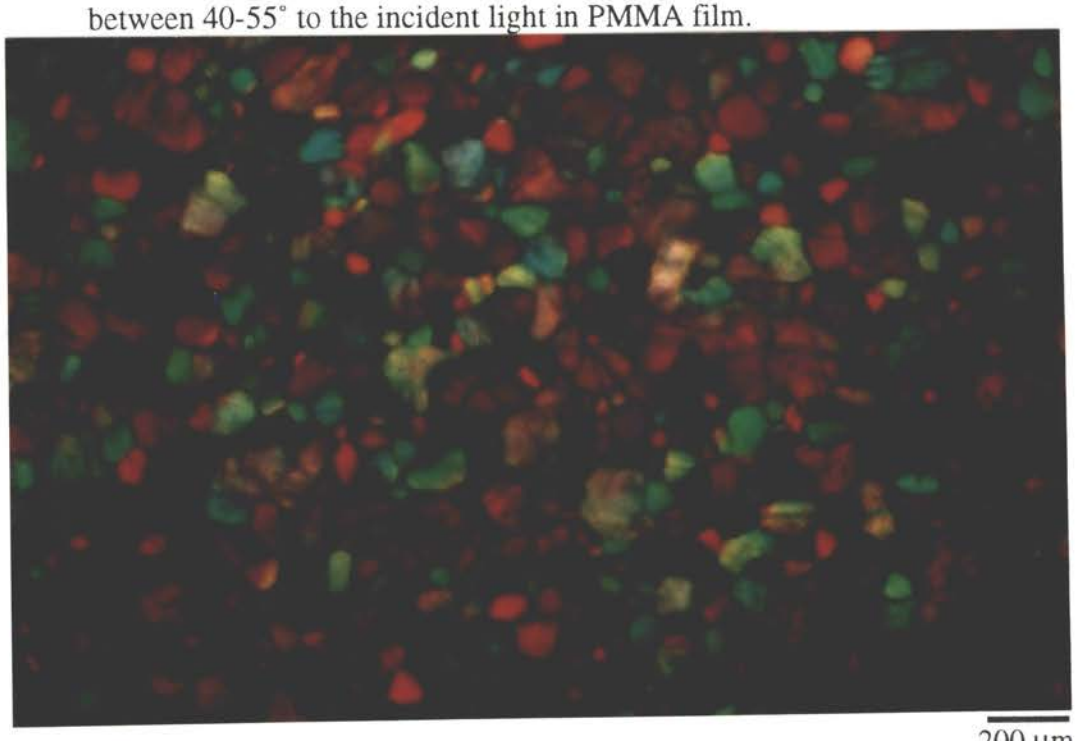

Figure 14. Polarizing microscope image of a 35 wt % 332 nm TPM-silica in MMA dispersion at an angle between 40-55° to the incident light.

When a glass cell containing TPM-silica in MMA dispersion was rotated about an axis parallel to the incident light normal to the plane of the cell, the crystallites not at extinction changed their intensity and color.[43,44] Figure 15a-d show the orthoscopic images of ordered 35 wt % 152 nm silica-MMA dispersion under two crossed polarizers of the polarizing microscope.

DISCUSSION

COLLOIDAL CRYSTALS IN MMA

The 152 nm diameter TPM-silica particles at concentrations between 35 and 45 weight percent in pure MMA spontaneously self assemble to form colloidal crystals. The electrostatic repulsive force arising from the dissociation of the surface hydroxyl groups is responsible for this phase transition. The surface coating of hydrophilic silica with TPM groups provides stability to the particles in MMA. Uncharged particles crystallize only when ϕ is at least 0.5 to 0.55. The close packing limit is at $\phi = 0.74$.[4] Therefore, our ϕ Ú 0.2 samples contain charged particles. The presence of acidic OH proves that these groups arise either from the parent silica or from hydrolysis of TPM or both.

The λ_{min} observed for the MMA dispersion shifts to longer wavelength as the weight percent of the particles decreases, which indicates the wavelength dependence on lattice spacings. Two different batches of TPM-silica particles of similar diameters when dispersed in MMA showed similar crystalline behavior and diffraction properties. In one batch, the TPM-silica particles were concentrated by sedimentation under gravitational force, and the other was concentrated by distilling out the solvent under reduced pressure. The 4 nm bandwidths of diffracted light from 264 μm cells are in excellent agreement with the calculated ($\Delta\lambda_o$) of 3.1 nm from dynamical diffraction theory.[45]

The structure of the colloidal crystals depends on surface charge, particle diameter, particle concentration, and the ionic strength of the medium. A variety of crystal morphologies, orientations and microstructures have been observed by different

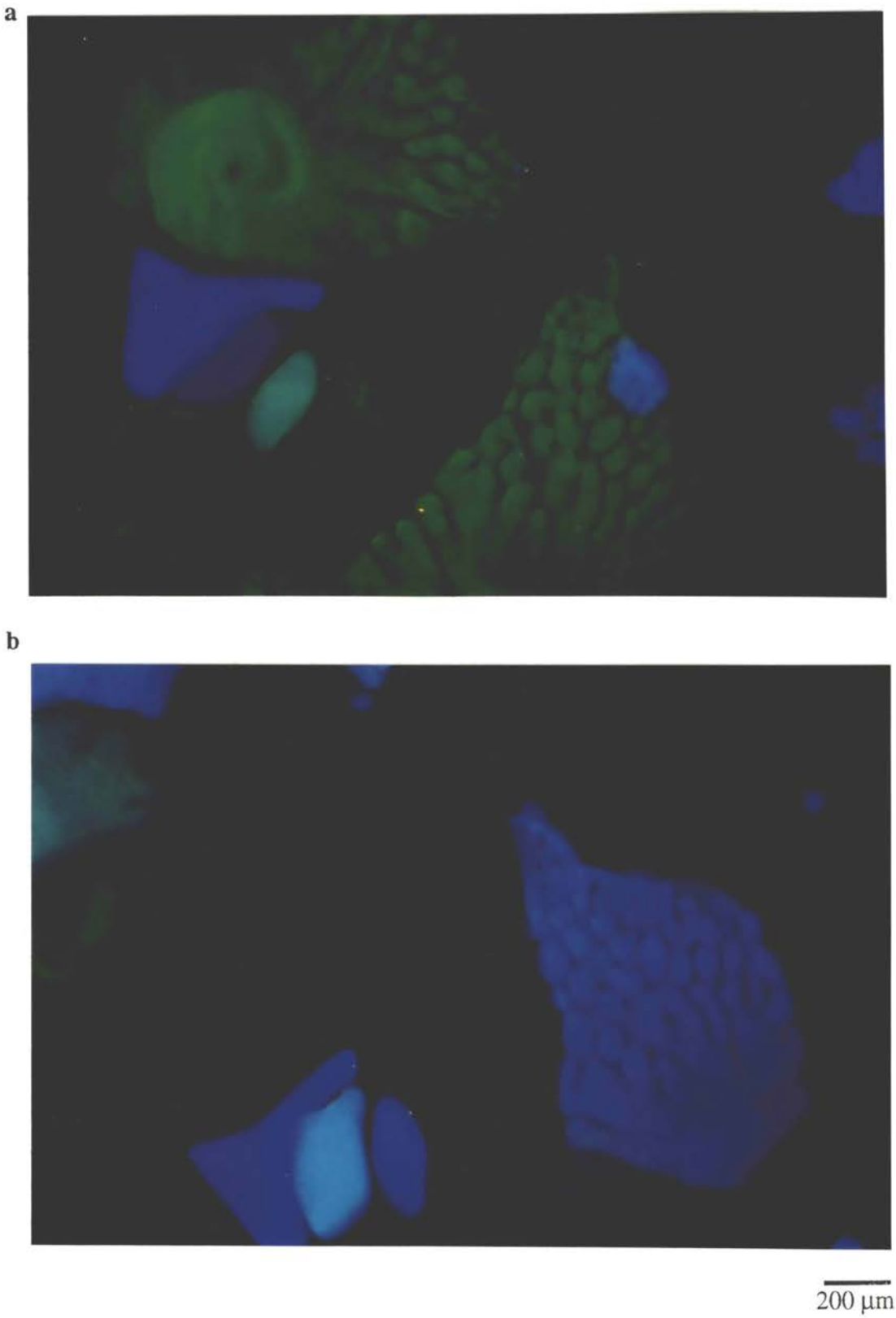

Figure 15. Polarizing microscope images of a 35 wt % 152 nm TPM-silica in MMA with incident light normal to the cell plane and at β-angle (a) 0, and (b) 30°.

Figure 15. Polarizing microscope images of a 35 wt % 152 nm TPM-silica in MMA with incident light normal to the cell plane and at β-angle (c) 60, and (d) 90°.

methods such as optical microscopy,[43,44] light scattering,[46] and electron microscopy.[47] Analysis of Kossel line patterns formed by scattering of light have revealed that highly charged particles at low concentration favor a bcc lattice, while less charged particles at high concentration favor a fcc lattice.[46] Moreover, it has been observed that light is diffracted from the d_{111} planes of fcc lattices and the d_{100} planes of bcc lattices oriented parallel to the surface of the glass cell. This also has been observed by optical microscopy where crystallites at extinction display brilliant colors when the incident light is not normal to the crystal planes.[43,44]

The formation of the colloidal crystals at different concentrations is also evident from via examination of material with polarizing microscopy and from iridescence observed directly. The most common structures for colloidal crystals of TPM-silica spheres in ethanol/toluene mixtures[8] are usually fcc, bcc, or a mixture of fcc and hcp structures. In the case of 160 nm diameter TPM-silica particles in ethanol/toluene mixtures, no crystallization was seen below $\phi = 0.194$ or above $\phi = 0.224$.[8] At $\phi = 0.197$ to 0.220, homogenous nucleation, and above $\phi = 0.220$, heterogeneous nucleation has been reported. In the case of silica in MMA, between 35 and 45 weight percent ($\phi =$ 0.195 and 0.225), the particles order into crystal lattices with the planes oriented parallel to the glass cell as evident from the polarizing microscopic images. As evident from Table III, the close agreement between the observed λ_{min} and the calculated λ_{min} using (a) Bragg equation (1) and (b) assumed diffraction from d_{111} planes of fcc lattice,[45] suggests that our TPM-silica particles in MMA dispersion order in a fcc lattice.

High degree of ordering of the crystallites, a smaller difference between the refractive indices of the particles and the monomer, and smaller particle diameters were found to narrow the bandwidth of the diffracted light from the dispersions. Using 332 nm TPM-silica particles in MMA in a 132 μm cell, we observed a 33 nm bandwidth of diffracted light, supports the effect of particle size. The degree of ordering of the

crystallites is reported also to depend on the cell thickness.[6,48] The thinner the sample cells, the greater the ordering of crystallites. We observe no significant differences in the bandwidths of spectral peaks between dispersions in 132 and 264 μm thick cells.

The blue shift of diffraction wavelength as a function of angle of incident light has been observed previously from polystyrene latex in water,[13,41] and from silica in MA dispersion and PMA composite films.[35] The blue shift is proportional to the *sin* θ function in the Bragg equation.

COLLOIDAL CRYSTAL IN PMMA COMPOSITES

Though the Bragg diffraction of visible light from the glassy film is evident from the transmission spectrum and from the polarizing microscope studies, there are marked differences between the colloidal dispersions and the composites. A blue shift in the rejection wavelength of the composite materials indicates that the colloidal crystals are compressed during photopolymerization. We have measured the dimensional changes that occur during polymerization and found that the thickness of the composite film was smaller compared to the length and width of the composite which remain unchanged.[35] The MMA diffuses into the epoxy used to seal the cell, and on polymerization, the PMMA adheres to the epoxy and not to the poly(dimethylsiloxane) coated glass cell. We have seen similar blue shifts on polymerization of a silica-MMA dispersion filled in an unsilylated glass cell. For a 35 weight percent silica in MMA, the expected 15.0 % decrease in volume only in the thickness of the composite on polymerization accounts for the 15.2 % decrease in *d*-spacing. The greater bandwidth of the diffraction peak of the composite film could be due to lower crystalline order of the particles in the polymer film than in the dispersion. Table VI shows the crystal parameters of TPM-silica in MMA dispersion and PMMA film, respectively.

The orthoscopic images of the polarizing microscope for the composite films show only a few colored crystallites and many at extinction, similar to that observed in the dispersions. No birefringence was observed from most of the film under two crossed polarizers when the incident plane polarized light was normal to the plane of the film which suggests presence of a single index of refraction in the polymer composite. When the composite films were rotated 40-55° to the incident light, the blue crystals throughout the film indicate that the order of the crystallites in the monomer was maintained and trapped in the solid matrix.

Table VI. Crystal Parameters of TPM-silica in MMA Dispersion and in PMMA Film[a]

	MMA		PMMA	
	I[b]	II[c]	I[d]	II[c]
volume fraction (ϕ)	0.195	0.195	0.2347	0.2347
suspension refractive index (n_s)	1.4192	1.4192	1.4804	1.4804
lattice parameter (a), nm	335.4	338.1	288.6	290.7
interplanar spacing (d_{111}), nm	193.6	195.2	164.6	165.5
Bragg diffracted wavelength (λ), nm	550.0	554.0	490.0	490.0
nearest neighboring spacing (D), nm	237.0	239.0	237.0	239.0
number of lattice planes	1363	1352	---	---
bandwidth, nm	3.1	3.4	3.7	11.6

[a] Most values are calculated from the equations in ref. 45 and ref. 10. [b] Calculated assuming diffraction from d_{111} planes of fcc lattice. [c] Calculated from transmission spectrum. [d] Calculated assuming a 15 % decrease in the thickness of the film.

CONCLUSIONS

Colloidal crystals of monodisperse TPM-silica grow in MMA dispersions at concentrations between 35 and 45 weight percent. Photopolymerization of the colloidal crystalline MMA dispersions yielded silica-PMMA composite films that Bragg diffract narrow bandwidths of visible light. The diffraction wavelength shifts to the blue by increasing the particle number. The characterization of the parent silica and the TPM-silica particles shows that the particles are coated with TPM coupling agent and that the particles are stable in MMA.

REFERENCES

1. Luck, W.; Klier, M.; Wesslau, H. *Ber. Bunsenges. Phys. Chem.* **1963**, *67*,75.
2. Hiltner, P. A.; Krieger, I. M. *J. Phys. Chem.* **1969**, *73*, 2386.
3. Okubo, T. Prog. *Polym. Sci.* **1993**, *18*, 481.
4. Pieranski, P. *Contemp. Phys.* **1983**, *24*, 25.
5. Hiltner, P. A.; Papir, Y. S.; Krieger, I. M. *J. Phys. Chem.* **1971**, *75*, 1881.
6. Philipse, A. P.; Vrij, A. *J. Coll. Interface Sci*. **1988**, *128*, 121.
7. Philipse, A. P.; Vrij, A. *J. Chem. Phys*. **1988**, *88*, 6459.
8. Dhont, J. K. G.; Smits, C.; Lekkerkerker, H. N. W. *J. Coll. Interface Sci.* **1992**, *152*, 386.
9. Ketelson, H. A.; Brook, M. A.; Pelton, R. H. *Polym. Adv. Tech.* **1995**, *6*, 335.
10. Sunkara H. B.; Jethmalani J. M.; Ford, W. T. *ACS Symp. Ser*. **1995**, *585*, 181.
11. Sunkara, H. B.; Jethmalani, J. M.; Ford, W. T. *Chem. Mater.* **1994**, *6*, 362.
12. Flaugh, P. L.; O'Donnell, S. E.; Asher, S. A. *Appl. Spectrosc*. **1984**, *38*, 848.
13. Asher, S. A.; Flaugh, P. L.; Washinger, G.; *Spectroscopy* **1986**, *1*, 26.
14. Gohrnan, P. A.; Bambakidis, G.; Spry, R. J.*A. Appl. Phys.* **1990**, *67*, 40.
15. Spry, R. J., U.S. Patent No. 4,986,635, 1991.
16. Asher, S. A., U.S. Patents Nos. 4,627,689 and 4,632,517, 1986.
17. Okubo, T. *Colloid Polym. Sci.* **1993**, *271*, 873.
18. Haacke, G.; Panzer, H. P.; Magliocco, L. G.; Asher, S. A. US Patent 5,266,238, 1993.
19. Asher, S. A.; Jagannathan S. US Patent 5,281,370, 1994.
20. Panzer, H. P., Giovanni, L.; Cohen, M. L.; Yen, W. S. US Patent 5,338,492, 1994.
21. Asher, S. A.; Holtz, J.; Liu, L.; Wu, Z. *J. Am. Chem. Soc.* **1994**, *116*, 4997.
22. Barbin, W. W.; Rodgers, M. B. In "Science and Technology of Rubber", Eds. Mark, J. E.; Erman, B.; Eirich, F. R. Academic Press: San Diego, CA, 1994, pp. 419-468.
23. Iler, R. K. *The Chemistry of Silica*; Wiley; New York, 1979; pp. 582-588.

24. Sanchez, C.; Ribot, F. *New J. Chem.* **1994**, *18*, 1007.

25. Mark, J. E.; Lee, C. Y.-C.; Biancone, P. A., Eds. *Hybrid Organic-Inorganic Composites*; ACS Symposium Series 585; American Chemical Society; Washington, DC, 1995.

26. Landry, C. J. T.; Coltrain, B. K.; Brady, B. K. *Polymer* **1992**, *33*, 1486.

27. Pope, E. J. A.; Asami, M.; Mackenzie, J. D. *J. Mater. Res.* **1989**, *4*, 1018.

28. Lin, H.; Day, D. E.; Stoffer, J.O. *Polym. Eng. Sci.* **1992**, *32*, 344.

29. Abramoff, B.; Covino, J; *J. Appl. Polym. Sci.* **1992**, *46*, 1785.

30. Nishiyama, N.; Horie, K.; Schick, R.; Ishida, H. *Polym. Commun.* **1990**, *31*, 380.

31. Nishiyama, N.; Ishizaki, T.; Horie, K.; Tomari, M.; Someya, M. *J. Biomed. Mater. Res.*, **1991**, *25*, 213.

32. Morikawa, A.; Yamaguchi, H.; Kakimoto, M.; Imai, Y. *Chem. Mater.* **1994**, *6*, 913.

33. Wang, S.; Ahmad, Z.; Mark, J. E. *Chem. Mater.* **1994**, *6*, 943.

34. Nishiyama, N.; Komatsu, K.; Fukai, K.; Nemoto, K.; Kumagai, M. *Composites*, **1995**, *26*, 309.

35. Jethmalani, J. M.; Ford, W. T. *Chem. Mater.* **1996**, *00*, 000.

36. Stober, W.; Fink, A.; Bohn, E. *J. Colloid Interface Sci*. **1968**, *26*, 62.

37. Badley, R. D.; Ford, W. T.; McEnroe, F. J.; Assink, R. A. *Langmuir*, **1990**, *6*, 792.

38. Okubo, T. *Langmuir* **1994**, *10*, 1695.

39. Okubo, T. *J. Chem. Phys.* **1987**, *87*, 6733.

40. Joseph, R.; Zhang, S.; Ford, W. T. *Macromolecules* **1996**, *29*, 1305.

41. Tarhan, I. I.; Watson, G. H. *Phys. Rev. Lett*. **1996**, *76*, 315.

42. Busch, R. W.; Ketley, A. D.; Morgan, C. R.; Whitt, D. G. *J. Radiat. Curing* **1980**, *7*, 20.

43. Monovoukas, Y.; Gast, A. P. *Phase Transitions* **1990**, 21.

44. Monovoukas, Y.; Gast, A. P. *Langmuir* **1991**, *7*, 460.

45. Spry, R. J.; Kosan, D. J. *Appl. Spectrosc*. **1986**, *40*, 782.

46. Clark, N. A.; Hurd, A. J.; Ackerson, B. J. *Nature* **1979**, *281*, 57.

47. Cohen, J. A.; Scales, D. J.; Ou-Yang, H. D.; Chaikin, P. M. *J. Coll. Interface Sci.* **1993**, *156*, 137.

48. Van Winkle, D. H.; Murray, C. A. *Phys. Rev.* **1986**, *34*, 562.

CHAPTER IV

TUNING THE DIFFRACTION OF VISIBLE LIGHT BY ORDERED SILICA-POLY(METHYL ACRYLATE) COMPOSITE FILMS

ABSTRACT

Composites of ordered colloidal crystals of amorphous monodisperse silica particles in amorphous poly(methyl acrylate) (PMA) films selectively Bragg diffract visible light. The 153 nm diameter colloidal silica particles are coated with 3-(trimethoxysilyl)propyl methacrylate (TPM) and ordered into colloidal crystals in methyl acrylate (MA) monomer, and the crystal order is locked into place by polymerization of the MA. Bragg diffraction from the films is detected spectrophotometrically as narrow peaks of low % transmission of visible light normal to the film plane. The diffraction wavelength is tuned by varying the d_{111}-spacing of the crystal lattice and by varying the Bragg angle. The variation in the lattice spacing is achieved by varying the particle size or particle concentration, by uniaxial stretching of the composite, and by swelling the composite with monomers such as styrene or methyl acrylate (MA) followed by photopolymerization of the imbibed monomers. As the particle concentration is increased from 35 to 45 weight percent, the ordered crystalline arrays of TPM-silica in MA dispersions show narrow diffraction peaks from 582 to 528 nm. After photopolymerization, the diffraction peaks are from 502 to 466 nm. Uniaxial stretching of the composite films shifts the peaks to 448-434 nm, swelling with MA or styrene red shifts them to 652-740 nm, and further photopolymerization of imbibed monomer, again blue shifts them to 550-632 nm.

INTRODUCTION

Silica-polymer composites often have improved optical, mechanical and thermal properties relative to the unfilled polymer.[1-5] In all previous composites, the silica is present as randomly distributed colloidal silica or silica fiber. The colloidal silica may be pre-formed or prepared *in situ* by either basic or acidic hydrolysis and condensation of tetraethyl orthosilicate (TEOS) or tetramethyl orthosilicate (TMOS).[1-5] Previously, we have ordered monodisperse amorphous colloidal silica in poly(methyl methacrylate) (PMMA) films.[6,7]

Monodisperse charged colloidal particles in aqueous and non-aqueous dispersions can self assemble into a three dimensional lattice known as a colloidal crystal. Several factors govern the formation, ordering and orientation of colloidal crystals, such as the size, surface charge, and concentration of particles, and the ionic strength of the medium.[6-15] With high particle volume fractions and low surface charges, face centered cubic (fcc) crystals form, while with low particle volume fractions and high surface charges, body centered cubic (bcc) crystals form.[6-9] Since the lattice spacings of these crystals usually exceed 100 nm, the dispersions efficiently Bragg diffract visible light.[6-26] Consequently, colloidal crystalline materials may be used in optical devices such as rejection filters, limiters and switches.[17-26] Our silica-polymer composite films are more robust than any previous colloidal crystalline materials. Ordered silica-PMMA films are thermoplastic like the parent polymer, and the narrow diffraction peaks in spectra of the films are retained even after heating to 150 °C.[6,7] The aim of the research reported here is to create films that will allow tuning of the diffraction wavelength by stretching and swelling.

Diffraction wavelengths from liquid colloidal dispersions have been tuned by varying the particle size,[12-15] particle concentration,[12-16] and Bragg angle.[17-21] A gradient of particle concentration, and consequently of diffraction wavelength, can be

created by particle sedimentation.[27-30] The diffraction wavelengths of hydrogels containing colloidal crystals of polystyrene latexes have been tuned by applying mechanical stress.[31-33] Here we show that diffraction wavelength decreases by photopolymerizing silica-MA (methyl acrylate) dispersions into polymer composites, and by uniaxially stretching the silica-PMA composites, and that the wavelength increases by swelling the silica-PMA composites with monomers.

RESULTS

BLUE SHIFT BY PARTICLE CONCENTRATION

Colloidal Crystals in MA. The colloidal silica was made by base hydrolysis and condensation of TEOS according to Stöber method.[6,7,34-36] The colloidal silica particles were then modified with 3-(trimethoxysilyl)propyl methacrylate (TPM) according to the method described by Philipse and Vrij as shown in Scheme 1.[6,7,37] The diameter of TPM-silica particles measured by TEM was found to be 153 nm with a polydispersity index (standard deviation to mean of 0.07) and 171 nm by dynamic light scattering (DLS).[38-42]

Scheme 1. Synthesis of TPM-silica Particles

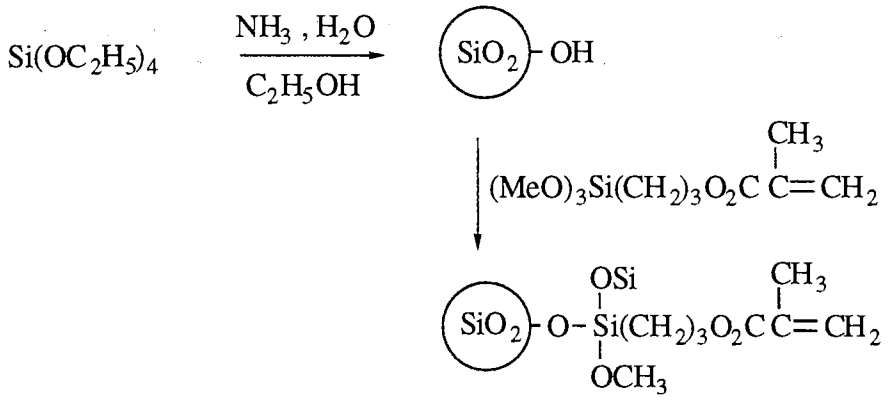

TPM-silica

The particle concentrations of 35, 40 and 45 wt% 153 nm TPM-silica in methyl acrylate (MA) dispersions diluted from 48 wt% concentrated dispersions were filled in silanized sandwiched glass cells and placed horizontally in an oven maintained at 25°C for nucleation and growth of the colloidal crystals. As these crystals have weak inter-particle interactions, the cells were handled carefully to minimize any external forces such as shear, thermal or electrical,[1-5,21,37] that could cause disruption during the nucleation and crystal growth. Iridescence from colloidal crystals at 35, 40 and 45 wt% TPM-silica in MA was observed within couple of minutes after filling 264 μm thickness cells.

As the structures of colloidal crystals of both polystyrene latexes in water[21,16-20] and silica spheres in ethanol/toluene mixtures[9] have been either bcc or fcc, or a mixture of fcc and hcp. Since only fcc has been observed by light scattering[8] and metallurgic microscopy[27-30] at high particle concentration and low surface charge, we believe that our TPM-silica particles at high particle concentrations and low surface charges may also order in to a fcc lattice in MA dispersions. The diffraction properties from the silica in MA dispersions are similar to that observed from silica in methyl methacrylate (MMA) dispersions and silica-PMMA composites.[6,7]

Figure 1 shows UV-visible transmission spectra from 35, 40 and 45 wt% 153 nm TPM-silica in MA dispersions, while Table I gives a comparison between the diffraction properties calculated using above equations from the MA dispersions and PMA composites. After a period of 6-8 hours, all MA dispersions showed narrow diffraction peaks (λ_{min}) between 582-528 nm based on particle concentrations. The d_{111}-spacing calculated from transmission spectra using the theory of Bragg diffraction[6,7,17-19] are given in Table II. The entire 20 x 70 mm cell, i.e., from top to bottom region and from one cell edge to the other showed diffraction wavelengths at the same λ_{min} at a given particle concentration using a 9 mm circular spectrophotometer beam profile.

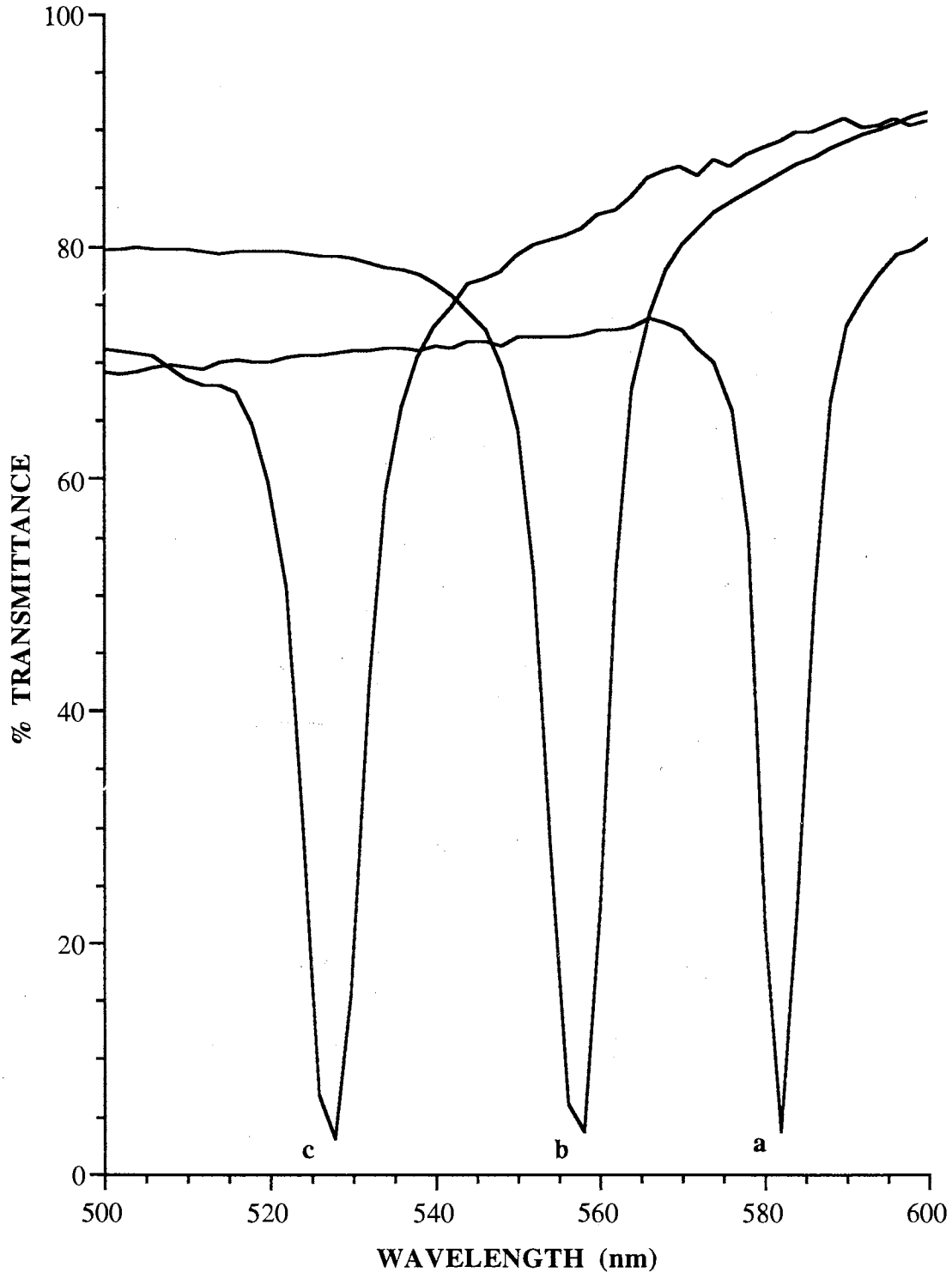

Figure 1. Transmission spectra of 153 nm TPM-silica particles in MA: (a) 35 wt%, (b) 40 wt% and (c) 45 wt%. Cell thickness = 264 μm.

Table I. Transmission of 153 nm TPM-silica in MA Dispersions and PMA Films

	before polymerization		after polymerization	
weight percent	λ_{min} (nm)	bandwidth[a] (nm)	λ_{min} (nm)	bandwidth[a] (nm)
35	582	4.2	502	14.7
40	556	6.2	482	12.8
45	528	5.8	466	13.5

[a] The bandwidths were measured at the half peak height.

Table II. Properties of MA Dispersions and PMA Composites

	MA dispersion			PMA composite			
weight percent	n_s	obsd d_{111}[a] (nm)	calcd d_{111}[b] (nm)	n_s	obsd d_{111}[a] (nm)	calcd d_{111}[c] (nm)	decrease in d_{111} (%)
35	1.4112	206.2	194.9	1.4721	170.5	170.5	17.3
40	1.4125	196.8	186.3	1.4712	163.8	163.7	16.8
45	1.4142	186.7	177.5	1.4700	158.5	156.8	16.0

[a] From Bragg equation, $\lambda = 2n_s d \sin\theta$, where n_s is the suspension refractive index. [b] From eq. (3) in ref. (7). [c] Based on monomer shrinkage during polymerization.

For example, 35 wt% silica MA dispersion filled in a 264 μm thick glass cell shows λ_{min} between 580-582 nm at cell edges, top, center and bottom regions of the cell. During the same period, the intensity of diffraction wavelengths were found to increase while the bandwidths measured at half height decreased as observed by UV-visible spectrophotometry.[3,10,11,26] The bandwidths measured at half-height were between 4.5-6.0 nm for 35-45 wt% TPM-silica in MA dispersions. These values are in slightly larger than the theoretically calculated values of 3.0-4.0 nm from eq. (15) in ref. (18).

We have also observed the growth of colloidal crystals by polarizing microscopy. The orthoscopic images between crossed polarizers showed many crystallites at extinction (no transmitted light), with d_{111} planes of fcc crystal parallel to the plane of the glass, only when incident light was normal to the crystal planes.[6,7,16-19,43] Upon rotation of the cells by an angle of 40-55° away from the incident light, brilliant blue and green colored crystallites of dimensions 50-200 μm were observed throughout the cell. The sizes of the colloidal crystallites were found to be smaller in case of 45 wt% dispersions as compared to 35 wt% dispersions.

We have also been able to order 142 nm and 330 nm TPM-silica particles in MA dispersions. A 40 wt% 142 nm TPM-silica MA dispersion shows narrow diffraction at 490 nm while a 40 wt% 330 nm TPM-silica MA dispersion shows a broad diffraction at 600 nm. Increasing the particle size leads to greater scattering of light with broad Bragg diffraction as compared to smaller sized particles which has also been previously observed in case of polystyrene spheres in water.[17-19]

Colloidal Crystals in PMA Composite. After a period of 6-8 hours, all MA dispersions containing 0.2 wt % photoinitiator (DMPA) to the monomer were photopolymerized using a medium pressure Hg-arc lamp to form the silica-PMA composite.[6,7] Copolymerization of the TPM groups on silica and the MA yields the composite as shown in Scheme 2. We have accomplished photopolymerization of a 35 wt% TPM-silica in MA dispersions with 0.05, 0.2, 1.0, and 5.0 wt% of DMPA and Figure 2 shows transmission spectra of silica-PMA composite formed by photopolymerization using 0.05-5.0 wt% DMPA. No change in the λ_{min} occurs at different initiator concentrations from the MA dispersions. The diffraction properties were found to be better in case of the composites made by photopolymerization of MA dispersions with 0.05 and 0.2 wt% DMPA as compared to that made with 1.0 or 5.0 wt%

DMPA. At 0.05 wt%, there were many ripples in the film, so we have used 0.2 wt% DMPA.

Scheme 2. Synthesis of TPM-silica-PMA Composite

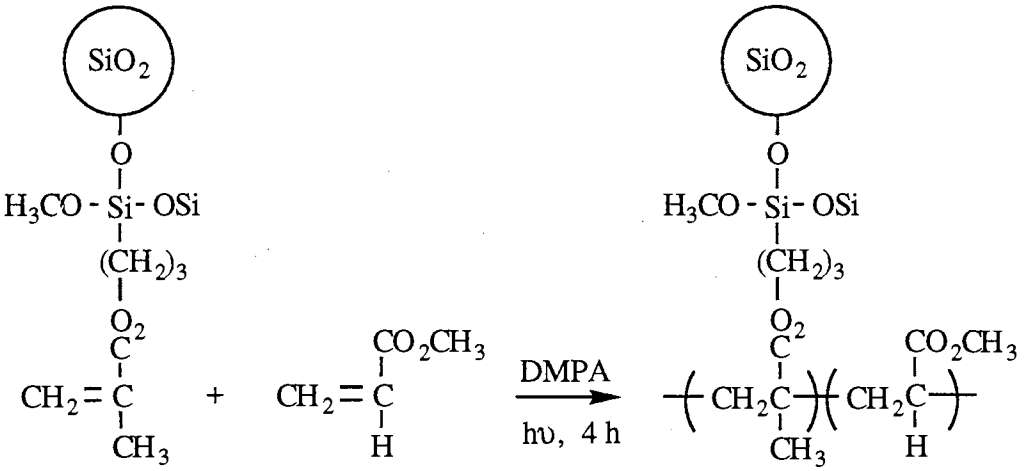

TPM-silica MA TPM-silica-PMA composite

Figure 3 shows the transmission spectra from 35, 40 and 45 wt% TPM-silica in PMA composite films, while Table I shows the diffraction properties from silica-PMA composites. On photopolymerization, the diffraction properties of PMA composites differ from MA dispersions in the manner that (a) λ_{min} values were blue shifted, (b) bandwidths measured at half-heights were weak and broad, and (c) λ_{min} values varied from one region to other at any given particle concentration. The typical half height bandwidths varied from 8.0-25.0 nm while the λ_{min} values varied by 10-20 nm between different regions of one sample. Narrow bandwidths of 8.0 to 12.0 nm were observed only from ordered and oriented crystals trapped in the polymer matrices. The bandwidths measured at half-heights usually observed form a solidified matrix containing the colloidal crystals range between 15 to 30 nm.[27-33] We have thus achieved a composite with a much narrower %T bandwidth of diffraction than polystyrene latexes in polyacrylamide gels.[31-33]

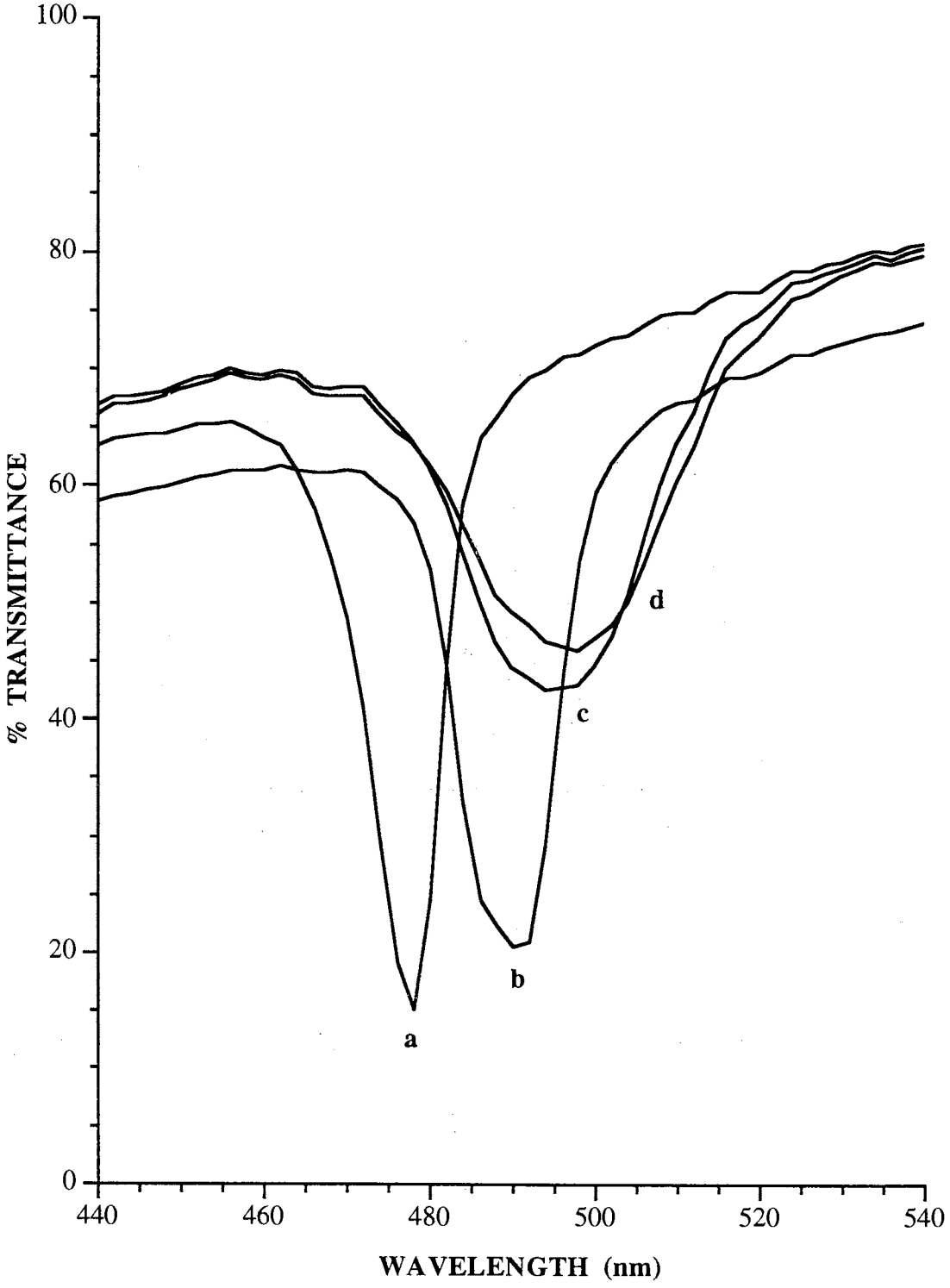

Figure 2. Transmission spectra of 35 wt % 153 nm TPM-silica particles in PMA: (a) 0.05, (b) 0.2, (c) 1.0, and (d) 5.0 wt % photoinitiator. Cell thickness = 264 μm.

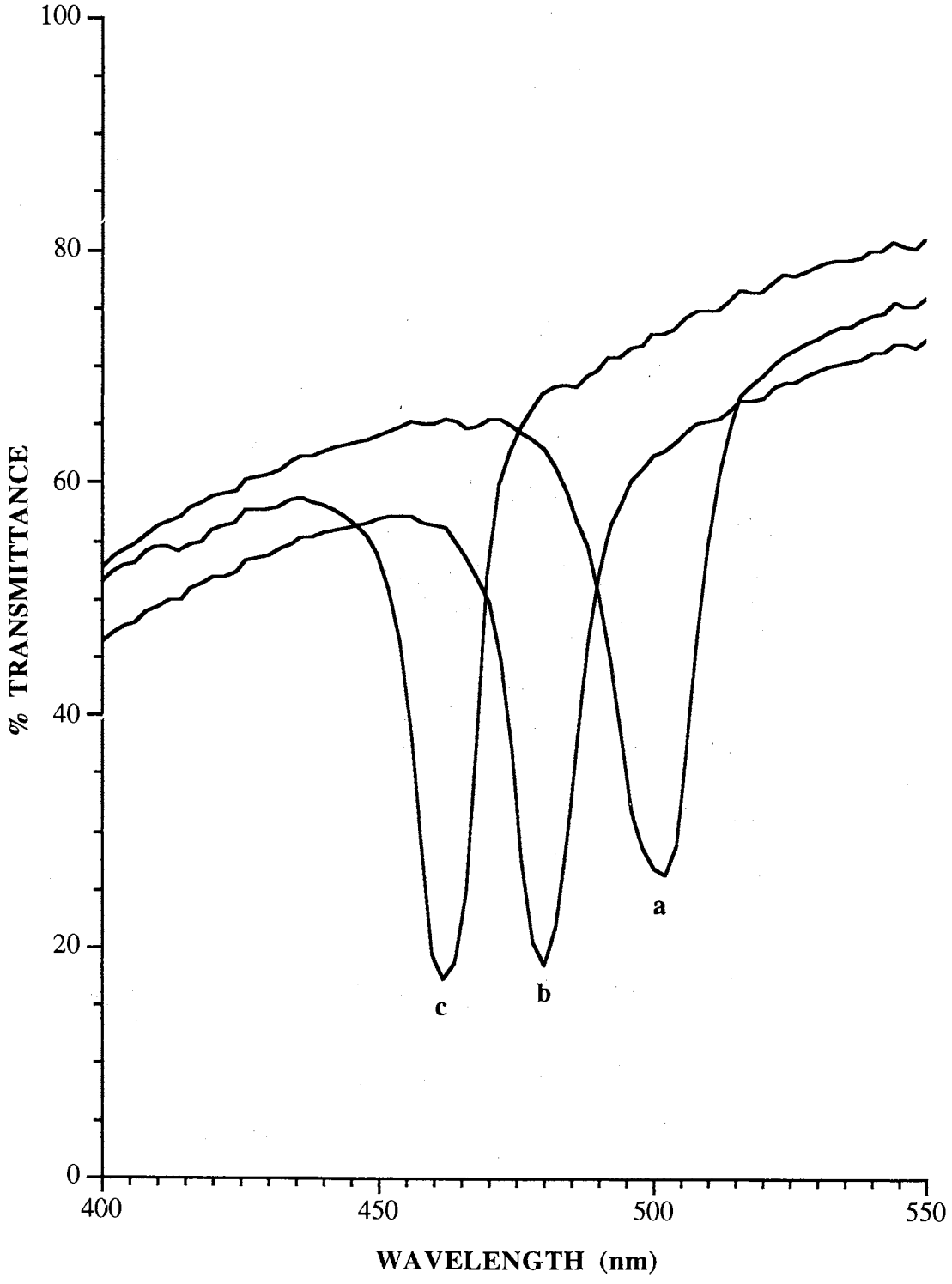

Figure 3. Transmission spectra of 153 nm TPM-silica particles in PMA: (a) 35 wt%, (b) 40 wt% and (c) 45 wt%. Cell thickness = 264 μm.

BLUE SHIFT BY STRETCHING THE ELASTOMERIC COMPOSITE FILM

The diffraction wavelength as observed by UV-visible spectrophotometry was tuned by uniaxially stretching 35, 40 and 45 wt% TPM-silica-PMA composites. Figure 4 shows the effect of stretching on the transmission spectra of 40 wt% TPM-silica PMA composite.

Table III shows the stretch ratio, diffraction wavelengths (λ_{min}) observed at different stretched lengths, difference between two consecutive diffraction wavelengths ($\Delta\lambda$), and bandwidths measured at half-height from a 40 wt% TPM-silica PMA composite film. As a film of original length L_o = 1.00 cm was stretched to L = 1.35 cm, the λ_{min} blue shifted from 486 nm to 440 nm. Beyond the length of 1.35 cm, the spectral peak became much weaker and broader as compared to the unstretched film.

Figure 5 shows a double Y-plot of λ_{min} and bandwidths measured at half-height versus the stretch ratio (L/L_o) for a 40 wt% TPM-silica-PMA composite. Similar trends in the diffraction properties were observed from 35 and 45 wt% TPM-silica-PMA composite films. The blue shift of the diffraction wavelengths as a function of uniaxial stretching was also observed from 35 and 45 wt% TPM-silica-PMA composite films. The λ_{min} in these two cases was found to blue shift from 502 nm to 448 nm for 35 wt% and 466 nm to 434 nm for 45 wt% silica-PMA composites at L/L_o = 1.35 as shown in Figures 6 and 7. All the composite films retracted to their original lengths after releasing the applied stress in 2-4 hours and showed diffraction peaks at λ_{min} within 2-4 nm of that observed from the unstretched films. The same composites on further stretching were found to show similar trends in the blue shift of diffraction wavelengths. Repeated stretching eventually broke the films. Tuning of Bragg diffraction in case of polystyrene particles in hydrogels only showed broad diffraction when subjected to strain.[31-33] These results show great promise towards making of tunable filters of visible light with narrow bandwidths of diffraction wavelengths.

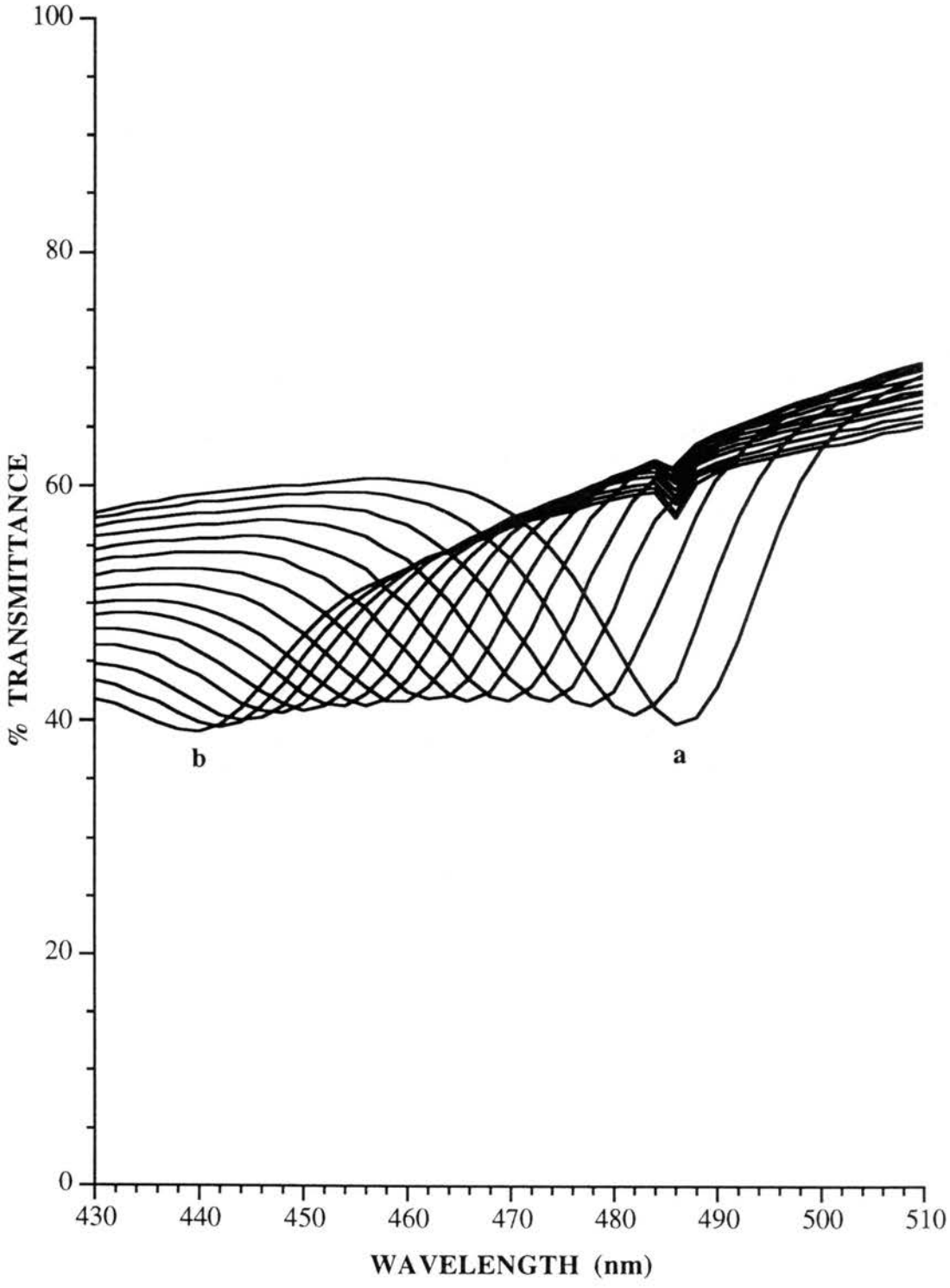

Figure 4. Transmission spectra of 153 nm TPM-silica in PMA (a) before and (b) after uniaxial stretching to $L/L_o = 1.35$. Intermediate spectra are from the film at $1 < L/L_o < 1.35$. The initially 228 μm thick film contained 40 wt% TPM-silica.

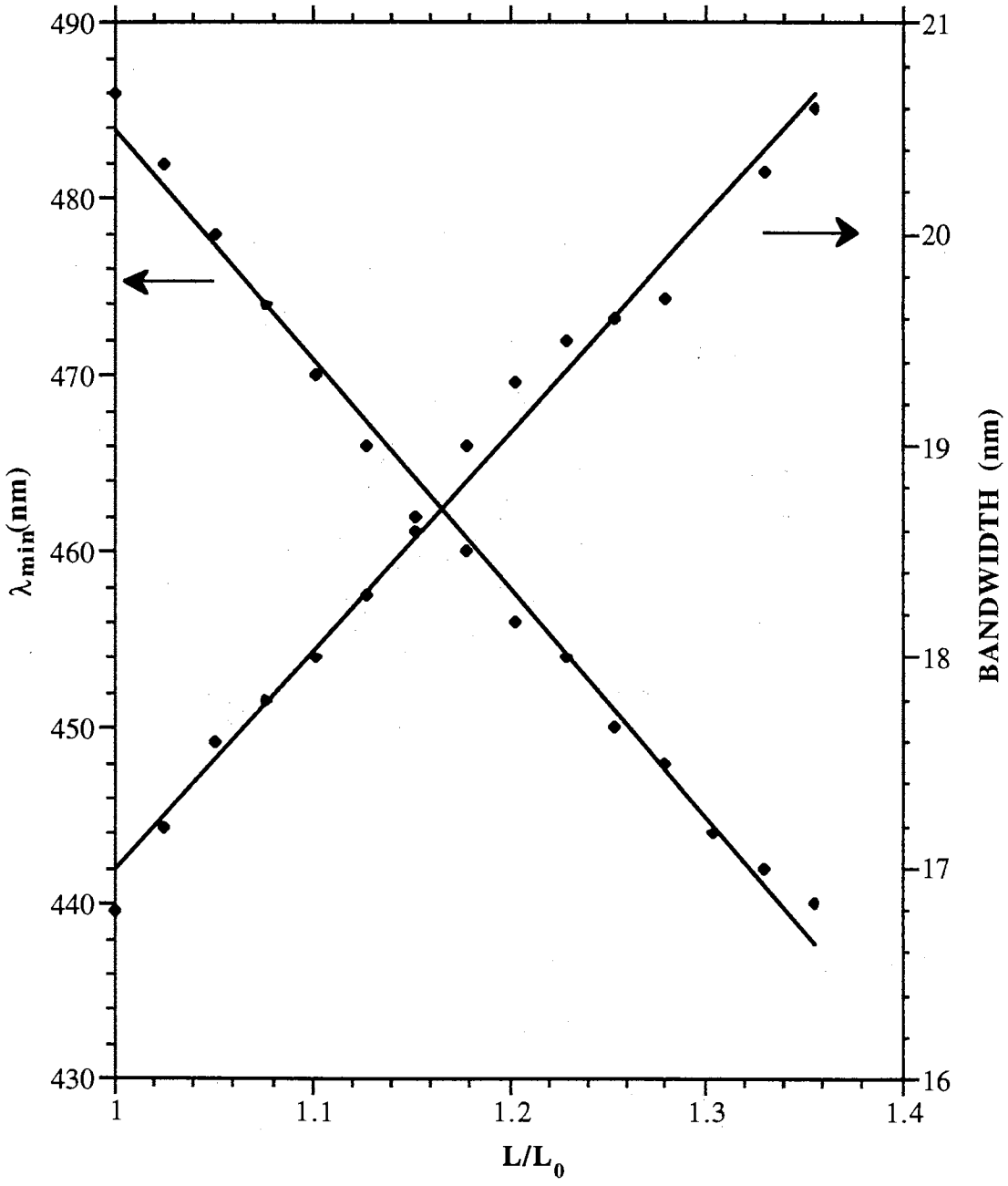

Figure 5. λ_{min} (nm) and bandwidth (nm) versus strain from spectra of Figure 4.

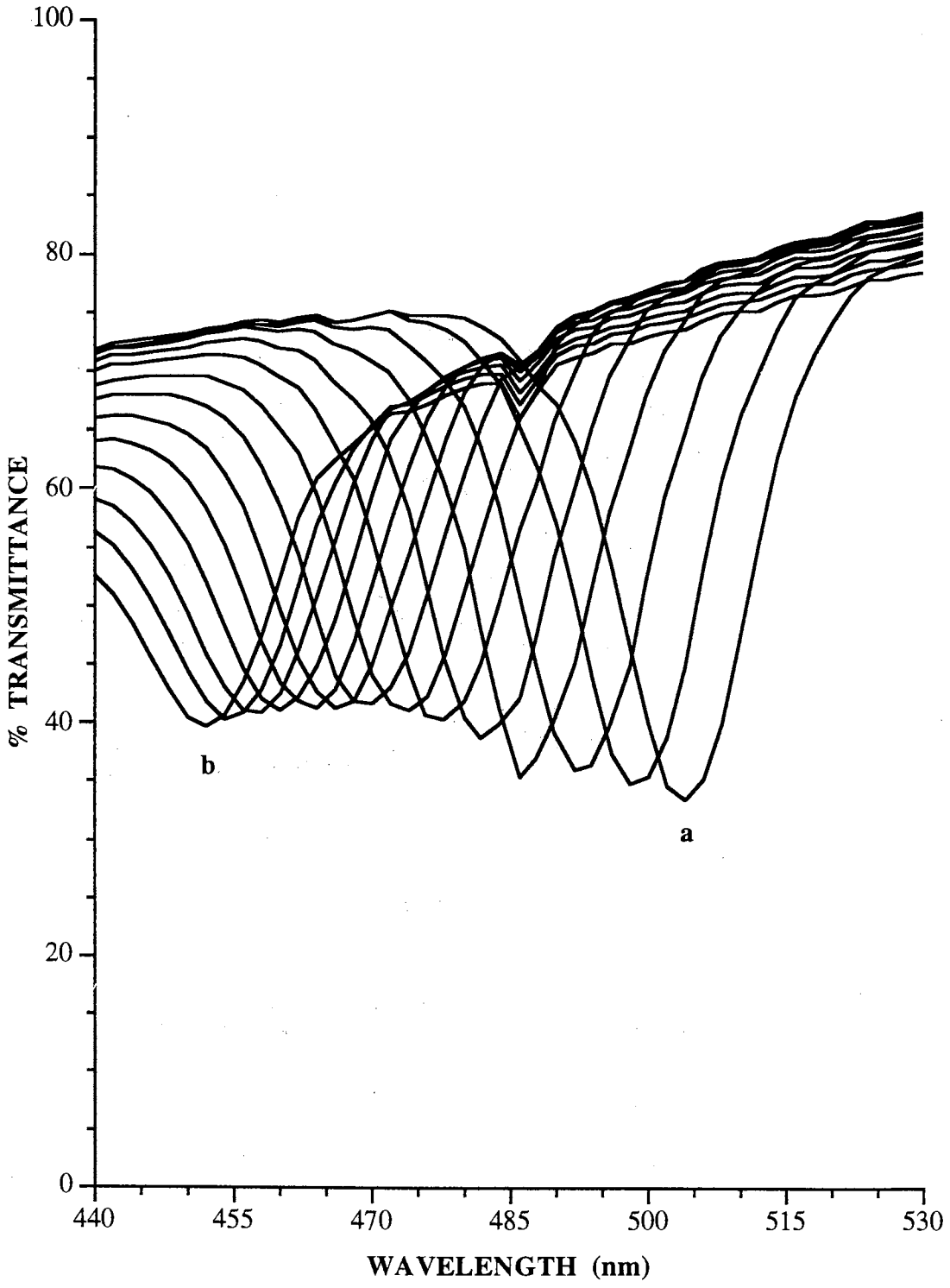

Figure 6. Transmission spectra of 153 nm TPM-silica in PMA (a) before and (b) after uniaxial stretching to $L/L_0 = 1.35$. Intermediate spectra are from the film at $1 < L/L_0 < 1.35$. The initially 228 μm thick film contained 35 wt% TPM-silica.

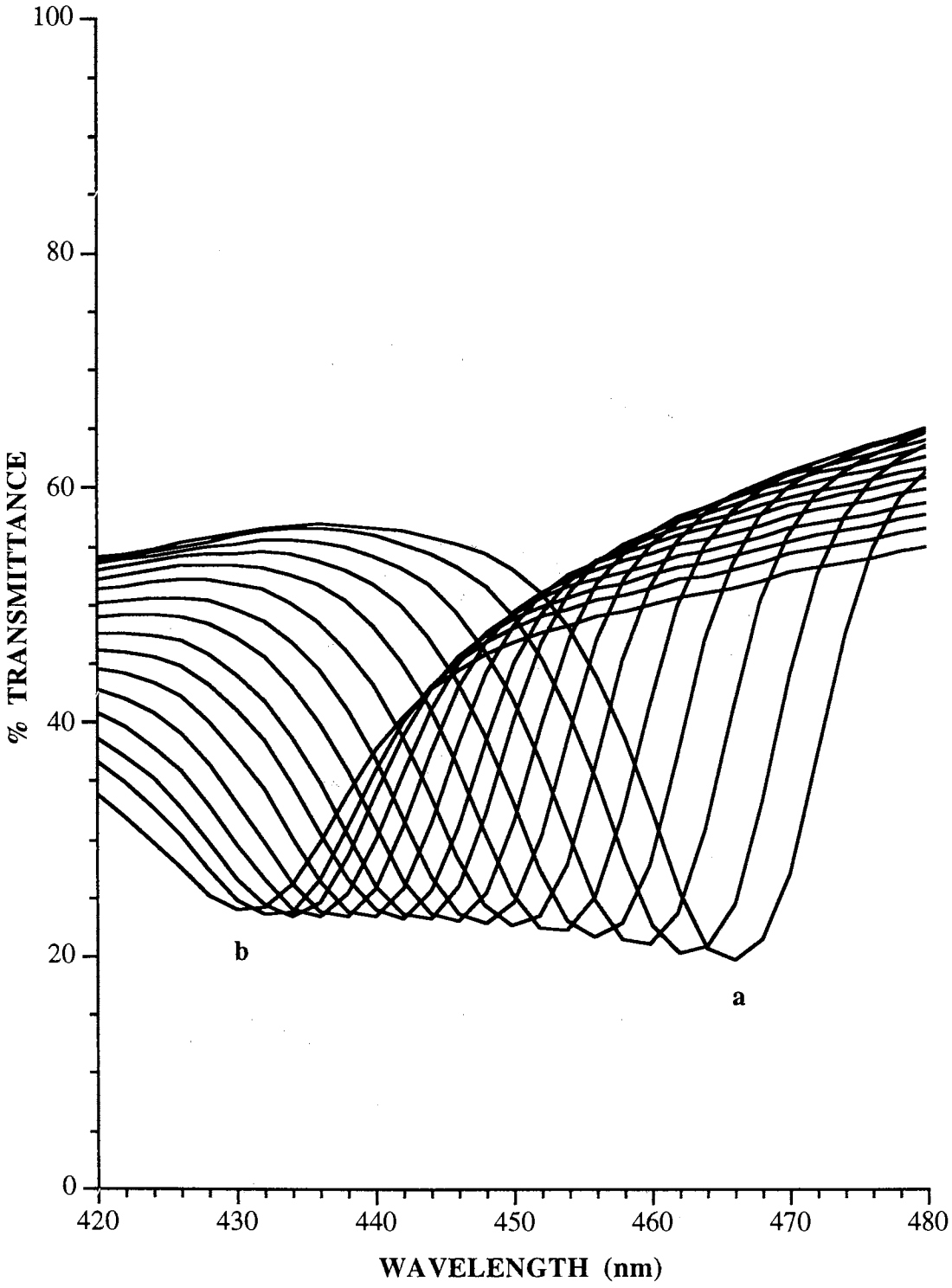

Figure 7. Transmission spectra of 153 nm TPM-silica in PMA (a) before and (b) after uniaxial stretching to $L/L_o = 1.35$. Intermediate spectra are from the film at $1 < L/L_o < 1.35$. The initially 228 μm thick film contained 45 wt% TPM-silica.

Table III. Transmission on Stretching a 40 wt% 153 nm TPM-silica-PMA Film

No.	L/L_0	λ_{min} (nm)	Bandwidth[a] (nm)
1	1.000	486	16.8
2	1.025	482	17.2
3	1.051	478	17.6
4	1.076	474	17.8
5	1.102	470	18.0
6	1.127	466	18.3
7	1.153	462	18.6
8	1.178	460	19.0
9	1.203	456	19.3
10	1.229	454	19.5
11	1.254	450	19.6
12	1.280	448	19.7
13	1.305	444	18.6
14	1.330	442	20.3
15	1.356	440	20.6

[a] Bandwidth measured at half-height.

RED SHIFT BY SWELLING OF THE ELASTOMERIC COMPOSITE FILM

The diffraction wavelength was red shifted by swelling the composites with monomers such as MA and styrene containing 1 wt% DMPA. Table IV shows λ_{min} from 40 wt% TPM-silica-PMA composite swollen with MA. Table V shows diffraction wavelength from a 35 wt% TPM-silica-PMA composite swollen with styrene.

Table IV. Transmission of a 40 wt% 153 nm TPM-silica-PMA Film Swollen with MA

dimensions (mm)	time (h)	λ_{min} (nm)	obsd d_{111}[a] (nm)	calcd d_{111} (nm)	bandwidth (nm)
70 x 20 x 0.264[b]	0	556	196.8	186.3	6.0
9.0 x 9.0 x 0.228[c]	0	506	172.0	163.7	11.3
11.0 x 11.0 x 0.295[d]	24	652 (655)	225.9	226.9[e]	13.3
10.5 x 10.5 x 0.287[f]	24	632 (637)	214.4	216.1[e]	14.2

[a] Calculated from the Bragg equation. [b] Dimensions of the entire sample of MA dispersion. [c] Dimensions of for a piece of the polymerized composite. [d] Swollen with MA and 1 weight percent initiator. [e] Calculated from the swollen dimensions of the composite. [f] After photopolymerization. The λ_{min} values in parentheses are calculated from the swollen dimensions of the composite.

Table V. Transmission of 35 wt% 153 nm TPM-silica-PMA Film Swollen with Styrene

time (h)	λ_{min} (nm)	bandwidth (nm)
0	502	12.1
4	680[a]	23.4
24	740[a]	14.1
24	724[b]	24.2
24	550[c]	18.9

[a] Swollen with styrene. [b] Swollen with styrene and 1 weight percent initiator. [c] After photopolymerization. [d] After thermal polymerization of imbibed styrene.

Figures 8 and 9 show transmission spectra at various time intervals from the composites that were swollen with MA and styrene, respectively. During the initial stages, diffusion of styrene the PMA composite led to uneven swelling in the film thickness. This uneven swelling occurred as a band of styrene diffused into the TPM-silica-PMA composite matrix. This phenomenon was observed as two diffraction peaks, one at 502 nm for unswollen region and other red shifted peak at 644 nm for partly swollen region of the composite.

Finally, only one peak at λ_{min} 680 nm was observed from the composite due to complete diffusion of styrene in the film thickness. In the case of the MA swollen composite, only one red shifted diffraction peak appeared at 652 nm. In 2-3 hours of swelling, the diffraction peak from the MA swollen composite was weak compared to the styrene swollen film which showed a strong diffraction peak. On swelling with MA and styrene, the diffraction bandwidths measured at half-heights from the swollen composites increased. The styrene swollen composite showed lower transmittance at wavelength away from the diffraction peak as compared to the MA swollen composite due to the higher refractive index of styrene. The glass-transition temperature (T_g) of the elastomeric unswollen TPM-silica-PMA composite was close to room temperature, while both MA and styrene swollen composites become gels with a much lower T_g at any given particle concentrations due to the plasticizing effect caused by monomer.

After a period of 6-8 hours, the composite films were further allowed to swell with MA and styrene containing 1 wt% DMPA in order to accomplish the photopolymerization of the imbibed monomers. During this second swelling period, the fully swollen size of the TPM-silica-crosslinked film was reached, and λ_{min} of the styrene swollen PMA composite film further red shifted the diffraction wavelength from 680 nm to 740 nm. The MA and styrene swollen composite films were then subjected to photopolymerization for a period of 3-4 hours.

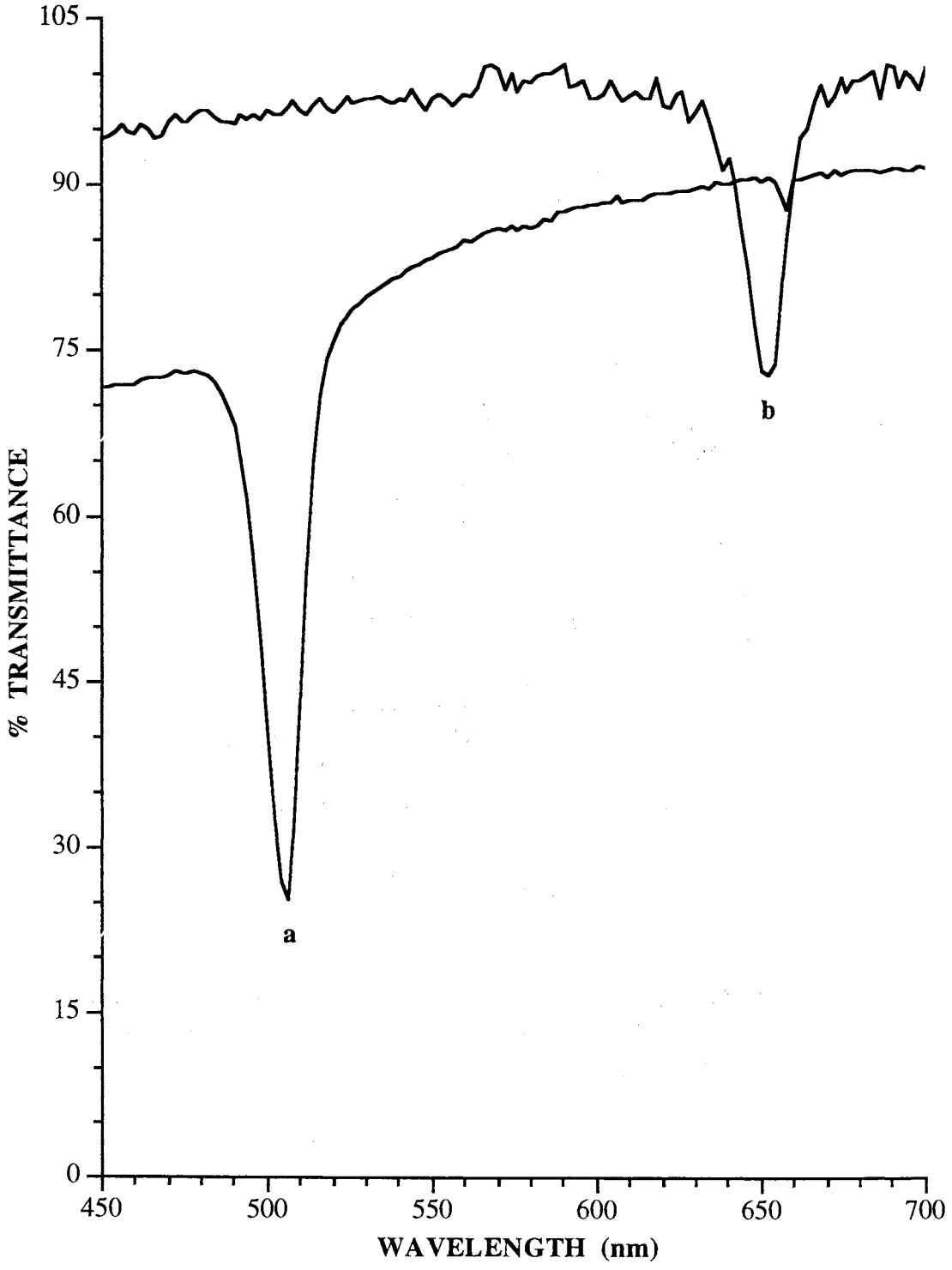

Figure 8. Transmission spectra of 153 nm TPM-silica-PMA composite (a) before and (b) after swelling with methyl acrylate. Before swelling the film contained 35 wt% TPM-silica and was 228 μm thick.

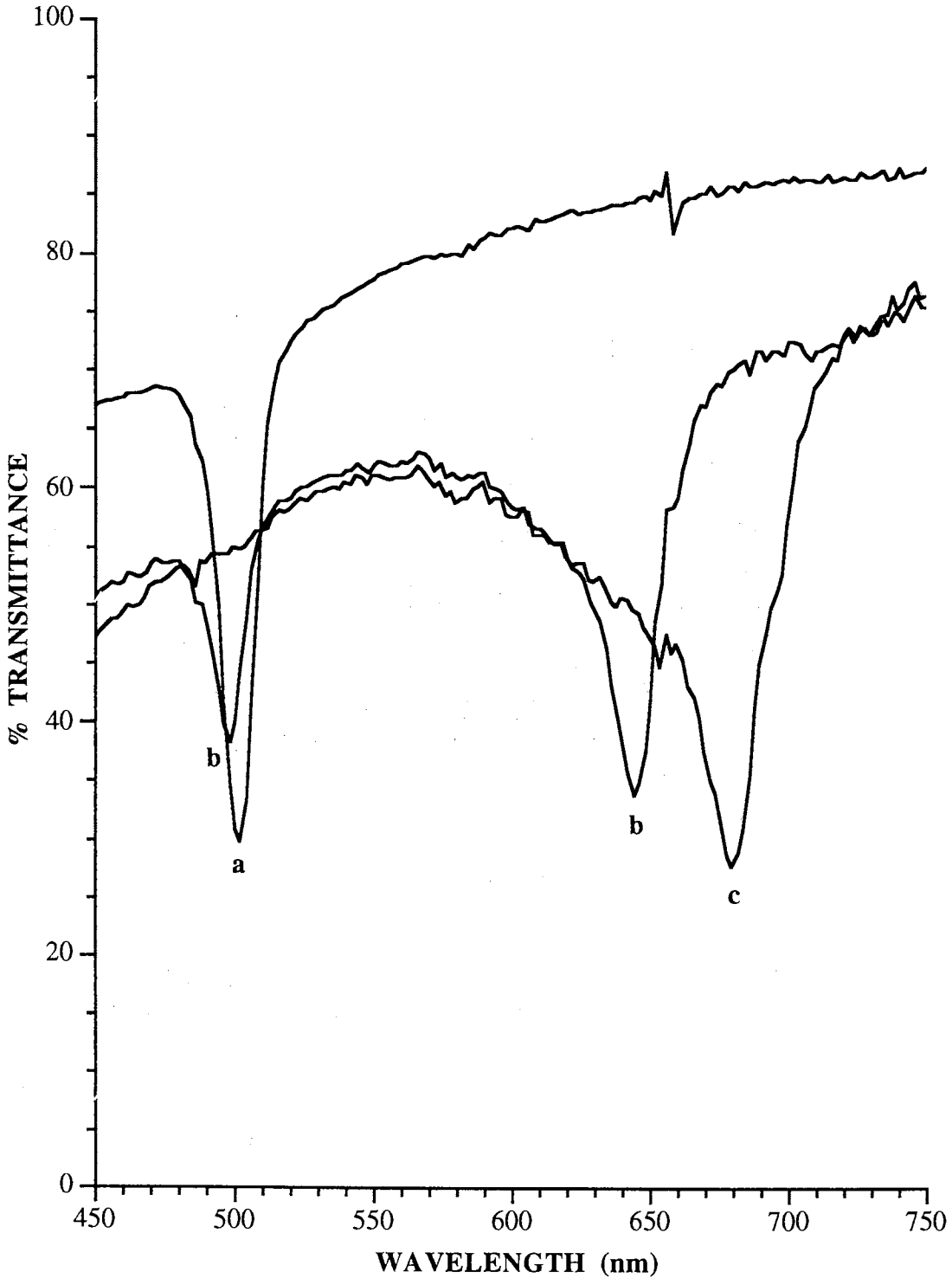

Figure 9. Transmission spectra of a 153 nm TPM-silica-PMA composite film swollen with styrene after (a) 0 h, (b) 2 h and (c) 4 h. Before swelling the film contained 35 wt% TPM-silica and was 228 μm thick.

The photopolymerization of the diffused MA was complete while that of diffused styrene was incomplete, and further thermal polymerization by heating in an oven at 90 °C formed the new composite film. Figures 10 and 11 show the diffraction wavelengths before and after photopolymerization from 35 wt% TPM-silica-PMA composites swollen with MA and styrene, respectively. The new PMA-PMA and PMA-PS composite films thus formed on photopolymerization show diffraction wavelengths at 632 and 550 nm, respectively. To understand the swelling behavior of the composite, we have measured the thickness and length and width before and after swelling and photopolymerization and compared to the diffraction phenomenon between the unswollen and swollen composites as shown in Table IV. We found, in the case of the PMA-PMA composite film, the Bragg diffraction at 506 nm from an unswollen film of thickness 228 μm was red shifted to 632 nm for the swollen film of thickness 287 μm. Figure 12 shows the dimensional changes which occur in the composite film during photopolymerization, swelling and photopolymerization of the added monomer. No macroscopic or microscopic phase separation was observed from the new polymer composite as observed from orthoscopic images between crossed polarizers of a polarizing microscope. Figure 13 shows the orthoscopic images of composite films held at an angle of 40-55° away from the incident light before and after swelling.[6,7,16,20] The images show blue colored crystals from the unswollen composite film and red with occasionally blue green colored crystals from the swollen composite. The dimensions of these crystals were found to vary from 50 to 200 μm. The blue green crystallites seen from swollen composites probably occur due to the different crystal orientations when compared to the red crystals.

BLUE SHIFT BY ROTATING DISPERSION AND COMPOSITE

We have also tuned of the λ_{min} by varying the Bragg angle, θ, where the PMA film was rotated at an angle away from the normal to the incident light of a UV-visible spectrophotometer.[22-26]

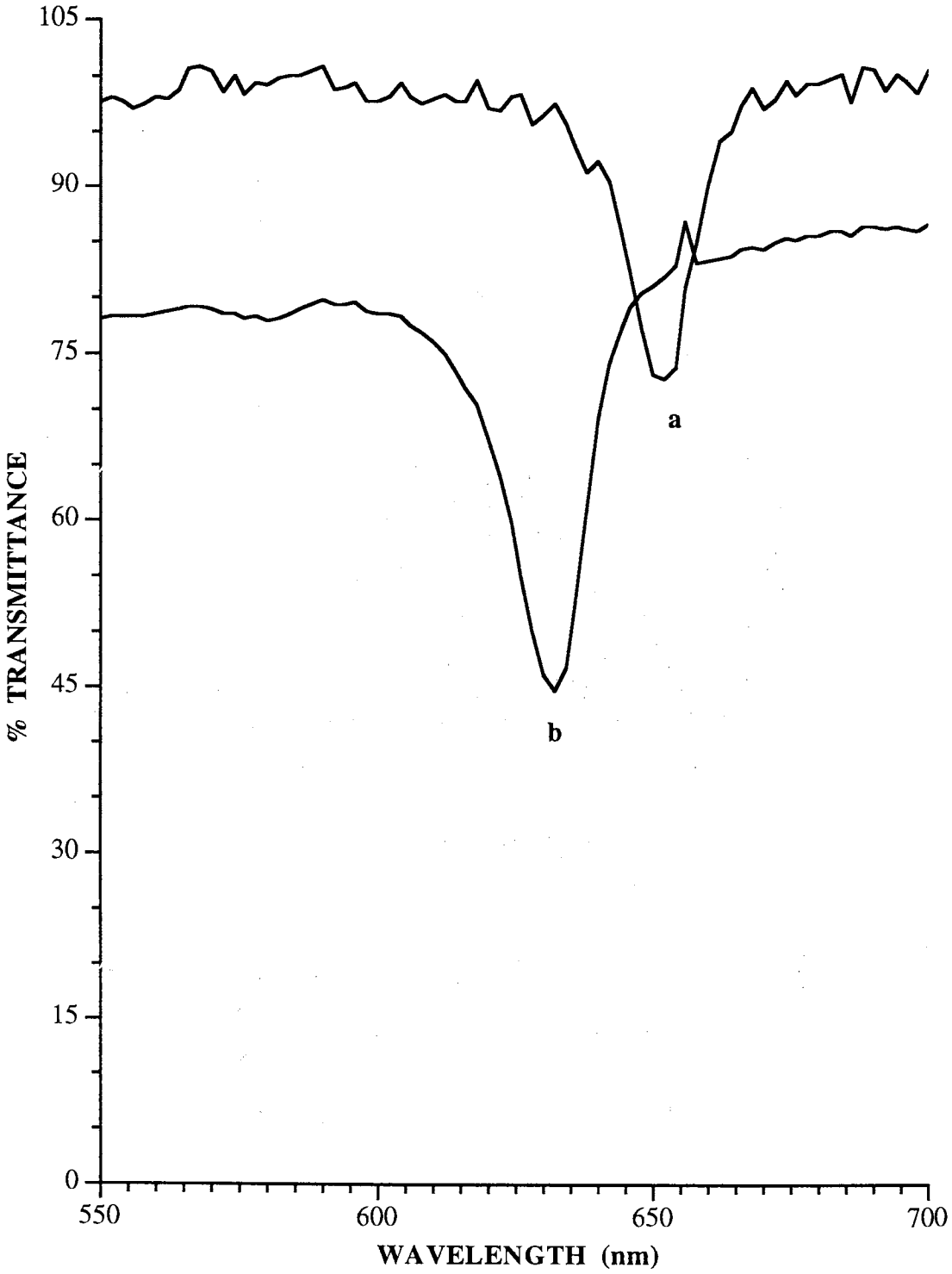

Figure 10. Transmission spectra of a 153 nm 35 wt% TPM-silica-PMA composite swollen with methyl acrylate (a) before and (b) after polymerization.

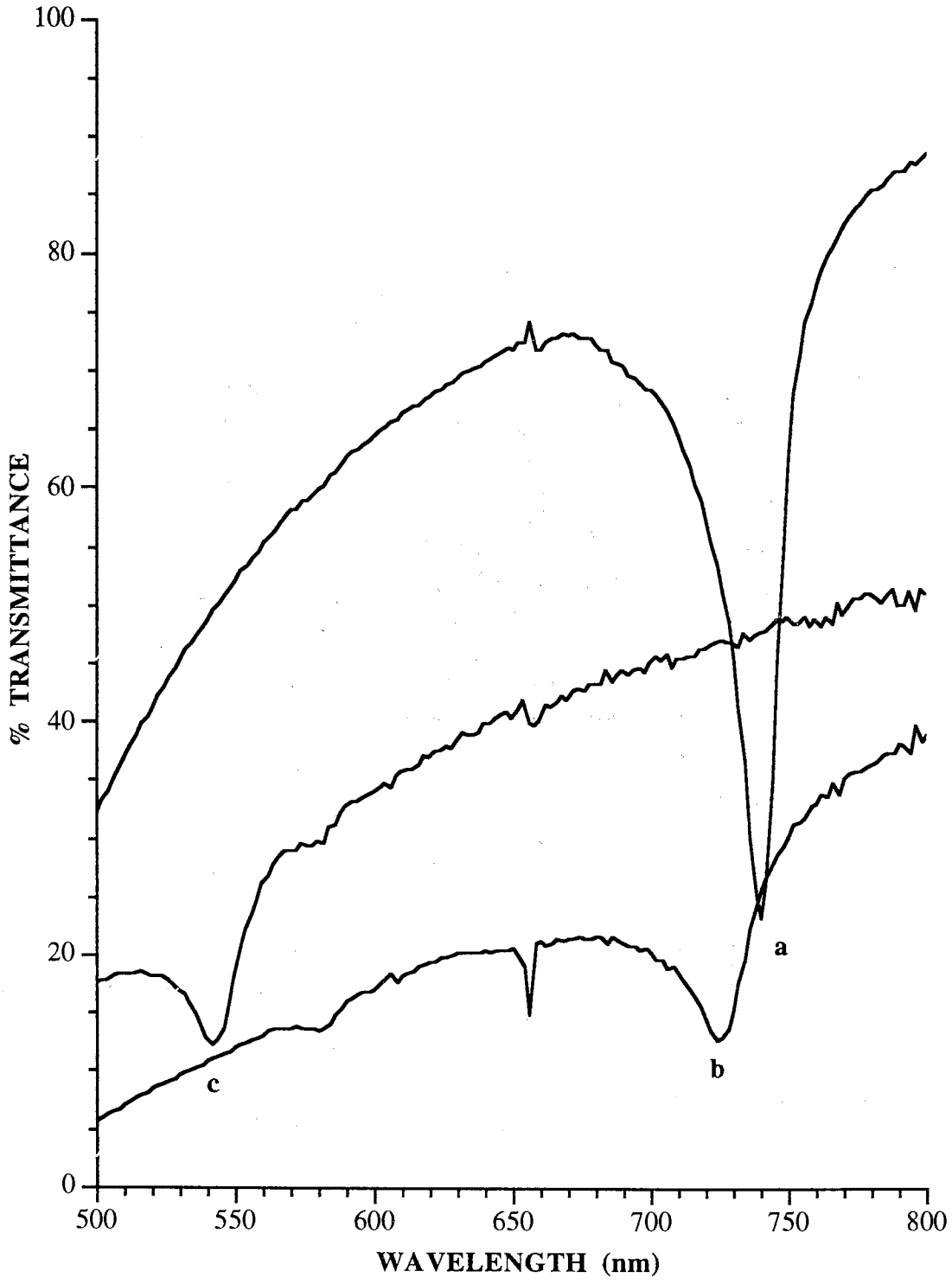

Figure 11. Transmission spectra of a 153 nm 35 wt% TPM-silica-PMA composite swollen with styrene (a) before, and (b) after photopolymerization, and (c) after heating at 90 °C.

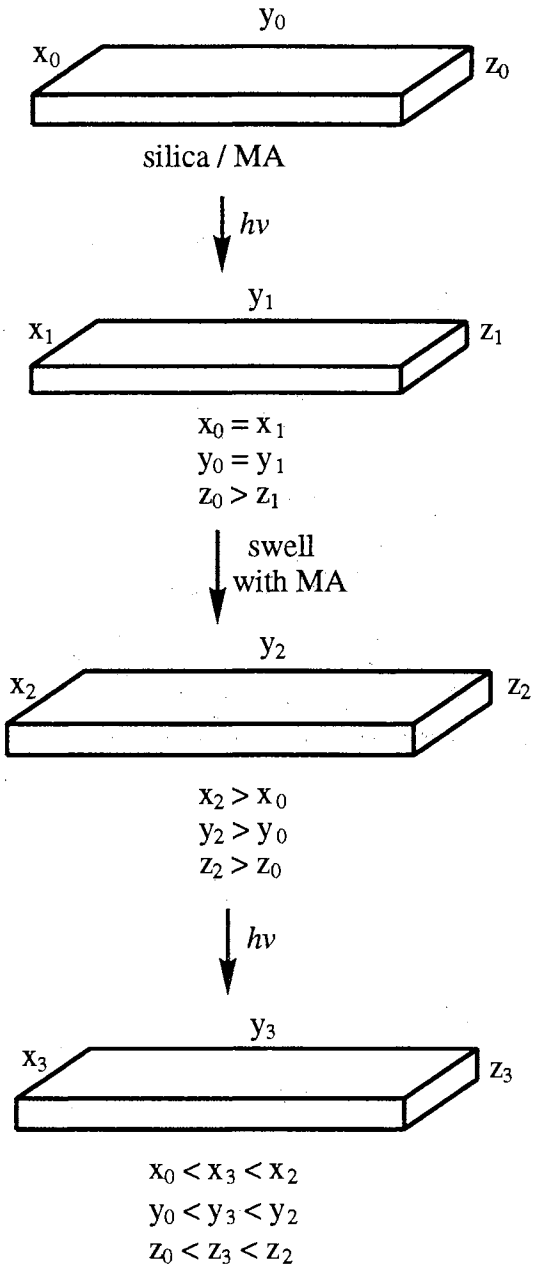

Figure 12. Dimensional changes during photopolymerization, swelling with MA and photopolymerization of imbibed MA from 40 wt% silica PMA composite. Measured dimensions are in Table IV.

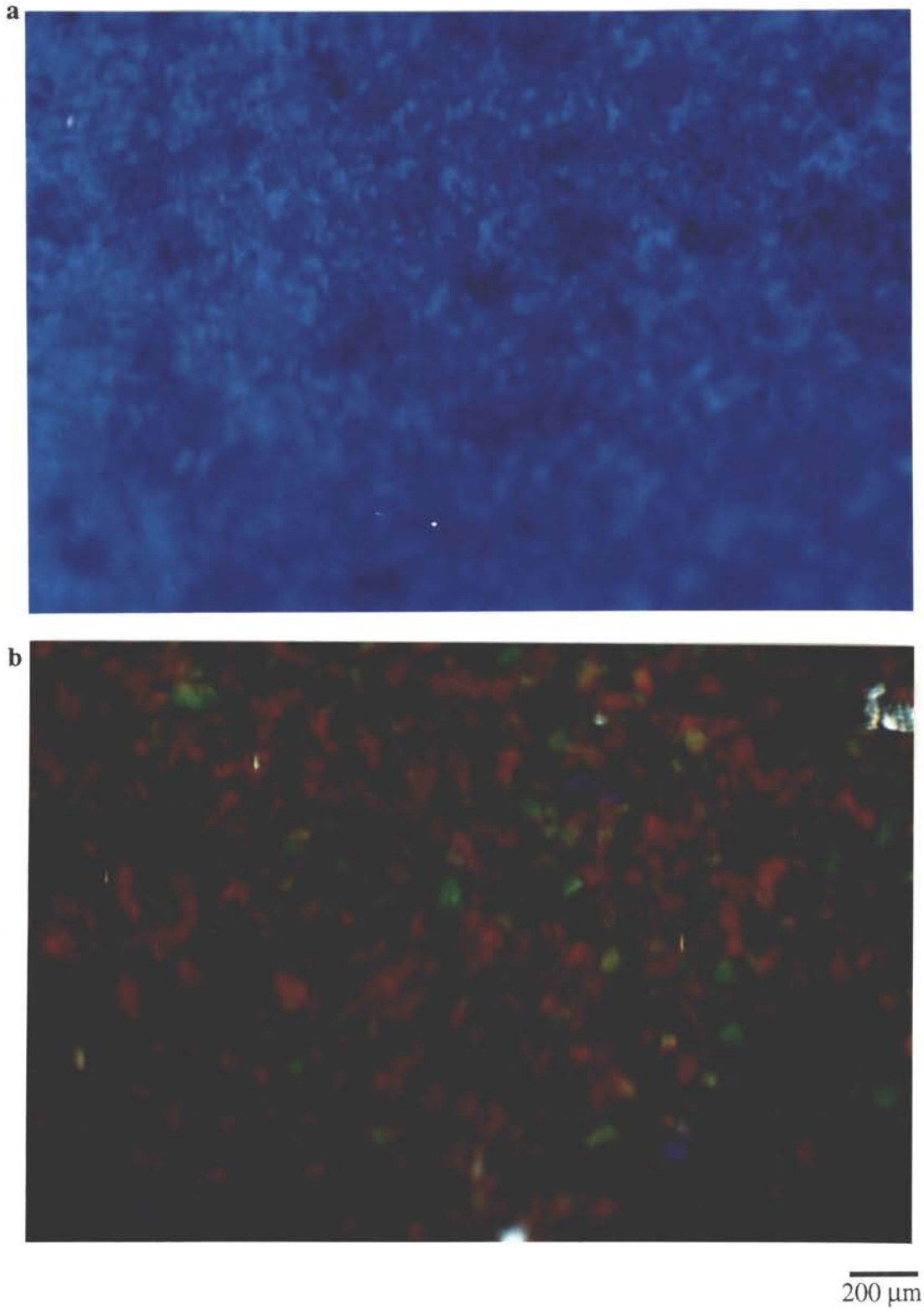

Figure 13. Orthoscopic images of a 153 nm TPM-silica-PMA composite film tilted 40-55° to the incident light between crossed polarizers before (top) and after (bottom) swelling with methyl acrylate.

Figures 14 and 15 show transmission spectra obtained by changing the Bragg angle and the blue shift of diffraction wavelength from a 40 wt% 153 nm TPM-silica in MA dispersion and PMA composite, respectively. Table VI shows the λ_{min} observed at different Bragg angles from a 40 wt% TPM-silica-MA dispersion and a 40 wt% TPM-silica-PMA composite film. By rotating the stage, the diffraction bandwidths measured at half-height at varied angles increased while the diffraction intensity decreased. Similar results have been observed from 35 and 45 wt % TPM-silica in MA dispersions and PMA composites.

Table VI. Transmission of 40 wt% 153 nm TPM-silica-MA Dispersion and PMA Composite as a Function of the Bragg Angle, θ.

	MA dispersion		PMA composite	
θ. (°)	λ_{min} (nm)	bandwidth (nm)	λ_{min} (nm)	bandwidth (nm)
90	556	7.3	490	13.7
84	554	7.5	490	13.7
82	552	7.3	488	13.7
80	550	8.1	486	12.6
78	548	8.1	486	12.1
76	546	8.3	482	12.6
74	544	8.5	480	12.6
72	540	8.9	478	12.1
70	538	8.9	476	12.1
68	534	9.0	472	11.3
66	530	9.3	---	---

The shifts of λ_{min} are consistent with the Bragg equation (1), and the angle of incidence from Snell's law of refraction (2),

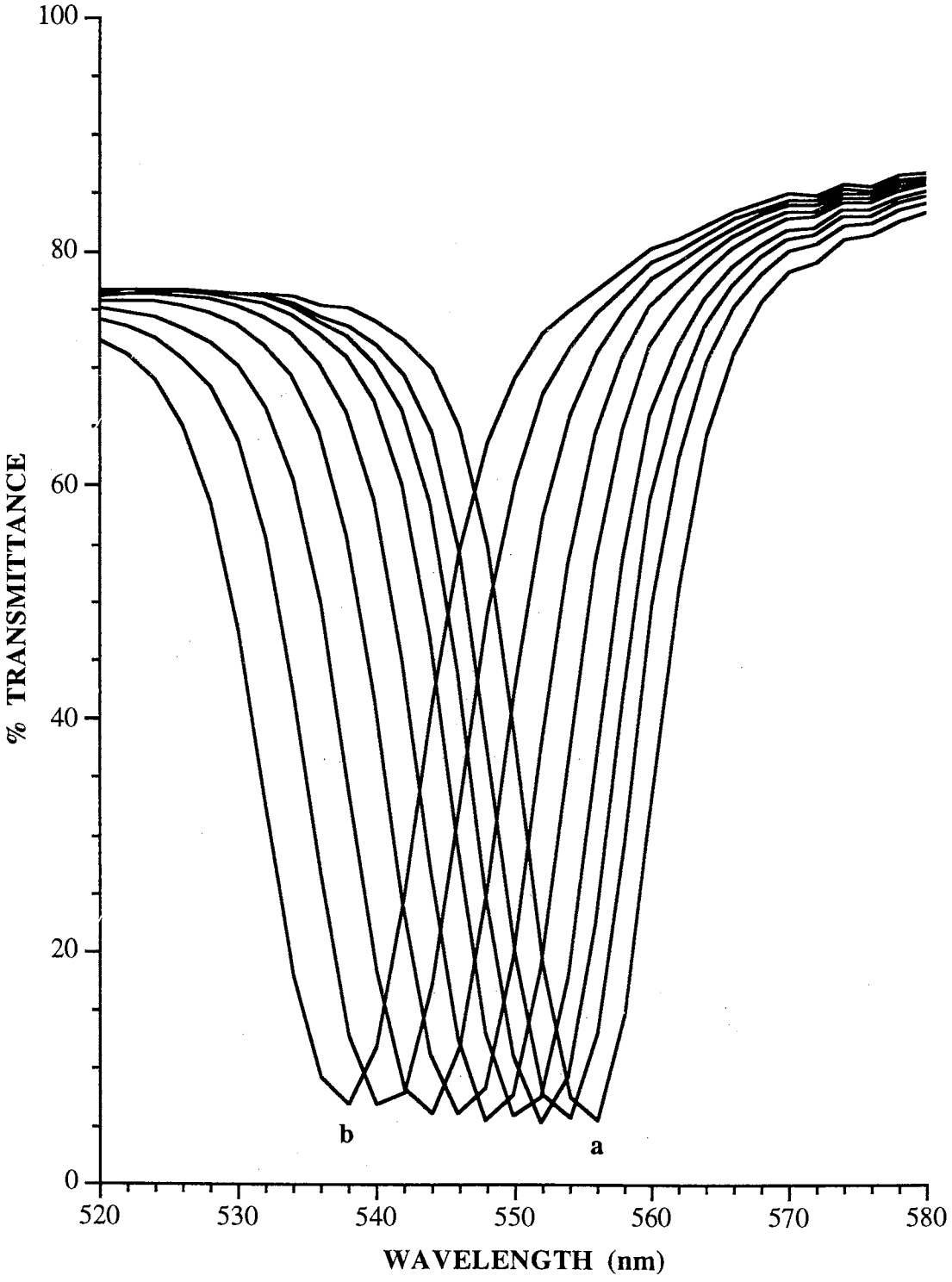

Figure 14. Transmission spectra of a 40 wt% 153 nm TPM-silica in MA dispersion as a function of angle of incidence: (a) 90° and (b) 66°. Film thickness = 264 μm. Data are in Table VI.

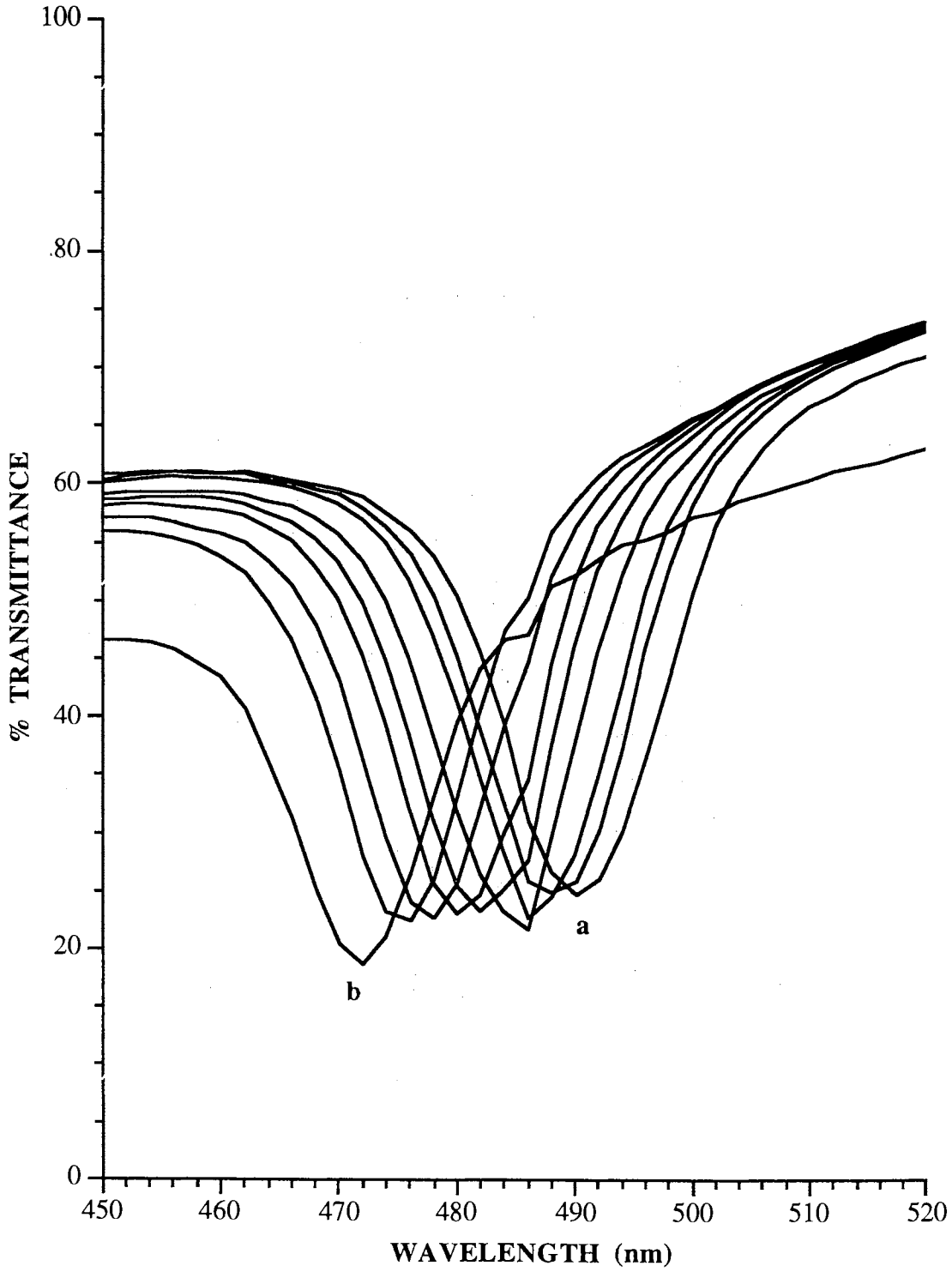

Figure 15. Transmission spectra of a 40 wt% 153 nm TPM-silica-PMA composite as a function of angle of incidence: (a) 90° and (b) 68°. Film thickness = 228 μm. Data are in Table VI.

$$\lambda = 2dn \sin\theta \quad (1)$$

where λ is the wavelength of diffracted light, d is the interplanar spacing, n is the refractive index of the dispersion and θ is the Bragg angle. Snell's law is given by

$$\theta = \cos^{-1}[(\cos\theta_1)/n] \quad (2)$$

where θ is the corrected Bragg angle, θ_1 is the observed glancing angle and n is the refractive index of the dispersion or the polymer composite, as previously observed for polystyrene latexes in water.[26] Figure 16 compares observed and calculated diffraction wavelengths with sin θ for MA dispersion and PMA composite.

SEM ANALYSIS

Figures 17a and 17b show the SEM pictures of the surface layer of 40 wt% TPM-silica particles in the unswollen PMA film, and the swollen PMA-PMA composite film, respectively. The films were microtomed normal to the film plane and the microtomed surfaces were also observed by the SEM. Figures 18a and 18b show the SEM pictures of surface layer of the microtomed section of unswollen PMA film, and the swollen PMA-PMA composite film, respectively. The micrographs show the regular hexagonal arrays of silica particles in the PMA composite films. The hexagonal order observed from these composites is similar to that observed from the SEM picture of surface layer of TPM-silica in PMMA composite film,[6,7] and of polystyrene latex in hydrogels by freeze fracture electron microscopy.[44-46] The increase in the interparticle distance as seen from the hexagonal arrays of the silica particles in the swollen film corresponds to the red shift of the diffraction wavelength. The cell parameter a, which increased from 339 nm for the unswollen PMA film to 402 nm for swollen repolymerized PMA composite, calculated from the micrographs, is larger than the a calculated from transmission spectra (327 nm and 375 nm, respectively).

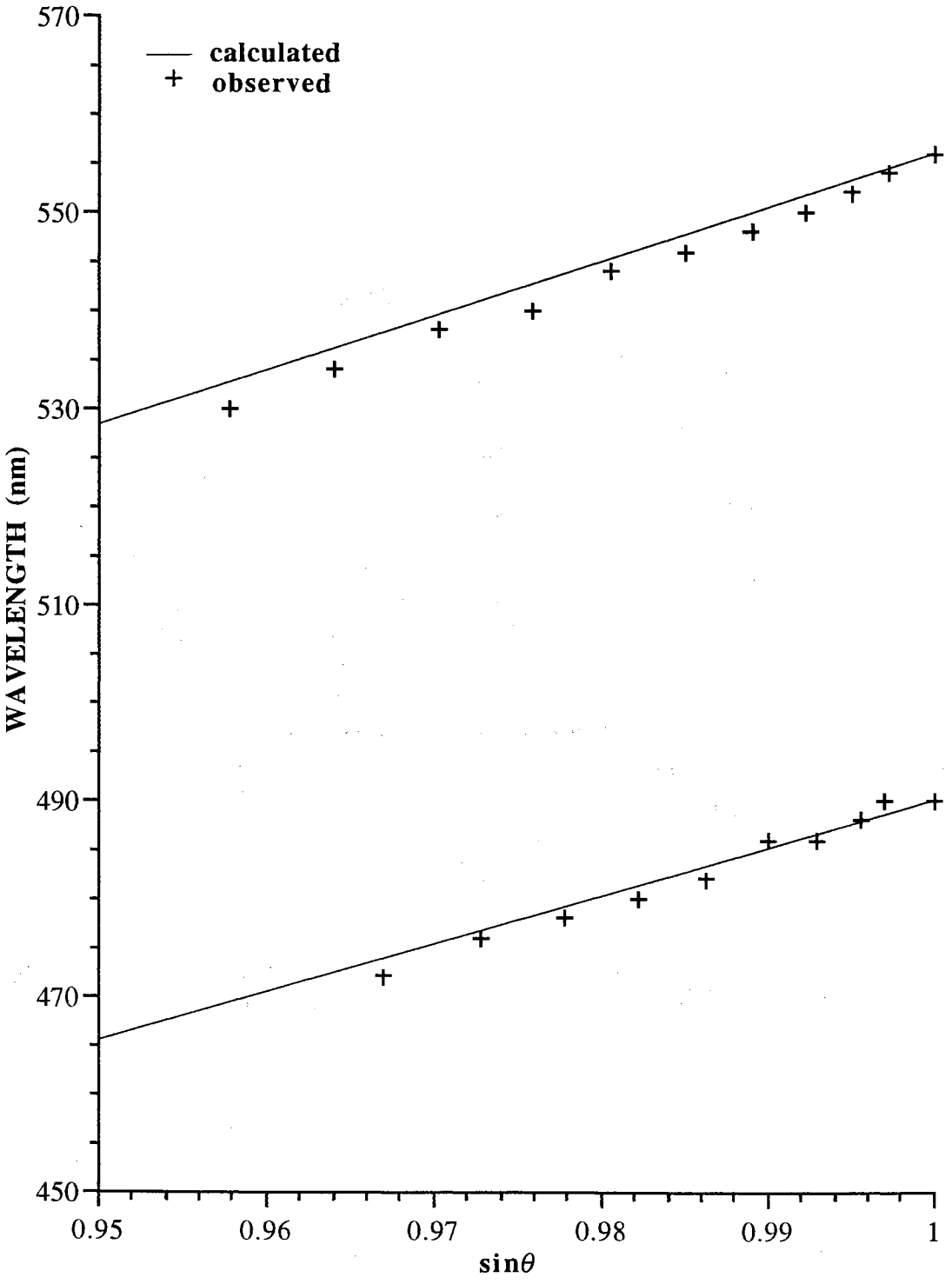

Figure 16. Plot of diffracted wavelength versus sin θ for the MA dispersion and PMA composite given in Table VI.

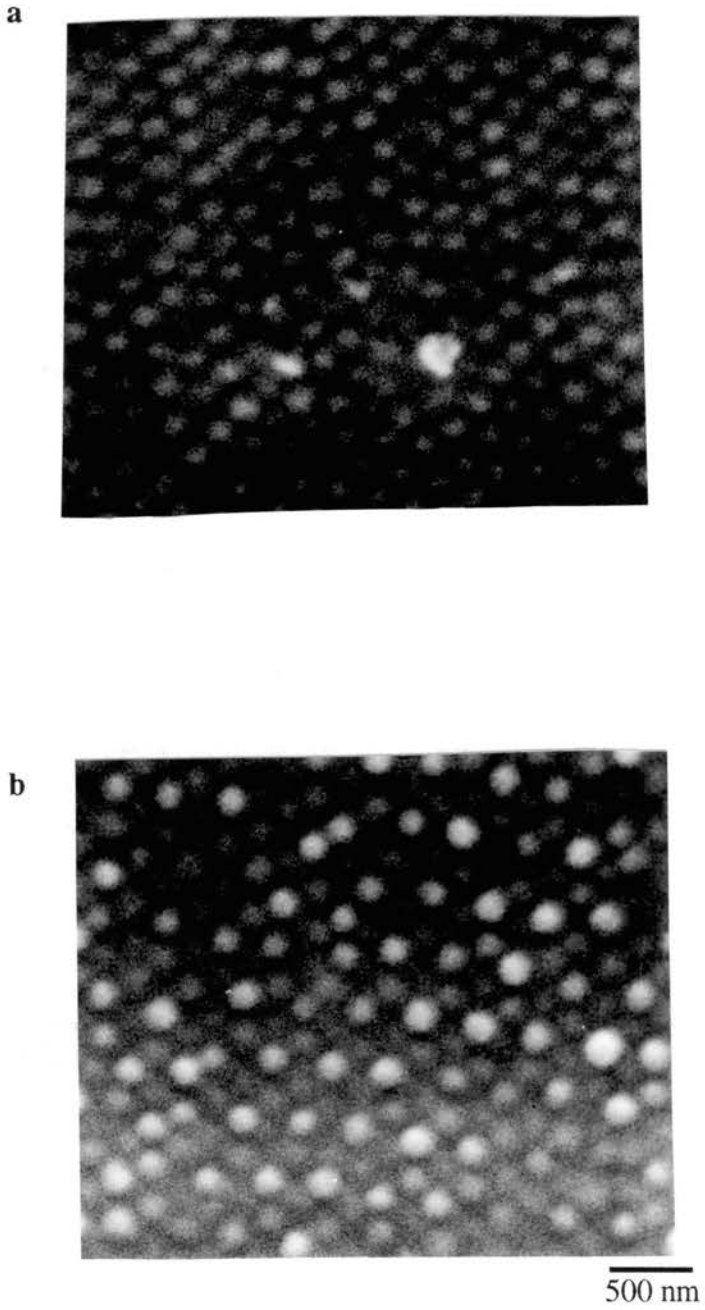

Figure 17. SEM image of a surface layer of a 40 wt % 153 nm TPM-silica-PMA composite film (a) before and (b) after swelling and photopolymerization of MA. Film thickness, (a) 228 μm and (b) 287 μm.

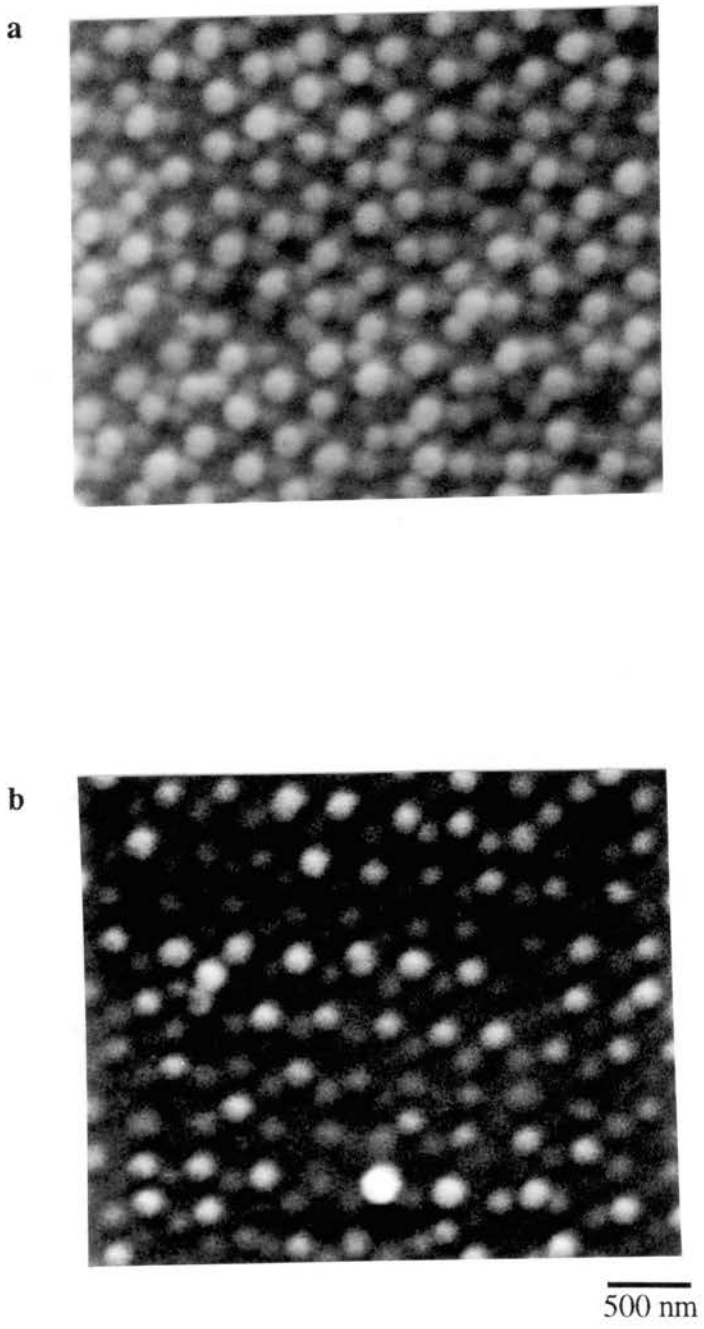

Figure 18. SEM image of a microtomed section of a 40 wt % 153 nm TPM-silica-PMA composite film (a) before and (b) after swelling and photopolymerization of MA. Film thicknesses are the same as in Figure 17.

DISCUSSION

As previous research on colloidal crystals showed that high particle concentrations of silica particles with low surface charge favor fcc lattice,[9] the 35-45 weight percent TPM-silica particles in MA dispersions also probably crystallize into fcc lattices. The d_{111} planes of the fcc crystals parallel to the film plane cause Bragg diffraction of visible light.[6,7,17-20,22-33] Bandwidths at half-height of peaks in visible spectra of films of the MA dispersions, and opacity to visible light between crossed polarizers, suggest crystallites with d_{111} planes parallel to the plane of the glass cells.

On photopolymerizing the monomer dispersions, appearance of low %T peaks in the transmission spectra of the composite films indicate that the crystal lattice, ordering and crystal orientation, especially, the d_{111} plane parallel to the film plane are trapped and maintained in the polymer matrix. A blue shift of the diffraction wavelength occurs from all composite films with varied particle concentrations due to the monomer shrinkage which compresses the crystal along the film thickness and thus the d_{111}-spacings.[6,7] Polymerization of MA to PMA occurs with a decrease in specific volume from 1.046 to 0.820 cm^3g^{-1}.[47] The shrinkage occurs entirely in the thickness of the film, not in the length or width, because the composite adheres to the epoxy used to seal the sandwich glass slides and not to the silanized glass surface. This phenomenon leads to a probable rhombohedral structure of the colloidal crystals in polymer composites as compared to the fcc structure for the monomer dispersions.

The d_{111}-spacings calculated from transmission spectra of the silica-PMA films are in good agreement with the d_{111}-spacings calculated by assuming monomer shrinkage only in the film thickness as seen in Table II. Thus, the d-spacing can be correlated to the 15% decrease only along the film thickness. The λ_{min} of the polymerized film varies from one region to another probably due to non-uniform decrease in thickness where certain regions may have greater contraction than the other regions, such that thinner

regions have smaller d_{111}-spacing than thicker ones. The intensity of the diffraction peak λ_{min} decreases for TPM-silica-PMA composite as compared to the MA dispersion due to smaller refractive index difference between TPM-silica to PMA as compared with TPM-silica to MA, while the broad bandwidth of diffraction wavelength from the composite is primarily due to some disordering and disorientation of the crystal lattice during photopolymerization.

By increasing the particle size, the diffraction wavelength shifts to the red due to the overall larger screening Debye-double layer around the particles at a given particle concentration in monomer dispersions. This is in agreement with varied sizes of polystyrene particles in water which show similar behavior of diffraction.[10,11]

By increasing the particle concentration from 35 to 45 wt%, the crystal cell dimensions decrease along with the interparticle distance and the d_{111}-spacings responsible for diffraction phenomenon decrease which causes a blue shift of the diffraction wavelength from the monomer dispersions and polymer films. This blue shift of diffraction wavelength is similar to that observed from dispersions of colloidal silica in ethanol/toluene,[9] or polystyrene latexes in water.[17-20,22-33]

The blue shift of λ_{min} as evident in Figure 4 and the inset of Figure 4 suggests that the d_{111}-spacing of the rhombohedral lattice decreases in the z-direction (or in the film thickness) as the films are uniaxially stretched to $L/L_o = 1.35$. On further stretching, the appearance of weak broad diffraction peaks from the composites suggest that either the uniform orientation of the crystallites or the order within the crystallites deteriorates as the crystals are compressed in the z-direction.[25] Similarly, even at $1 < L/L_o \leq 1.35$, the increase in the half height bandwidth of λ_{min} is probably due to the decrease of inter- or intracrystalline order. As long as the film of 40% silica in PMA is not stretched to $L/L_o > 1.35$, it behaves as an elastomer with a very slow viscoelastic response, regaining its macroscopic dimensions and its crystal dimensions, as measured by visible spectra,

within 4 hours after releasing the stress. These silica-PMA composites provide more convenient control of the diffraction wavelength by stretching than do polyacrylamide gels containing polystyrene latexes.[25,26]

We have not been able to grow colloidal crystals of 153 nm monodisperse silica in MA or MMA at concentrations of less than 35 weight percent, and consequently the diffraction wavelengths of the polymer films are limited to ≤ 510 nm. This problem has been solved by swelling colloidal crystalline silica PMA films with more monomer and retention of crystalline order. Polymerization of the imbibed monomer gives a robust film with λ_{min} = 632 nm shown in Figure 10. The red shifts of λ_{min} in the spectra of Figures 8-11 show that swelling the composite matrix with MA or styrene increases the d_{111}-spacings of the crystal lattice. During swelling by styrene there were two diffraction peaks for two different d_{111}-spacings, one for unswollen and the other for partly swollen regions of different thickness in the film. As time progresses, the appearance of only one diffraction peak from the composite film suggests that it is completely swollen with the monomer, and one d_{111}-spacing is now present in the film thickness. The d_{111}-spacing of 225.9 nm calculated from the Bragg equation and λ_{min} of the MA swollen composite, agrees well with the d_{111}-spacing of 226.9 nm calculated from the thickness of the film assuming that the crystal lattice swells to the same extent as the matrix.

On photopolymerization of added monomers, blue shifts of diffraction wavelengths are due to shrinkage of the thickness of the two composites as discussed above. The agreement between d_{111}-spacings of 214.4 nm calculated from transmission spectra and that calculated from the film thickness (d_{111} = 216.1 nm) indicates that photopolymerization shrinks the swollen crystal lattice to the same extent as the polymer matrix. The diffraction wavelengths from the new composites as seen in Figures 7 and 8 suggest presence of similar order and orientation of colloidal crystallites trapped into the swollen polymer matrix.

All the above mentioned techniques for tuning the diffraction wavelengths involve either increasing or decreasing the d-spacings of the crystal lattice. The blue shift of the diffraction wavelength as seen by changing the Bragg angle shows that the λ_{min} can be altered by changing θ. As θ is varied, the $sin\theta$ value in equation (1) decreases and thus the diffraction wavelength shifts to the blue.[16-20] The blue shift of λ_{min} is consistent with the Bragg equation only when the refractive index is corrected using Snell's Law as previously discussed for polystyrene latex in water.[26]

Since the films between crossed polarizers are not birefringent to light normal to the surface, and blue-green crystallites appear when the film is tilted 40-55°, the lattice plane causing diffraction is parallel to the plane of the glass as observed previously with a silica-PMMA composite.[6,7] The changes from transmission of blue-green to red through crossed polarizers by colloidal crystals when the polymer composite swells is due to the increased d_{111} spacing. The hexagonal order observed in the SEM pictures of the surface layer and the microtomed layer also indicates that d_{111} planes are parallel to the film plane and that the particle order is trapped by photopolymerization.[6,7,44-46] The tuning of diffraction wavelengths of the silica-PMA films by stretching and swelling is due to its elastomeric properties. Copolymerization between the methacrylate groups of the silane coupling agent, TPM, and the acrylate groups, links the silica particles to the PMA matrix, so that the silica effectively acts as a crosslinker of the PMA. This prevents the polymer film from dissolving in more monomer and provides the elastic force to restore the stretched film to its original dimensions after stress is released.

CONCLUSIONS

We have been able to grow TPM-silica colloidal crystals in MA dispersions between 35 and 45 wt% particle concentrations. Photopolymerization of the MA dispersions yield silica-PMA composites that Bragg diffracts narrow bandwidths of visible light. The Bragg diffraction wavelength shifts to the blue by decreasing the

particle size and by increasing the particle concentrations in MA dispersions. By stretching the composite films, and by changing the Bragg angle, the diffraction wavelength shifts to the blue, which allows the composite films to be employed as tunable filters. On swelling the composite film with monomers and photopolymerizing the imbibed monomers, the diffraction wavelength shifts to the red.

REFERENCES

1. Iler, R. K. *The Chemistry of Silica*; Wiley; New York, 1979; pp 582-588.
2. Sanchez, C.; Ribot, F. *New J. Chem.* **1994**, *18*, 1007.
3. Mark, J. E.; Lee, C. Y.-C.; Biancone, P. A., Eds. *Hybrid Organic-Inorganic Composites*; ACS Symposium Series 585; American Chemical Society; Washington, DC, 1995.
4. Landry, C. J. T.; Coltrain, B. K.; Brady, B. K. *Polymer* **1992**, *33*, 1486.
5. Pope, E. J. A.; Asami, M.; Mackenzie, J. D. *J. Mater. Res.* **1989**, *4*, 1018.
6. Sunkara, H. B.; Jethmalani, J. M.; Ford, W. T. *Chem. Mater.* **1994**, *6*, 362.
7. Sunkara H. B.; Jethmalani J. M.; Ford, W. T. *ACS Symp. Ser.* **1995**, *585*, 181.
8. Carlson, R. J.; Asher, S. A. *Appl. Spectrosc.* **1984**, *38*, 297.
9. Dhont, J. K. G.; Smits, C.; Lekkerkerker, H. N. W. *J. Coll. Interface Sci.* **1992**, *152*, 386.
10. Kesavamoorthy, R. Tandon, S.; Xu, S.; Jagannathan, S.; Asher, S. A. *J. Coll. Interface Sci.* **1992**, *153*, 188.
11. Okubo, T. *Langmuir* **1994**, *10*, 1695.
12. Hiltner, P. A.; Krieger, I. M. *J. Phys. Chem.* **1969**, *73*, 2386.
13. Okubo, T. *Colloid Polym. Sci.* **1993**, *271*, 190.
14. Okubo, T. *J. Chem. Soc., Faraday Trans. 1* **1986**, *82*, 3163.
15. Okubo, T. *J. Chem. Soc., Faraday Trans. 1* **1986**, *82*, 3175.
16. Clark, N. A.; Hurd, A. J.; Ackerson, B. J. *Nature* **1979**, *281*, 57.
17. Rundquist, P. A.; Photinos, P.; Jagannathan, S.; Asher, S. A. *J. Chem. Phys.* **1989**, *91*, 4932.
18. Spry, R. J.; Kosan, D. J. *Appl. Spectrosc.* **1986**, *40(6)*, 782.
19. Monovoukas, Y.; Gast, A. P. *Langmuir* **1991**, *7*, 460.
20. Monovoukas, Y.; Gast, A. P. *Phase Transitions* **1990**, *21*, 183.

21. Krieger, I. M.; Hiltner, P. A. *Polymer Colloids Proceedings*, ACS Symposium on Polymer Colloids, Fitch, R., Ed. Plenum Press; New York, 1971, 63.
22. Asher, S. A.; Kesavamoorthy, R.; Jagannathan, S.; Rundquist, P. A. *Nonlinear Optics III* **1992**, *SPIE Vol. 1626*, 238.
23. Asher, S. A. US Patent 4,627,689, 1986.
24. Asher, S. A.; Jagannathan S. US Patent 5,281,370, 1994.
25. Flaugh, P. L.; O'Donnell, S. E.; Asher, S. A. *Appl. Spectrosc.* **1984**, *38(6)*, 847.
26. Asher, S. A.; Flaugh, P. L.; Washinger, G. *Spectroscopy* **1986**, *1*, 26.
27. Okubo, T. *Prog. Polym. Sci.* **1993**, *18*, 481.
28. Okubo, T. *Colloid Polym. Sci.* **1993**, *271*, 873.
29. Okubo, T. *J. Chem. Phys.* **1987**, *86*, 2394.
30. Okubo, T. *J. Chem. Phys.* **1988**, *88*, 6581.
31. Asher, S. A.; Holtz, J.; Liu, L.; Wu, Z. *J. Am. Chem. Soc.* **1994**, *116*, 4997.
32. Panzer, H. P., Giovanni, L.; Cohen, M. L.; Yen, W. S. US Patent 5,338,492, 1994.
33. Haacke, G.; Panzer, H. P.; Magliocco, L. G.; Asher, S. A. US Patent 5,266,238, 1993.
34. Stöber, W.; Fink, A.; Bohn, E. *J. Colloid Interface Sci*. **1968**, *26*, 62.
35. Bogush, G. H.; Tracy, M. A.; Zukoski, C. F. *J. Non-Cryst. Solids* **1988**, *104*, 95.
36. Badley, R. D.; Ford, W. T.; McEnroe, F. J.; Assink, R. A. *Langmuir* **1990**, *6*, 792.
37. Philipse, A. P.; Vrij, A. *J. Coll. Interface Sci*. **1988**, *128*, 121.
38. Sunkara H. B.; Jethmalani J. M.; Ford, W. T. *J. Polym. Sci. Polym. Chem. Ed.* **1992**, *30*, 1917.
39. Pusey, P. N.; van Megen, W. *J. Chem. Phys.* **1984**, *80*, 3513.
40. Ackerson, B. J.; Clark, N. A. *J. Phys*. (Paris) **1981**, *42*, 929.
41. Pecora, R., Ed. *Dynamic Light Scattering-Applications of Photon Correlation Spectroscopy*, Plenum Press, New York, 1985.
42. Nobbmann, U. M.S. thesis, Oklahoma State University, 1991.

43. Hiltner, P. A.; Papir, Y. S.; Krieger, I. M. *J. Phys. Chem.* **1971**, *75*, 1881.

44. Goodwin, J. W.; Ottewill, R. H.; Parentich, A. *J. Phys. Chem.* **1986**, *84*, 1580.

45. Cohen, J. A.; Scales, D. J.; Ou-Yang, H. D.; Chaikin, P. M. *J. Coll. Interface Sci.* **1993**, *156*, 137.

46. Kamenetzky, E. A.; Magliocco, L. G.; Panzer, H. P. *Science*, **1994**, *264*, 207.

47. Scientific Polymer Products, Inc. Catalog, Ontario, New York, 1991-92.

CHAPTER V

CRYSTAL STRUCTURES OF FILMS OF MONODISPERSE COLLOIDAL SILICA IN POLY(METHYL ACRYLATE)

ABSTRACT

Composite films of amorphous monodisperse colloidal silica particles in poly(methyl acrylate) (PMA) selectively Bragg diffract visible light. The 153 nm diameter silica particles coated with 3-(trimethoxysilyl)propyl methacrylate (TPM) in liquid methyl acrylate (MA) spontaneously form a face centered crystal (fcc) lattice with d_{111} planes parallel to the plane of the glass cell. Photopolymerization of MA solidifies the crystal order. Since decrease in the volume during polymerization proceeds by decrease in the film thickness only, the fcc lattice transforms to a rhombohedral lattice. The *d*-spacings and the lattice parameter *a*, calculated from optical Bragg diffraction of the composites, correlate well with those measured from scanning electron micrographs.

INTRODUCTION

Inorganic filler materials in polymer composites often improve mechanical and thermal stabilities compared with the pure polymer matrix.[1-5] Colloidal silica in composites may be pre-formed or prepared *in situ* by hydrolysis and condensation of tetraethyl orthosilicate (TEOS) or tetramethyl orthosilicate (TMOS).[1-5] In all examples of silica-polymer composites previous to ours, silica particles or silica fibers were randomly distributed. We have reported preparation and Bragg diffraction of composites of ordered monodisperse amorphous colloidal silica particles in poly(methyl methacrylate) (PMMA) films, PMA, and other acrylic polymer films.[6-8]

Monodisperse charged colloidal particles in aqueous and non-aqueous liquids spontaneously self assemble into a three dimensional lattice known as a colloidal crystal. Several factors influence the formation, ordering and orientation of colloidal crystals.[6-16] So far, the colloidal particles are found to order in either ABA or ABC stacks, which leads to either fcc, body-centered cubic (bcc) or hexagonal close-packed (hcp) lattices. Particles with low surface charge form fcc lattices at high concentrations, while particles with high surface charge form bcc lattices at low particle concentrations.[6-10] The dimensions of colloidal crystal lattices usually exceed 100 nm, causing Bragg diffraction of visible light.[6-28] Consequently, materials containing colloidal crystals have potential applications as optical rejection filters, limiters and switches.[18-28] We have made silica-PMMA composite films that are mechanically and thermally more robust than any previous colloidal crystalline materials.[6-8]

The crystal microstructures, morphologies, orientations and simulations of colloidal particles in aqueous and non-aqueous dispersions have been studied under the stresses of shear, electrical fields, confinement between two plates, and elevated temperatures using light scattering,[29-35] metallurgical microscopy,[36-39] optical

microscopy,[40,41] real-time digital-imaging of particles,[42-45] x-ray topography,[46] freeze fracture microscopy,[47] scanning and transmission electron microscopy,[48-50] and ultra small angle X-ray diffraction (USAXRD).[51,52] During crystallization of polystyrene latexes in water, confocal laser scanning microscopy experiments have shown that the particle order begins at the bottom surface and extends upwards through layers of the stacked particles.[16] The analyses of Kossel rings and Bragg spots caused by light scattering indicate that the d_{111} planes of the fcc structure, the 100 planes of the hcp structure or the d_{110} planes of the bcc structures are normal to the incident light. Coexistence of fcc and bcc or fcc and hcp lattices has been observed at certain particle concentrations in dispersions of both polystyrene latexes in water and colloidal silica in ethanol-toluene mixtures.[10] Hexagonal arrays of colloidal particles in optical and metallurgical microscopic images suggest that d_{111}-planes of fcc and d_{110}-planes of bcc lattices lie parallel to the plane of the glass observation cells. A theoretical model has been proposed for the formation of colloidal crystals and diffraction of light under shear forces.[53]

In our earlier report on the Bragg diffraction of visible light by silica-PMA composites,[8] we proposed that photopolymerization of TPM-silica-MA dispersions reduces their volumes 16-17 % by decrease only in the thickness of the composite, which transforms the fcc lattice to a rhombohedral lattice or decreases the distance between the hexagonal planes of the hcp lattice. We also proposed that on swelling the elastomeric composite with MA and on polymerization of the imbibed monomer, the crystal remains rhombohedral or hcp but expands in all three dimensions. This report gives the analysis of the colloidal crystal structures of silica-PMA composites by scanning electron microscopy (SEM). Comparisons of the crystal parameter a, and the d spacings of the crystal structures calculated from optical Bragg diffraction and measured from SEM analysis will be helpful to understand the crystal structures in the composite films.

RESULTS AND DISCUSSION

SILICA-PMA COMPOSITE

A 40 wt % dispersion of 153 nm diameter TPM-silica particles in MA (**A**) became iridescent 1-2 minutes after filling the glass cells, and the wavelength of λ_{min} (minimum transmittance) due to Bragg diffraction was 552 nm. Figure 1 shows the transmission spectra of an MA dispersion and a PMA composite of TPM-silica, and Table I reports the diffraction wavelengths and bandwidths. By polarizing microscopic observation, the sample contained 50-200 μm crystals over its entire area. Silica spheres like ours at 0.344 to 0.380 g mL^{-1} in low dielectric ethanol/toluene mixtures form fcc or mixtures of fcc and hcp colloidal crystals, and the d_{111} or 100 planes Bragg diffract visible light.[10]

Table I. Transmission of TPM-silica in MA Dispersion and PMA Composite[a]

Sample	λ_{min} (nm)	obsd d_{111} (nm)	calcd d_{111}[b] (nm)	bandwidth (nm)
A	552	195	186	6
B	488	166	166	7[c]

[a] Studies were done using 40 wt % 153 nm TPM-silica. [b] Calculated from the Bragg equation assuming an fcc lattice for the MA dispersion, and a 15.1% decrease in the d_{111} spacing for the PMA composite. [c] The diffraction band had a broad shoulder.

During crystallization, the particles form layers of two-dimensional hexagonal order, and the spacing between the layers corresponds to the λ_{min} of diffracted wavelength. The stacking of the layers could lead to at least three different structures. If the layers order in a ABC manner, fcc crystals with most dense d_{111} planes form parallel to the plane of the glass. If the layered stacks order in a ABA manner, hcp crystals with 100 planes form parallel to the plane of the glass. However, both fcc and hcp lattices could coexist in the thickness of the dispersion.

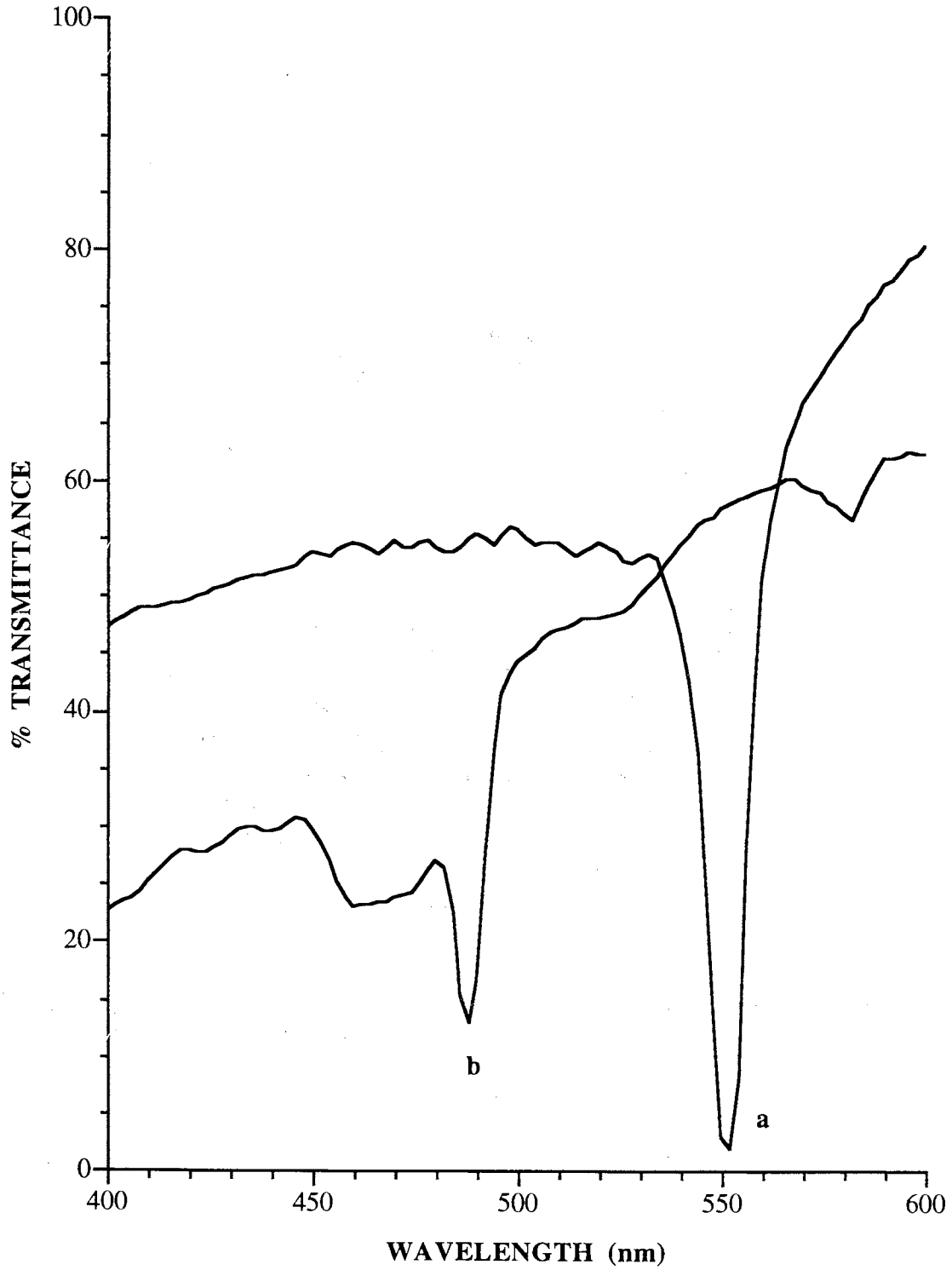

Figure 1. Transmission spectra of 40 wt % 153 nm TPM-silica particles (a) in MA monomer and (b) in PMA composite.

The MA dispersion containing 0.2 wt % photoinitiator (based on monomer) was irradiated to copolymerize MA and the TPM groups on silica to yield the silica-PMA composite (**B**).[6-8] After photopolymerization, the transmission spectrum was blue shifted with a broad shoulder, and λ_{min} varied from one position to another in the composite film. The shoulder in the spectrum of the composite film probably is due to the coexistence of crystals having d_{111} planes parallel and crystals having d_{111} not parallel to the film plane, which along with less order of the particles may cause broadening of the diffraction bandwidths. The blue shift of the narrower peak of **B** results from a decrease in the specific volume of the matrix during polymerization. Only the thickness of the film decreased, not the length and width, because the PMA adhered to the epoxy resin that sealed the edges of the cells but not to the poly(dimethylsiloxane)-coated glass surface. If the crystal structure of the monomer dispersion was fcc with d_{111} planes parallel to the film plane, and during polymerization the particle positions changed only in the direction normal to that plane, the crystal structure in the polymerized film is rhombohedral. If the particles ordered in a hcp lattice in monomer dispersion, the spacing between the 100 planes would decrease to the same extent as in an fcc lattice, and the lattice would remain hcp. In case of coexistence of fcc and hcp lattices, the fcc would transform to a rhombohedral and hcp will remain hcp with smaller interplanar spacings. The d_{111}-spacings calculated from transmission spectra of the silica-PMA films at most regions are in good agreement with the d_{111}-spacings calculated by assuming monomer shrinkage only in the film thickness, as seen in Table I. Because of uneven shrinkage in the film thickness, the λ_{min} varies from one region to another, and the thinner regions have smaller d_{111}-spacings than the thicker regions.

SWELLING THE COMPOSITE FILM

The λ_{min} of the TPM-silica PMA composite shifts to the red during swelling with MA (containing 1 wt % photoinitiator) (**C**). Irradiation for 3-4 h polymerized the

imbibed MA to form a new PMA composite film **(D)**. Figure 2 shows the transmission spectra. The diffraction properties and dimensions of the sample before and after swelling with MA and photopolymerization are reported in Table II.

Table II. Transmission of a 153 nm TPM-silica-PMA Film Swollen with MA[a]

Sample identity	dimensions (mm)	time (h)	λ_{min} (nm)	d_{111} (nm)	bandwidth (nm)
B	9.0 x 8.75 x 0.470	0	512	174	8[b]
C	11.0 x 10.75 x 0.622	24	678	236	13
D	10.6 x 10.25 x 0.600	24	656	222	14

[a] Initial particle concentration = 40 wt %. [b] The diffraction band had a broad shoulder.

Figure 3 illustrates the dimensions at each stage of formation of the composite film. At one 470 μm thick location of the unswollen silica-PMA composite film, λ_{min} shifted from 512 nm to 676 nm after swelling with MA. Further polymerization of the swollen silica-PMA composite produced a 600 μm thick film with λ_{min} = 656 nm. During the swelling and repolymerization process, the Bragg diffraction wavelengths from the composite films at various stages corresponded with the thickness of the films. No phase separation was observed in orthoscopic images of the new composite between crossed polarizers. During swelling with MA, the in-plane dimensions of the sample were not constrained at all, and the only force normal to the plane was due to the weight of the microscope slide. The macroscopic dimensions after swelling and repolymerizing increased 1.32 and 1.22 times in thickness and 1.27 and 1.17 times in the other two dimensions, respectively compared with the original silica-PMA film. Thus, if the original film has a rhombohedral crystal structure and/or an hcp structure, and particle positions change in proportion to the macroscopic sample dimensions, both the MA-swollen film and the repolymerized film also have a rhombohedral and/or hcp structures.

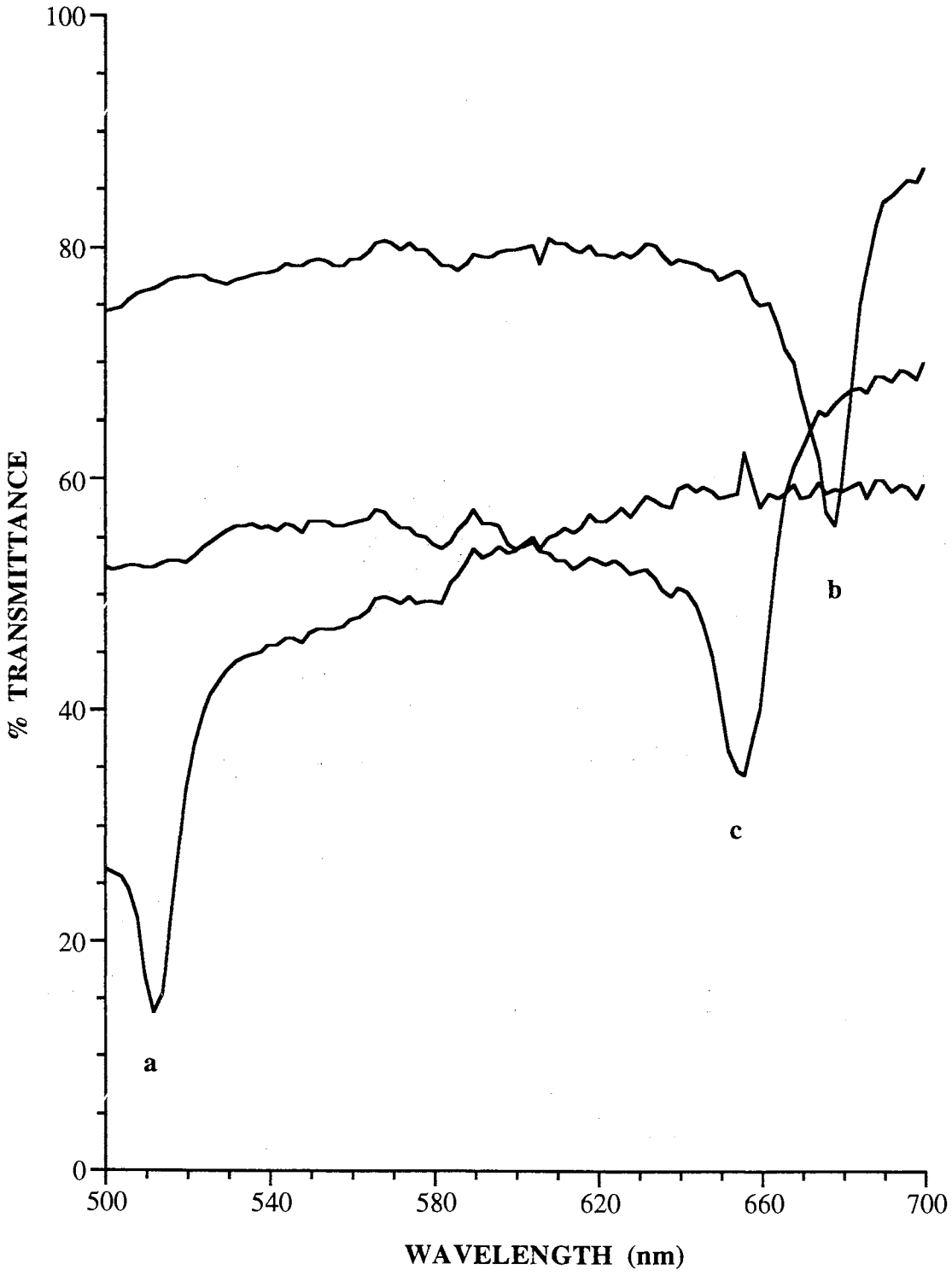

Figure 2. Transmission spectra of a 40 wt % 153 nm TPM-silica-PMA composite (a) before, (b) after swelling with methyl acrylate and (c) after polymerization.

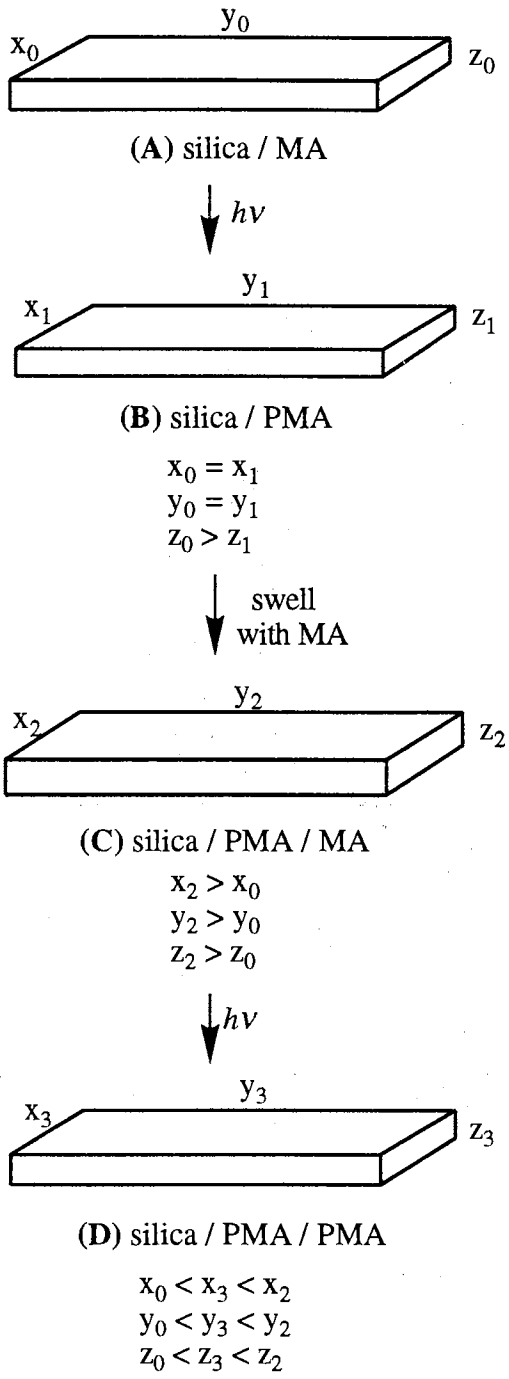

Figure 3. Dimensional changes during photopolymerization, swelling with MA and photopolymerization of imbibed MA of a 40 wt % silica-PMA composite. Measured dimensions are in Table II.

COMPUTER MODELING

Since an hcp lattice remains hcp during photopolymerization, after swelling, and after polymerization of the imbibed MA, we have modeled only the transformation of an fcc lattice to a rhombohedral lattice. The positional coordinates of silica particles in a fcc unit cell were modeled using ChemDraw v. 2.0. The lower two models in Figure 4 show the side view of parallel d_{111} planes of an fcc lattice in MA and of a rhombohedral lattice in a PMA composite. The top two models in the figure show the numbering of particles in the two crystal lattices. The interparticular distances in both the fcc and rhombohedral unit cells are given in Table III. The cartesian coordinates and the interparticular internal angles of an fcc unit cell are given in Tables IV and V, respectively. Since, in our spectrophotometric experiments, photopolymerization of MA causes a 15.1 % decrease in the Bragg diffraction wavelength, the d_{111}-spacings of the original fcc lattice were decreased by 15 % in the thickness only to give a rhombohedral lattice. We assume no change of in-plane particle positions because the in-plane macroscopic dimensions of the sample did not change.

The positional cartesian coordinates and the interparticular internal angles of an rhombohedral unit cell are given in Tables VI and VII, respectively. During the lattice compression, the interparticle distances within a d_{111} plane of the lattice do not change, but the lattice parameter a and the d_{111}-spacings become smaller.

The models of the fcc and rhombohedral lattices assume regular hexagonal particle order in the d_{111} planes, and rectangles or parallelograms of particles in the d_{110} planes of the fcc or rhombohedral lattice. The interparticular distances a and d_{111} spacings of 10.00 and 5.77 units for the model unit cell of fcc transform to 9.53 and 4.91 units for the unit cell of the rhombohedral lattice.

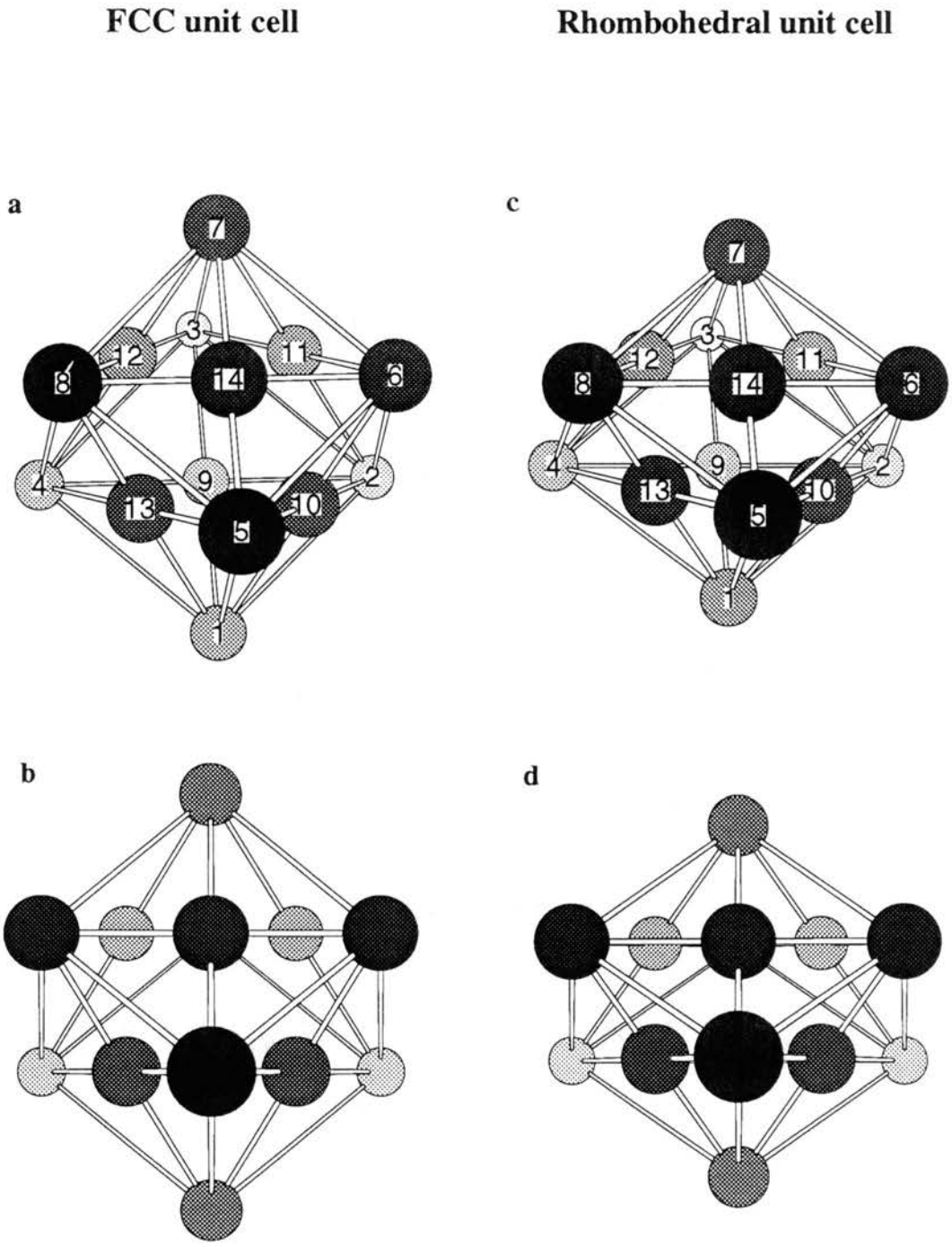

Figure 4. Computer generated models of (a and b) a unit cell of an fcc lattice and (c and d) a unit cell of a rhombohedral lattice.

Table III. Distances (arbitrary units) of TPM-silica in FCC and Rhombohedral Lattice

FCC		Rhombohedral	
Si(1)-Si(2)	10.000	Si(1)-Si(2)	9.527
Si(1)-Si(4)	10.000	Si(1)-Si(4)	9.527
Si(1)-Si(5)	10.000	Si(1)-Si(5)	9.527
Si(1)-Si(9)	7.069	Si(1)-Si(9)	6.382
Si(1)-Si(10)	7.069	Si(1)-Si(10)	6.382
Si(1)-Si(13)	7.069	Si(1)-Si(13)	6.369
Si(2)-Si(3)	10.000	Si(2)-Si(3)	9.527
Si(2)-Si(6)	10.000	Si(2)-Si(6)	9.527
Si(2)-Si(9)	7.070	Si(2)-Si(9)	7.074
Si(2)-Si(10)	7.070	Si(2)-Si(10)	7.074
Si(2)-Si(11)	7.069	Si(2)-Si(11)	6.383
Si(3)-Si(4)	10.000	Si(3)-Si(4)	9.528
Si(3)-Si(7)	10.000	Si(3)-Si(7)	9.526
Si(3)-Si(9)	7.071	Si(3)-Si(9)	6.380
Si(3)-Si(11)	7.071	Si(3)-Si(11)	7.069
Si(3)-Si(12)	7.070	Si(3)-Si(12)	7.072
Si(4)-Si(8)	10.000	Si(4)-Si(8)	9.527
Si(4)-Si(9)	7.071	Si(4)-Si(9)	7.076
Si(4)-Si(12)	7.070	Si(4)-Si(12)	6.382
Si(4)-Si(13)	7.070	Si(4)-Si(13)	7.075
Si(5)-Si(6)	10.000	Si(5)-Si(6)	9.526
Si(5)-Si(8)	10.000	Si(5)-Si(8)	9.528
Si(5)-Si(10)	7.072	Si(5)-Si(10)	7.074
Si(5)-Si(13)	7.071	Si(5)-Si(13)	7.084
Si(5)-Si(14)	7.070	Si(5)-Si(14)	6.380
Si(6)-Si(7)	10.000	Si(6)-Si(7)	9.527
Si(6)-Si(10)	7.072	Si(6)-Si(10)	6.381
Si(6)-Si(11)	7.070	Si(6)-Si(11)	7.075
Si(6)-Si(14)	7.070	Si(6)-Si(14)	7.071
Si(7)-Si(8)	10.000	Si(7)-Si(8)	9.525
Si(7)-Si(11)	7.072	Si(7)-Si(11)	6.384
Si(7)-Si(12)	7.072	Si(7)-Si(12)	6.389
Si(7)-Si(14)	7.072	Si(7)-Si(14)	6.387
Si(8)-Si(12)	7.070	Si(8)-Si(12)	7.068
Si(8)-Si(13)	7.072	Si(8)-Si(13)	6.382
Si(8)-Si(14)	7.071	Si(8)-Si(14)	7.072

The rhombohedral lattice has a 15% smaller d_{111}-spacing and is otherwise the same as the fcc lattice.

Table IV. Cartesian Coordinates of TPM-silica Particles in a FCC Lattice

	x	y	z
Si(1)	-0.000259	-8.659500	0.005264
Si(2)	7.070374	-2.889206	-4.080276
Si(3)	-0.001022	2.881073	-8.166428
Si(4)	-7.071487	-2.889800	-4.079666
Si(5)	-0.000687	-2.881454	8.166992
Si(6)	7.070450	2.888779	4.080444
Si(7)	0.000259	8.659500	-0.005264
Si(8)	-7.070847	2.889771	4.079865
Si(9)	-0.000061	-2.889862	-4.079773
Si(10)	3.534561	-2.886261	2.042542
Si(11)	3.535858	2.884247	-2.043106
Si(12)	-3.535614	2.884476	-2.043182
Si(13)	-3.534805	-2.886032	2.042465
Si(14)	0.000046	2.888123	4.080994

Table V. Internal Angles (°) of TPM-silica in a FCC Lattice

Si(2)-Si(1)-Si(4)	90.011	Si(3)-Si(4)-Si(12)	45.000	Si(12)-Si(7)-Si(14)	59.997
Si(2)-Si(1)-Si(5)	90.005	Si(3)-Si(4)-Si(13)	89.993	Si(4)-Si(8)-Si(5)	90.000
Si(2)-Si(1)-Si(9)	44.993	Si(8)-Si(4)-Si(9)	89.997	Si(4)-Si(8)-Si(7)	90.011
Si(2)-Si(1)-Si(10)	44.993	Si(8)-Si(4)-Si(12)	45.004	Si(4)-Si(8)-Si(12)	45.005
Si(2)-Si(1)-Si(13)	90.000	Si(8)-Si(4)-Si(13)	45.019	Si(4)-Si(8)-Si(13)	45.004
Si(4)-Si(1)-Si(5)	90.000	Si(9)-Si(4)-Si(12)	59.992	Si(4)-Si(8)-Si(14)	90.004
Si(4)-Si(1)-Si(9)	45.004	Si(9)-Si(4)-Si(13)	59.985	Si(5)-Si(8)-Si(7)	90.002
Si(4)-Si(1)-Si(10)	90.007	Si(12)-Si(4)-Si(13)	60.000	Si(5)-Si(8)-Si(12)	90.000
Si(4)-Si(1)-Si(13)	44.993	Si(1)-Si(5)-Si(6)	89.992	Si(5)-Si(8)-Si(13)	45.005
Si(5)-Si(1)-Si(9)	90.004	Si(1)-Si(5)-Si(8)	89.995	Si(5)-Si(8)-Si(14)	44.991
Si(5)-Si(1)-Si(10)	45.004	Si(1)-Si(5)-Si(10)	44.986	Si(7)-Si(8)-Si(12)	45.016
Si(5)-Si(1)-Si(13)	45.000	Si(1)-Si(5)-Si(13)	44.986	Si(7)-Si(8)-Si(13)	90.000
Si(9)-Si(1)-Si(10)	59.997	Si(1)-Si(5)-Si(14)	89.990	Si(7)-Si(8)-Si(14)	45.009
Si(9)-Si(1)-Si(13)	59.997	Si(6)-Si(5)-Si(8)	89.995	Si(12)-Si(8)-Si(13)	59.992
Si(10)-Si(1)-Si(13)	59.997	Si(6)-Si(5)-Si(10)	45.009	Si(12)-Si(8)-Si(14)	60.008
Si(1)-Si(2)-Si(3)	89.995	Si(6)-Si(5)-Si(13)	89.990	Si(13)-Si(8)-Si(14)	59.989
Si(1)-Si(2)-Si(6)	90.000	Si(6)-Si(5)-Si(14)	45.000	Si(1)-Si(9)-Si(2)	90.009
Si(1)-Si(2)-Si(9)	44.997	Si(8)-Si(5)-Si(10)	89.993	Si(1)-Si(9)-Si(3)	180.000
Si(1)-Si(2)-Si(10)	44.997	Si(8)-Si(5)-Si(13)	45.009	Si(1)-Si(9)-Si(4)	90.000
Si(1)-Si(2)-Si(11)	90.000	Si(8)-Si(5)-Si(14)	45.004	Si(2)-Si(9)-Si(3)	90.002
Si(3)-Si(2)-Si(6)	90.004	Si(10)-Si(5)-Si(13)	59.982	Si(2)-Si(9)-Si(4)	180.000
Si(3)-Si(2)-Si(9)	45.009	Si(10)-Si(5)-Si(14)	59.997	Si(3)-Si(9)-Si(4)	89.992
Si(3)-Si(2)-Si(10)	90.000	Si(13)-Si(5)-Si(14)	59.997	Si(1)-Si(10)-Si(2)	90.009
Si(3)-Si(2)-Si(11)	45.004	Si(2)-Si(6)-Si(5)	90.005	Si(1)-Si(10)-Si(5)	90.011
Si(6)-Si(2)-Si(9)	90.000	Si(2)-Si(6)-Si(7)	90.000	Si(1)-Si(10)-Si(6)	180.000
Si(6)-Si(2)-Si(10)	45.014	Si(2)-Si(6)-Si(10)	45.000	Si(2)-Si(10)-Si(5)	180.000
Si(6)-Si(2)-Si(11)	44.993	Si(2)-Si(6)-Si(11)	44.995	Si(2)-Si(10)-Si(6)	89.992
Si(9)-Si(2)-Si(10)	59.989	Si(2)-Si(6)-Si(14)	90.000	Si(5)-Si(10)-Si(6)	89.990
Si(9)-Si(2)-Si(11)	60.003	Si(5)-Si(6)-Si(7)	90.000	Si(2)-Si(11)-Si(3)	90.011
Si(10)-Si(2)-Si(11)	60.003	Si(5)-Si(6)-Si(10)	45.009	Si(2)-Si(11)-Si(6)	90.009
Si(2)-Si(3)-Si(4)	90.000	Si(5)-Si(6)-Si(11)	90.004	Si(2)-Si(11)-Si(7)	180.000
Si(2)-Si(3)-Si(7)	89.992	Si(5)-Si(6)-Si(14)	44.986	Si(3)-Si(11)-Si(6)	180.000
Si(2)-Si(3)-Si(9)	45.000	Si(7)-Si(6)-Si(10)	90.000	Si(3)-Si(11)-Si(7)	89.990
Si(2)-Si(3)-Si(11)	44.991	Si(7)-Si(6)-Si(11)	45.014	Si(6)-Si(11)-Si(7)	89.990
Si(2)-Si(3)-Si(12)	89.995	Si(7)-Si(6)-Si(14)	45.014	Si(3)-Si(12)-Si(4)	90.011
Si(4)-Si(3)-Si(7)	90.002	Si(10)-Si(6)-Si(11)	59.992	Si(3)-Si(12)-Si(7)	90.000
Si(4)-Si(3)-Si(9)	45.009	Si(10)-Si(6)-Si(14)	59.994	Si(3)-Si(12)-Si(8)	180.000
Si(4)-Si(3)-Si(11)	90.002	Si(11)-Si(6)-Si(14)	60.009	Si(4)-Si(12)-Si(7)	180.000
Si(4)-Si(3)-Si(12)	44.997	Si(3)-Si(7)-Si(6)	90.005	Si(4)-Si(12)-Si(8)	90.000
Si(7)-Si(3)-Si(9)	89.995	Si(3)-Si(7)-Si(8)	89.995	Si(7)-Si(12)-Si(8)	89.990
Si(7)-Si(3)-Si(11)	45.011	Si(3)-Si(7)-Si(11)	45.009	Si(1)-Si(13)-Si(4)	90.009
Si(7)-Si(3)-Si(12)	45.005	Si(3)-Si(7)-Si(12)	44.998	Si(1)-Si(13)-Si(5)	90.014
Si(9)-Si(3)-Si(11)	59.990	Si(3)-Si(7)-Si(14)	90.000	Si(1)-Si(13)-Si(8)	180.000
Si(9)-Si(3)-Si(12)	59.997	Si(6)-Si(7)-Si(8)	90.005	Si(4)-Si(13)-Si(5)	180.000
Si(11)-Si(3)-Si(12)	60.006	Si(6)-Si(7)-Si(11)	45.000	Si(4)-Si(13)-Si(8)	89.988
Si(1)-Si(4)-Si(3)	89.997	Si(6)-Si(7)-Si(12)	90.000	Si(5)-Si(13)-Si(8)	89.992
Si(1)-Si(4)-Si(8)	90.007	Si(6)-Si(7)-Si(14)	45.000	Si(5)-Si(14)-Si(6)	90.014
Si(1)-Si(4)-Si(9)	44.997	Si(8)-Si(7)-Si(11)	90.004	Si(5)-Si(14)-Si(7)	180.000
Si(1)-Si(4)-Si(12)	89.995	Si(8)-Si(7)-Si(12)	45.000	Si(5)-Si(14)-Si(8)	90.011
Si(1)-Si(4)-Si(13)	44.993	Si(8)-Si(7)-Si(14)	45.005	Si(6)-Si(14)-Si(7)	89.992
Si(3)-Si(4)-Si(8)	89.993	Si(11)-Si(7)-Si(12)	59.997	Si(6)-Si(14)-Si(8)	180.000
Si(3)-Si(4)-Si(9)	45.009	Si(11)-Si(7)-Si(14)	59.997	Si(7)-Si(14)-Si(8)	89.985

Table VI. Cartesian Coordinates of TPM-silica Particles in a Rhombohedral Lattice

	x	y	z
Si(1)	0.036362	-6.034439	-0.012909
Si(2)	7.083420	-1.084610	-4.087570
Si(3)	-0.018692	3.780090	-8.169281
Si(4)	-7.066132	-1.178452	-4.103806
Si(5)	0.006012	-1.142776	8.162323
Si(6)	7.045792	3.813080	4.083786
Si(7)	-0.057098	8.676773	0.002014
Si(8)	-7.096222	3.714462	4.071014
Si(9)	0.009323	-1.129654	-4.095795
Si(10)	3.543000	-1.111618	2.036240
Si(11)	3.506668	3.790756	-2.042389
Si(12)	-3.557312	3.739487	-2.046738
Si(13)	-3.527573	-1.163834	2.022476
Si(14)	-0.024826	3.759979	4.079178

Table VII. Internal Angles (°) of TPM-silica in a Rhombohedral Lattice

Si(2)-Si(1)-Si(4)	95.912	Si(3)-Si(4)-Si(12)	47.920	Si(12)-Si(7)-Si(14)	67.206
Si(2)-Si(1)-Si(5)	95.889	Si(3)-Si(4)-Si(13)	89.911	Si(4)-Si(8)-Si(5)	95.985
Si(2)-Si(1)-Si(9)	47.948	Si(8)-Si(4)-Si(9)	89.922	Si(4)-Si(8)-Si(7)	84.185
Si(2)-Si(1)-Si(10)	47.943	Si(8)-Si(4)-Si(12)	47.885	Si(4)-Si(8)-Si(12)	42.056
Si(2)-Si(1)-Si(13)	98.816	Si(8)-Si(4)-Si(13)	42.057	Si(4)-Si(8)-Si(13)	47.952
Si(4)-Si(1)-Si(5)	95.992	Si(9)-Si(4)-Si(12)	56.257	Si(4)-Si(8)-Si(14)	90.067
Si(4)-Si(1)-Si(9)	47.962	Si(9)-Si(4)-Si(13)	59.924	Si(5)-Si(8)-Si(7)	84.155
Si(4)-Si(1)-Si(10)	98.879	Si(12)-Si(4)-Si(13)	56.241	Si(5)-Si(8)-Si(12)	90.014
Si(4)-Si(1)-Si(13)	47.952	Si(1)-Si(5)-Si(6)	84.111	Si(5)-Si(8)-Si(13)	48.030
Si(5)-Si(1)-Si(9)	98.881	Si(1)-Si(5)-Si(8)	84.010	Si(5)-Si(8)-Si(14)	42.036
Si(5)-Si(1)-Si(10)	47.945	Si(1)-Si(5)-Si(10)	42.063	Si(7)-Si(8)-Si(12)	42.134
Si(5)-Si(1)-Si(13)	48.037	Si(1)-Si(5)-Si(13)	41.954	Si(7)-Si(8)-Si(13)	81.249
Si(9)-Si(1)-Si(10)	67.352	Si(1)-Si(5)-Si(14)	81.105	Si(7)-Si(8)-Si(14)	42.105
Si(9)-Si(1)-Si(13)	67.315	Si(6)-Si(5)-Si(8)	95.844	Si(12)-Si(8)-Si(13)	56.280
Si(10)-Si(1)-Si(13)	67.353	Si(6)-Si(5)-Si(10)	42.052	Si(12)-Si(8)-Si(14)	60.016
Si(1)-Si(2)-Si(3)	84.094	Si(6)-Si(5)-Si(13)	89.948	Si(13)-Si(8)-Si(14)	56.366
Si(1)-Si(2)-Si(6)	84.106	Si(6)-Si(5)-Si(14)	47.922	Si(1)-Si(9)-Si(2)	89.995
Si(1)-Si(2)-Si(9)	42.056	Si(8)-Si(5)-Si(10)	89.920	Si(1)-Si(9)-Si(3)	180.000
Si(1)-Si(2)-Si(10)	42.064	Si(8)-Si(5)-Si(13)	42.061	Si(1)-Si(9)-Si(4)	89.981
Si(1)-Si(2)-Si(11)	81.102	Si(8)-Si(5)-Si(14)	47.922	Si(2)-Si(9)-Si(3)	90.014
Si(3)-Si(2)-Si(6)	95.856	Si(10)-Si(5)-Si(13)	59.922	Si(2)-Si(9)-Si(4)	180.000
Si(3)-Si(2)-Si(9)	42.040	Si(10)-Si(5)-Si(14)	56.276	Si(3)-Si(9)-Si(4)	90.011
Si(3)-Si(2)-Si(10)	89.985	Si(13)-Si(5)-Si(14)	56.304	Si(1)-Si(10)-Si(2)	90.000
Si(3)-Si(2)-Si(11)	47.900	Si(2)-Si(6)-Si(5)	95.895	Si(1)-Si(10)-Si(5)	89.997
Si(6)-Si(2)-Si(9)	90.019	Si(2)-Si(6)-Si(7)	84.141	Si(1)-Si(10)-Si(6)	180.000
Si(6)-Si(2)-Si(10)	42.049	Si(2)-Si(6)-Si(10)	47.943	Si(2)-Si(10)-Si(5)	180.000
Si(6)-Si(2)-Si(11)	47.953	Si(2)-Si(6)-Si(11)	42.073	Si(2)-Si(10)-Si(6)	90.005
Si(9)-Si(2)-Si(10)	60.032	Si(2)-Si(6)-Si(14)	89.972	Si(5)-Si(10)-Si(6)	90.000
Si(9)-Si(2)-Si(11)	56.280	Si(5)-Si(6)-Si(7)	84.150	Si(2)-Si(11)-Si(3)	90.035
Si(10)-Si(2)-Si(11)	56.296	Si(5)-Si(6)-Si(10)	47.948	Si(2)-Si(11)-Si(6)	89.974
Si(2)-Si(3)-Si(4)	95.903	Si(5)-Si(6)-Si(11)	89.967	Si(2)-Si(11)-Si(7)	180.000
Si(2)-Si(3)-Si(7)	84.144	Si(5)-Si(6)-Si(14)	42.056	Si(3)-Si(11)-Si(6)	180.000
Si(2)-Si(3)-Si(9)	47.946	Si(7)-Si(6)-Si(10)	81.214	Si(3)-Si(11)-Si(7)	90.019
Si(2)-Si(3)-Si(11)	42.073	Si(7)-Si(6)-Si(11)	42.071	Si(6)-Si(11)-Si(7)	89.974
Si(2)-Si(3)-Si(12)	89.951	Si(7)-Si(6)-Si(14)	42.100	Si(3)-Si(12)-Si(4)	90.028
Si(4)-Si(3)-Si(7)	84.176	Si(10)-Si(6)-Si(11)	56.296	Si(3)-Si(12)-Si(7)	89.946
Si(4)-Si(3)-Si(9)	47.955	Si(10)-Si(6)-Si(14)	56.294	Si(3)-Si(12)-Si(8)	180.000
Si(4)-Si(3)-Si(11)	89.990	Si(11)-Si(6)-Si(14)	59.947	Si(4)-Si(12)-Si(7)	180.000
Si(4)-Si(3)-Si(12)	42.052	Si(3)-Si(7)-Si(6)	95.860	Si(4)-Si(12)-Si(8)	90.056
Si(7)-Si(3)-Si(9)	81.252	Si(3)-Si(7)-Si(8)	95.833	Si(7)-Si(12)-Si(8)	89.971
Si(7)-Si(3)-Si(11)	42.082	Si(3)-Si(7)-Si(11)	47.904	Si(1)-Si(13)-Si(4)	90.091
Si(7)-Si(3)-Si(12)	42.124	Si(3)-Si(7)-Si(12)	47.931	Si(1)-Si(13)-Si(5)	90.009
Si(9)-Si(3)-Si(11)	56.325	Si(3)-Si(7)-Si(14)	98.734	Si(1)-Si(13)-Si(8)	180.000
Si(9)-Si(3)-Si(12)	56.287	Si(6)-Si(7)-Si(8)	95.854	Si(4)-Si(13)-Si(5)	180.000
Si(11)-Si(3)-Si(12)	59.943	Si(6)-Si(7)-Si(11)	47.952	Si(4)-Si(13)-Si(8)	89.992
Si(1)-Si(4)-Si(3)	84.090	Si(6)-Si(7)-Si(12)	98.704	Si(5)-Si(13)-Si(8)	89.911
Si(1)-Si(4)-Si(8)	84.012	Si(6)-Si(7)-Si(14)	47.917	Si(5)-Si(14)-Si(6)	90.030
Si(1)-Si(4)-Si(9)	42.063	Si(8)-Si(7)-Si(11)	98.662	Si(5)-Si(14)-Si(7)	180.000
Si(1)-Si(4)-Si(12)	81.053	Si(8)-Si(7)-Si(12)	47.900	Si(5)-Si(14)-Si(8)	90.037
Si(1)-Si(4)-Si(13)	41.961	Si(8)-Si(7)-Si(14)	47.934	Si(6)-Si(14)-Si(7)	89.983
Si(3)-Si(4)-Si(8)	95.809	Si(11)-Si(7)-Si(12)	67.152	Si(6)-Si(14)-Si(8)	180.000
Si(3)-Si(4)-Si(9)	42.040	Si(11)-Si(7)-Si(14)	67.198	Si(7)-Si(14)-Si(8)	89.951

SEM ANALYSIS

Our earlier reports showed SEM images of hexagonal particle orders only of the surface layers of silica-PMMA[6,7] and silica-PMA[8] composites and not the particle order in the bulk. Now we have microtomed the composites both parallel and perpendicular to the film surface to observe the bulk particle order. The SEM images of the 40 wt % TPM-silica-PMA composite and the swollen repolymerized silica-PMA composite microtomed parallel to the film plane, show hexagonal order.

Figure 5a shows the SEM images of the 40 wt % TPM-silica-PMA composite microtomed parallel to the surface, while Figure 5b shows the model hexagonal arrays of the particles which represent d_{111} planes of a rhombohedral lattice. Similarly, Figures 6a and 6b show the SEM image of the swollen repolymerized silica-PMA composite microtomed parallel to the film plane and the model particle arrays for 100 planes of an hcp lattice, respectively. Similar order of polystyrene particles in hydrogels also has been observed by freeze fracture electron microscopy.[47] By measuring the center-to-center interparticular distance in the hexagonal order, the D_0 in the d_{111} planes of the rhombohedral lattice or the lattice constant a of an hcp lattice was measured.[54]

The SEM images of the 40 wt % TPM-silica-PMA composite and the swollen repolymerized composite obtained from films microtomed perpendicular to the film plane are shown in Figures 7a and 8a. The arrangements of particles in parallelograms represent either d_{110} planes of rhombohedral or 110 planes of hcp crystals. As shown in Figures 7b and 8b, the interparticle distances between the ordered diagonal arrays give the constant a of the rhombohedral lattice or the constant c of hcp, which is twice the d spacing, while the interparticle distances between the horizontal planes (which bisect the diagonal arrays at an acute angle) give the d_{111} spacings of a unit cell of rhombohedral lattice.

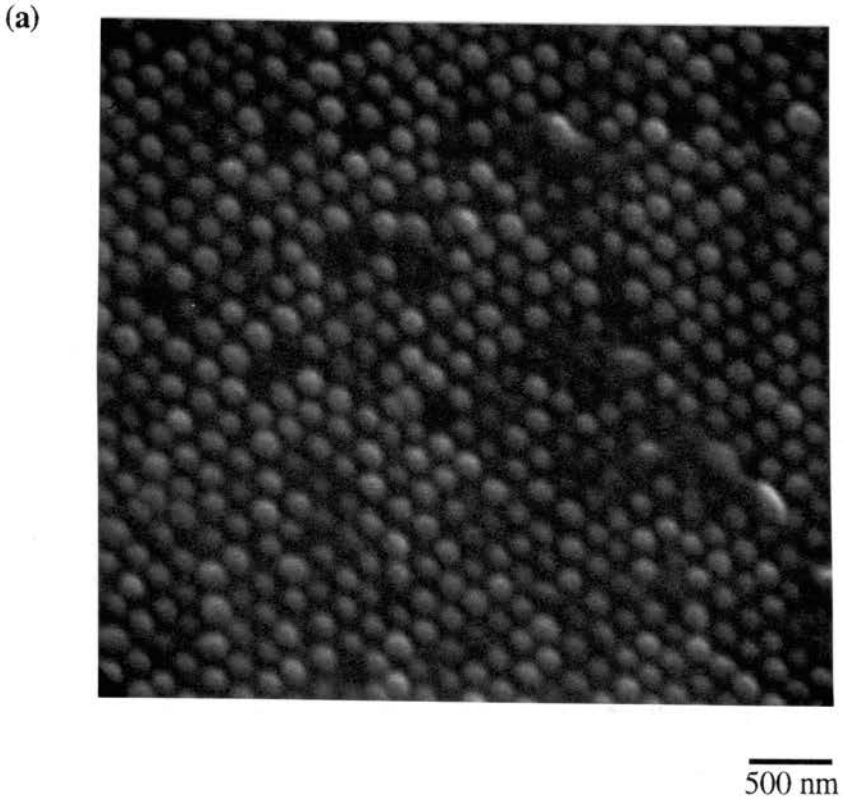

Figure 5. (a) SEM image of a 40 wt % 153 nm TPM-silica-PMA composite film, microtomed parallel to film plane and (b) regular hexagonal model of a d_{111} plane. Film thickness = 470 μm.

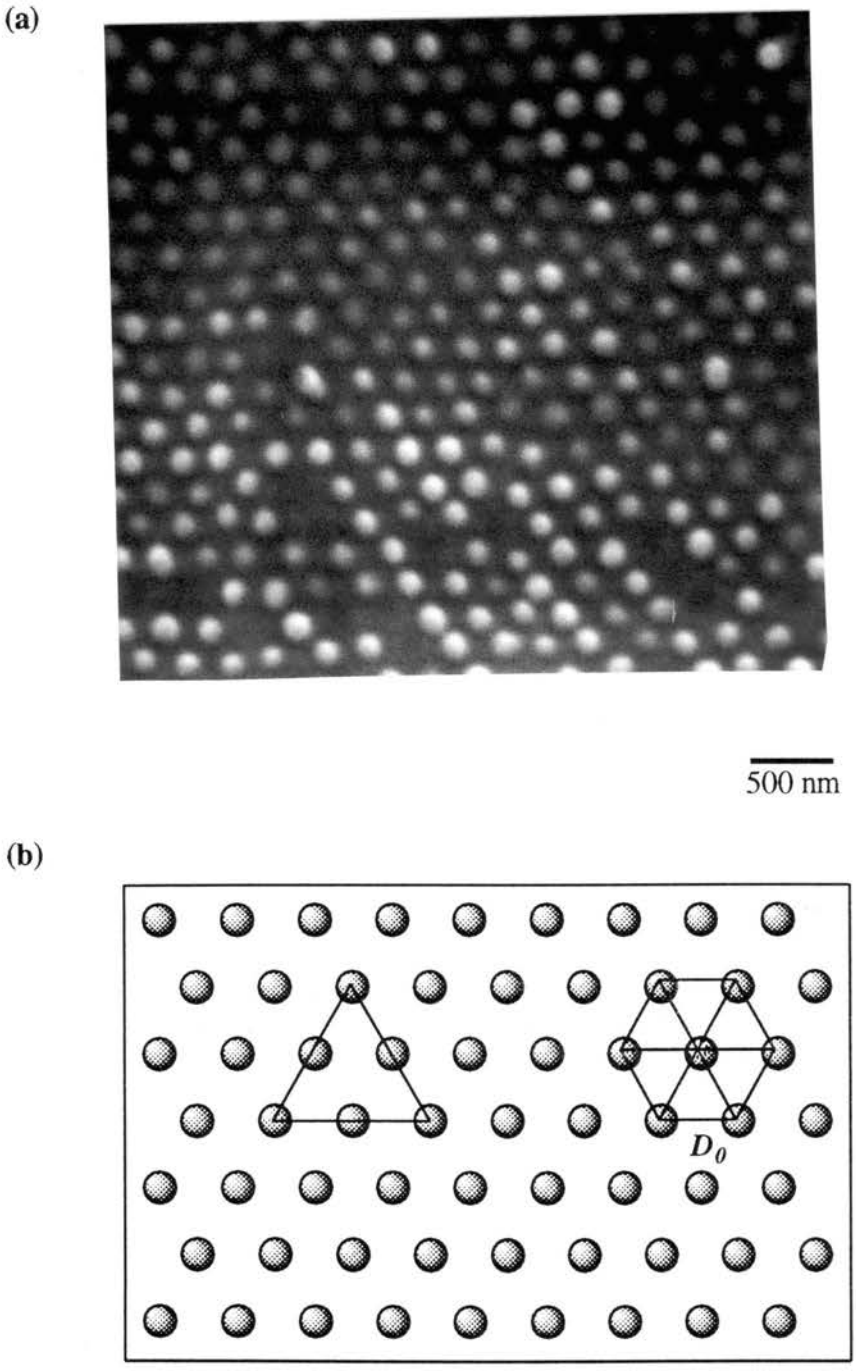

Figure 6. (a) SEM image of a 40 wt % 153 nm TPM-silica-PMA composite film swollen with MA, polymerized, and microtomed parallel to film plane and, (b) regular hexagonal model of a d_{111} plane. Film thickness = 590 μm.

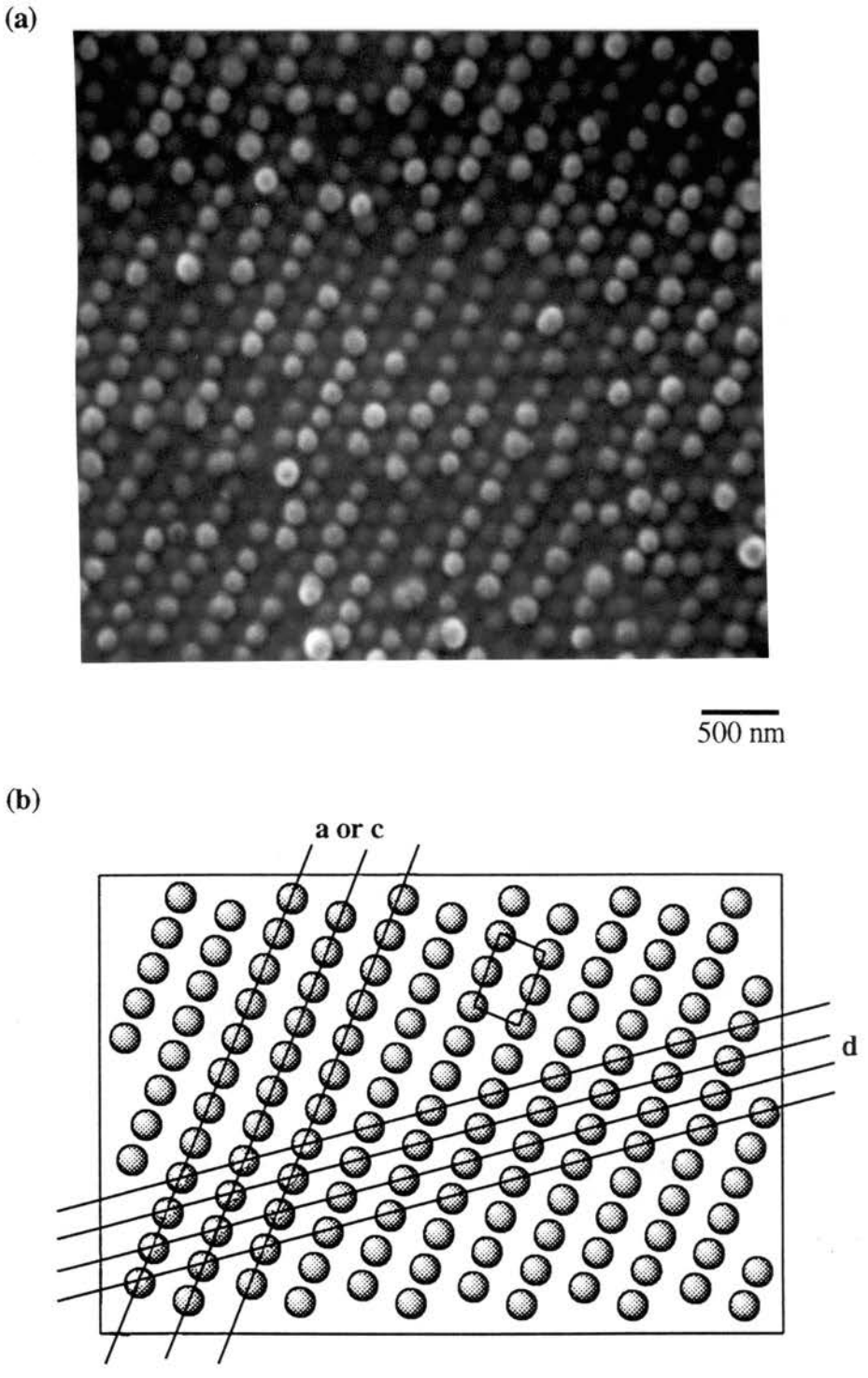

Figure 7. (a) SEM image of a 40 wt % 153 nm TPM-silica-PMA composite film, microtomed perpendicular to the film plane and (b) rectangular particle order of a d_{110} plane. Film thickness = 470 μm.

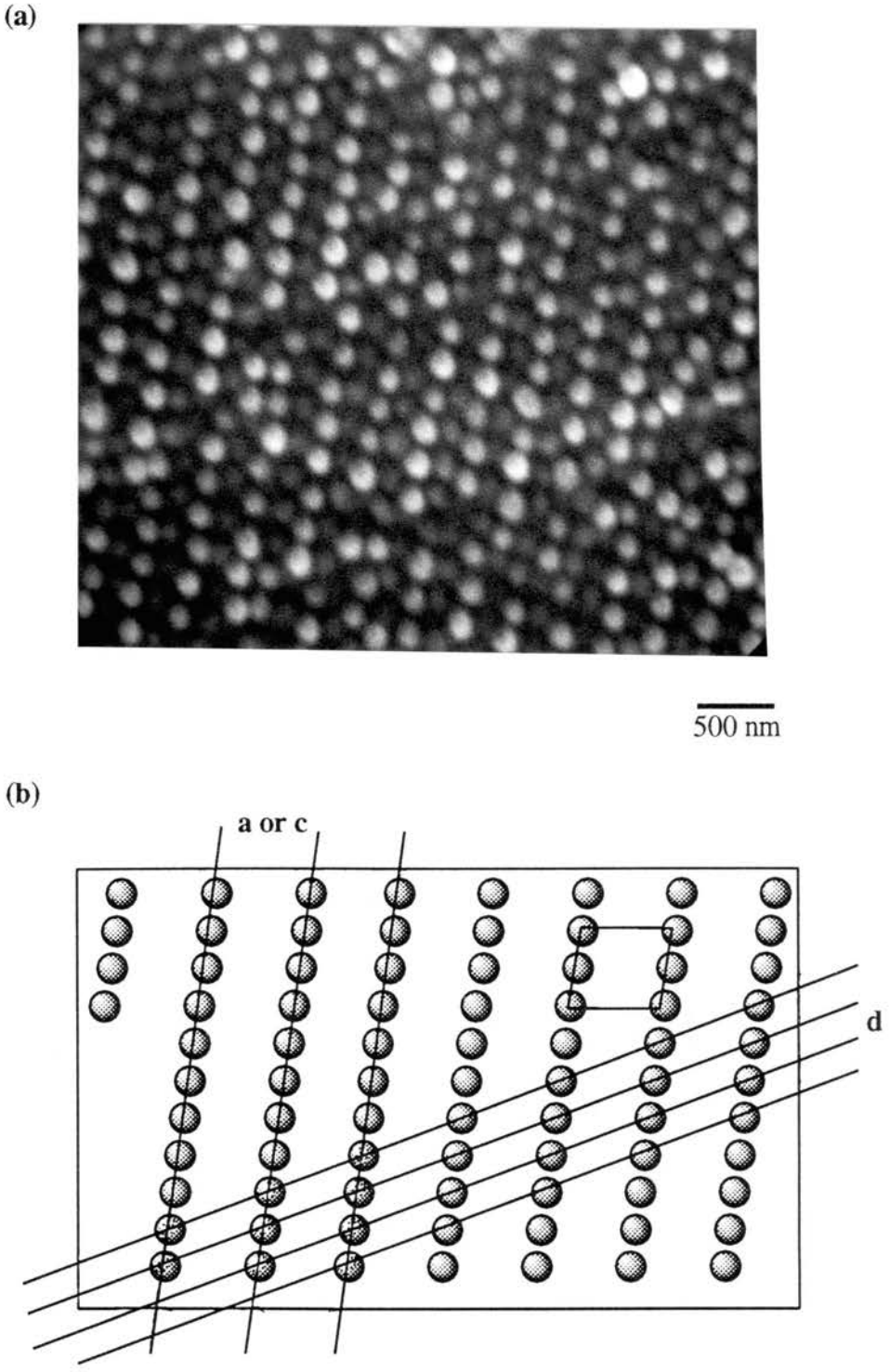

Figure 8. (a) SEM image of a 40 wt % 153 nm TPM-silica-PMA composite film swollen with MA, polymerized, and microtomed perpendicular to the film plane (b) parallelogram like particle order of a d_{110} plane. Film thickness = 590 μm.

In Table VIII, the lattice constant *a* and the *d* spacings measured from the SEM micrographs assuming a rhombohedral crystal structure, and the lattice constants *a*, *c*, and the *d* spacing of an hcp lattice are in close agreement with *a*, *c* and *d* calculated from optical diffraction of TPM-silica in PMA and swollen repolymerized PMA films. This supports our model of a rhombohedral crystal structure in the original composite film that remains rhombohedral on swelling with MA and on polymerization of imbibed MA.

Table VIII. Crystal Parameters of Ordered 153 nm TPM-silica in PMA Composite

		SEM[a]			Bragg diffraction[b]				
		fcc and hcp			fcc		hcp		
plane	2D order	a (nm)	d_{111} (nm)	c (nm)	a (nm)	d_{111} (nm)	a (nm)	d_{111} (nm)	c (nm)
110[c]	parallelogram	325	167	----	322	166	----	----	----
100[c]	hexagon	218	----	----	----	----	221	----	----
110[c]	rectangle	----	165	330	----	----	----	166	332
110[d]	parallelogram	413	225	----	393	222	----	----	----
100[d]	hexagon	304	----	----	----	----	310	----	----
110[d]	rectangle	----	206	413	----	----	----	222	445

[a] Crystal parameters *a* and *d* calculated from the interparticular distance from the SEM images, assuming a rhombohedral crystal structure. [b] Calculated from the Bragg equation assuming a rhombohedral crystal structure. [c] These planes were observed from the polymerized TPM-silica-PMA composite (B). [d] These planes were observed from the swollen and repolymerized composite (D). The blank spaces in the table indicate that the crystal lattice spacings could not be calculated from the microtomed section of the films.

CONCLUSIONS

Monodisperse TPM-silica in an MA dispersion self assembles into hexagonally ordered planes which then form either a fcc lattice or a mixture of fcc and hcp lattices. On

photopolymerization of MA, the fcc lattice is transformed to a rhombohedral lattice since the monomer volume change occurs only in the thick part of the composite. The silica-PMA composite swelled with MA and then shrank during further polymerization of the imbibed MA. Bragg diffraction wavelengths, observed spectrophotometrically as narrow % T peaks at each stage of the process, are in close agreement with the proposed lattice transformations. Although the SEM analysis only provides two-dimensional structural information, the interparticle spacings measured from the SEM images support the proposed lattice transformations.

REFERENCES

1. Iler, R. K. *The Chemistry of Silica*; Wiley; New York, 1979; pp 582-588.
2. Sanchez, C.; Ribot, F. *New J. Chem.* **1994**, *18*, 1007.
3. Mark, J. E.; Lee, C. Y.-C.; Biancone, P. A., Eds. *Hybrid Organic-Inorganic Composites*; ACS Symposium Series 585; American Chemical Society; Washington, DC, 1995.
4. Landry, C. J. T.; Coltrain, B. K.; Brady, B. K. *Polymer* **1992**, *33*, 1486.
5. Pope, E. J. A.; Asami, M.; Mackenzie, J. D. *J. Mater. Res.* **1989**, *4*, 1018.
6. Sunkara, H. B.; Jethmalani, J. M.; Ford, W. T. *Chem. Mater.* **1994**, *6*, 362.
7. Sunkara H. B.; Jethmalani J. M.; Ford, W. T. *ACS Symp. Ser.* **1995**, *585*, 181-191.
8. Jethmalani, J.; Ford, W. T. *Chem.. Mater.*, **1996**, *8*, 000.
9. Pieranski, P. *Contemp. Phys.*, **1983**, *24*, 25.
10. Dhont, J. K. G.; Smits, C.; Lekkerkerker, H. N. W. *J. Coll. Interface Sci.* **1992v**, *152*, 386.
11. Okubo, T. *Langmuir* **1994**, *10*, 1695.
12. Hiltner, P. A.; Krieger, I. M. *J. Phys. Chem.* **1969**, *73*, 2386.
13. Okubo, T. *Colloid Polym. Sci.* **1993**, *271*, 190.
14. Okubo, T. *J. Chem. Soc., Faraday Trans. 1*, **1986**, *82*, 3163.
15. Okubo, T. *J. Chem. Soc., Faraday Trans. 1*, **1986**, *82*, 3175.
16. Dosho, S.; Ise, N.; Ito, K.; Iwai, S.; Kitano, H.; Matsuoka, H.; Nakamura, H.; Okumura, H.; Ono, T.; Sogami, I. S.; Ueno, Y.; Yoshida, H.; Yoshiyama, T. *Langmuir*, **1993**, *9*, 394.
17. Krieger, I. M.; Hiltner, P. A. *Polymer Colloids Proceedings*, ACS Symposium on Polymer Colloids, Ed. R. Fitch, Plenum Press, New York, NY, 1971, 63.
18. Asher, S. A.; Kesavamoorthy, R.; Jagannathan, S.; Rundquist, P. A. *Nonlinear Optics III* **1992**, *SPIE Vol. 1626*, 238.
19. Asher, S. A. US Patent 4,627,689, 1986.

20. Asher, S. A.; Jagannathan S. US Patent 5,281,370, 1994.

21. Flaugh, P. L.; O'Donnell, S. E.; Asher, S. A. *Appl. Spectrosc.* **1984**, *38*, 847.

22. Asher, S. A.; Flaugh, P. L.; Washinger, G. *Spectroscopy* **1986**, *1*, 26.

23. Okubo, T. *Prog. Polym. Sci.* **1993**, *18*, 481.

24. Okubo, T. *Colloid Polym. Sci.* **1993**, *271*, 873.

25. Okubo, T. *J. Chem. Phys.* **1988**, *88*, 6581.

26. Asher, S. A.; Holtz, J.; Liu, L.; Wu, Z. *J. Am. Chem. Soc.* **1994**, *116*, 4997.

27. Panzer, H. P., Giovanni, L.; Cohen, M. L.; Yen, W. S. US Patent 5,338,492, 1994.

28. Haacke, G.; Panzer, H. P.; Magliocco, L. G.; Asher, S. A. US Patent 5,266,238, 1993.

29. Williams, R; Crandall, R. S. *Phys. Lett.* **1974**, *48A*, 225.

30. Clark, N. A.; Hurd, A. J.; Ackerson, B. J. *Nature*, **1979**, *281*, 57.

31. Carlson, R. J.; Asher, S. A. *Appl. Spectrosc.* **1984**, *38*, 297.

32. Yoshiyama, T. *Polymer*, **1986**, *27*, 827.

33. Rundquist, P. A.; Photinos, P.; Jagannathan, S.; Asher, S. A. *J. Chem. Phys.* **1989**, *91*, 4932.

34. Monovoukas, Y.; Gast, A. P. *J. Coll. Interface Sci.* **1989**, *128*, 533.

35. Kesavamoorthy, R. Tandon, S.; Xu, S.; Jagannathan, S.; Asher, S. A. *J. Coll. Interface Sci.* **1992**, *153*, 188.

36. Kose, A.; Ozaki, M.; Takano, K.; Kobayashi, Y.; Hachisu, S. *J. Coll. Interface Sci.* **1973**, *44*, 330.

37. Hachisu, S.; Yoshimura, S. *Nature*, **1980**, *283*, 188.

38. Ise, N.; Okubo, T.; Sugimura, M.; Ito, K.; Nolte, H. J. *J. Chem. Phys.*, **1983**, *78*, 536.

39. Okubo, T. *J. Chem. Phys.* **1987**, *86*, 2394.

40. Monovoukas, Y.; Gast, A. P. *Phase Transitions* **1990**, *21*, 183.

41. Monovoukas, Y.; Gast, A. P. *Langmuir* **1991**, *7*, 460.

42. Van Winkle, D. H.; Murray, C. A. *Phys. Rev.A.*, **1986**, *34*, 562.

43. Murray, C. A.; Van Winkle, D. H. *Phys. Rev. Lett.* **1987**, *58*, 1200.

44. Murray, C. A.; Wenk, R. A. *Phys. Rev. Lett.* **1989**, *62*, 1643.

45. Hug, J. E.; Van Swol, F.; Zukoski, C. F. *Langmuir*, **1995**, *11*, 111.

46. Yoshimura, T.; Sogami, I. S. *Langmuir*, **1987**, *3*, 851.

47. Cohen, J. A.; Scales, D. J.; Ou-Yang, H. D.; Chaikin, P. M. *J. Coll. Interface Sci.* **1993**, *156*, 137.

48. Goodwin, J. W.; Ottewill, R. H.; Parentich, A. *J. Phys. Chem.* **1986**, *84*, 1580.

49. Kamenetzky, E. A.; Magliocco, L. G.; Panzer, H. P. *Science*, **1994,** *264*, 207.

50. Ishizu, K.; Sugita, M.; Kotsubo, H.; Saito, R. *J. Colloid Interface Sci*. **1995**, *169*, 456.

51. Matsuoka, H.; Ise, N. *Chemtracts Macromol. Chem.* **1993**, *4*, 59.

52. Konishi, T.; Ise, N. *J. Am. Chem. Soc.* **1995**, *117*, 8422.

53. Loose, W.; Ackerson, B. J. *J. Chem. Phys.* **1994**, *101*, 7211.

54. Cullity, B. D. *Elements of X-ray Diffraction*, Addison-Wesley Publishing Company, Inc.; Massachusetts, 1978, pp 330-337.

CHAPTER VI

THERMAL PROPERTIES OF SILICA POLYMER COMPOSITES

ABSTRACT

Colloidal crystals of monodisperse amorphous 152 nm TPM-silica particles are trapped in PMMA and PMA composite films. Differential scanning calorimetry (DSC) analyses show that the crystal order increases the glass transition (T_g) temperatures compared with the PMMA films which contain randomly distributed silica particles and pure PMMA film. Thermogravimetric analysis (TGA) of the PMA composite films containing ordered, randomly distributed and aggregated silica particles show decomposition temperatures between 375 and 410 °C.

INTRODUCTION

Inorganic-organic composites have improved optical, mechanical and thermal properties compared to either of the two components. Most of these composites are blends of immiscible inorganics in organic polymers, where the degree of mixing increases the strength and tensile modulus of the final composites. Among the inorganics, carbon black and silica have been most widely used as fillers to reinforce the organic polymers.[1-4] To increase the compatibility between the silica and the polymer matrix, surface coupling agents such as TPM or polymers of MMA, styrene, and N-vinylcarbazole have been grafted on the surface of colloidal silica.[5-7]

Hybrids of silica with polyimide,[8,9] poly(tetramethylene oxide)[10] and polyacrylonitrile[11] have been made where TEOS undergoes either acidic or basic hydrolysis in a solution containing functionalized silane copolymer to colloidal particles. One such example is that of a MMA-co-TPM polymer where the alkoxy silane groups undergo hydrolysis via the sol-gel approach to form silica particles that are randomly distributed in the PMMA matrix. Such hybrid materials have increased T_g's compared with pure PMMA films.[2,12] In the case of polyimide-silica made by the sol-gel approach in polyamic acid followed by heating at high temperatures to form the polyimides, the T_g was reduced by increasing the silica content, the decomposition temperature was not affected, and the amount of residue left behind was proportional to the silica content.[8]

Tacticity in the backbone of PMMA has been known to influence the T_g values. Pure syndiotactic PMMA has a T_g of 160 °C and pure isotactic PMMA has a T_g of 43 °C.[13,14] Commercial PMMA and PMMA made by other polymerization techniques have yielded mixtures of syndiotactic and isotactic structures.

Monodisperse charged colloidal particles in aqueous and non-aqueous dispersions spontaneously self assemble into a three dimensional lattice known as a colloidal crystal.

We have ordered monodisperse amorphous colloidal TPM-silica in MMA and MA dispersions. On photopolymerization of the monomer dispersions, the colloidal crystals are stabilized in the silica-polymer composites.[15-17] Covalent linkage between the TPM-silica particles and the PMMA or PMA matrix enhances the mechanical properties, stabilizes the crystal order and orientations as compared to other ordered colloidal crystals in aqueous or non-aqueous dispersions. Ordered silica-PMMA films are thermoplastic like the parent polymer, robust and stable even after heating to 150 °C, while the silica-PMA composites are elastomeric, and the diffraction wavelength has been tuned by stretching and swelling.[15-17] The aim of the research reported here is to understand the effect of the ordering of silica particles on the thermal properties of the composite films.

RESULTS AND DISCUSSION

DSC ANALYSIS

The T_g's of pure PMMA, PMMA composite with randomly distributed TPM-silica and PMMA composite film with colloidal crystals of TPM-silica trapped in the matrices were analyzed by DSC at a scan rate of 10 K/min. Figures 1, 2 and 3 show the thermograms for pure PMMA, randomly distributed TPM-silica in PMMA and ordered TPM-silica in PMMA composite films, respectively. All films were scanned at least three to four times and the T_g's of the fourth scan were interpolated and are given in Table I. The first two scans on such composite films showed weak T_g values, and therefore the composites were analyzed four times. Two different batches of ordered TPM-silica in PMMA were analyzed

We have observed an increase in the T_g of PMMA from 102 to 116 °C by only incorporating 152 or 153 nm TPM-silica which is randomly distributed in the PMMA matrix. The increase could arise due to the presence of silica as filler and due to the

cross-linking effect produced by the copolymerization of the methacrylate end of TPM with the PMMA matrix.

Table I. Glass Transition Temperatures (T_g) of PMMA Films [a]

sample	T_g (°C)[b]	T_g (°C)[c]
pure PMMA film[d]	102	102
PMMA composite without colloidal crystals	116	117
PMMA composite with colloidal crystals	124	125

[a] The reported T_g values (± 1 °C)are from the third or fourth heating. [b] PMMA with 35 wt % 152 nm TPM-silica particles. [c] PMMA with 40 wt % 153 nm TPM-silica particles. [d] PMMA films were made by photopolymerizing MMA dispersions with 1 wt % DMPA similar to other silica-PMMA composites.

It is well-known that the tacticity of the polymer affects the T_g, and the reported T_g of a 0.59 syndiotactic, 0.31 heterotactic and 0.10 isotactic PMMA was 114.2 °C.[18] For a pure syndiotactic PMMA and a pure isotactic PMMA, the T_g has been estimated to be 160 °C and 43 °C, respectively.[13] These discrepancies in the tacticities arise from various methods of PMMA syntheses. At this time, we are not sure if the increase in the T_g values for the randomly distributed silica in PMMA is due to silica which acts as a filler, or to crosslinking between the silica particles and the PMMA matrix. We have also seen an increase in the T_g value from 116 to 125 °C, when colloidal crystals of silica having dimensions 100 to 250 μm are trapped in the PMMA matrix. This may also be due to the presence of regular spatial distribution of silica particles in the matrix which reduces the motion of the polymer chains. At this time, we are not sure about the reason for the increase in the T_g of the silica-PMMA composite. The possible influence of tacticity can be tested by measuring the ratio of syndiotactic and isotactic structural units in the composite films, and such work is under way at our laboratory.

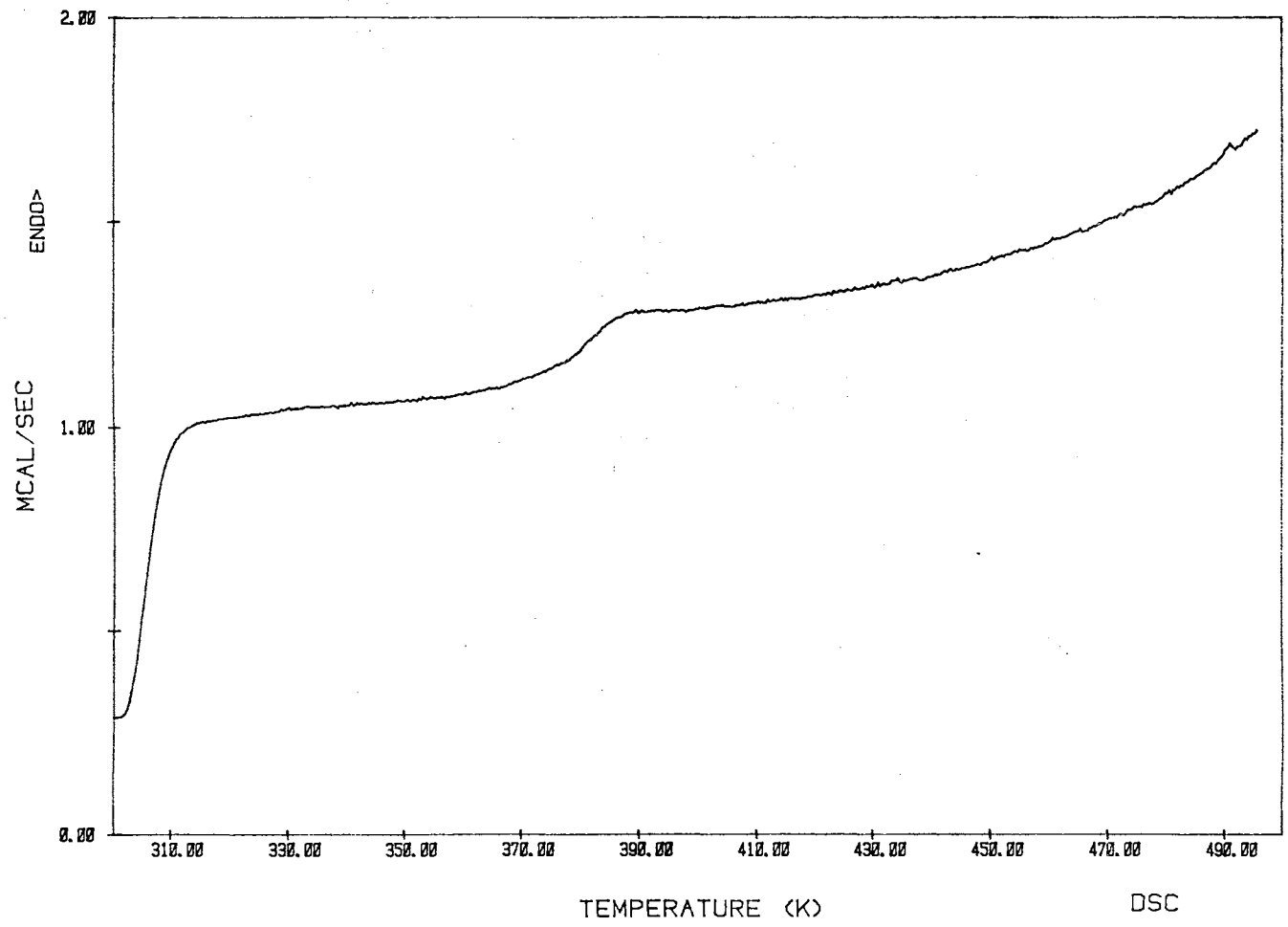

Figure 1. DSC thermogram of a pure PMMA film at a scan rate of 10 K/min (sample weight = 20 mg).

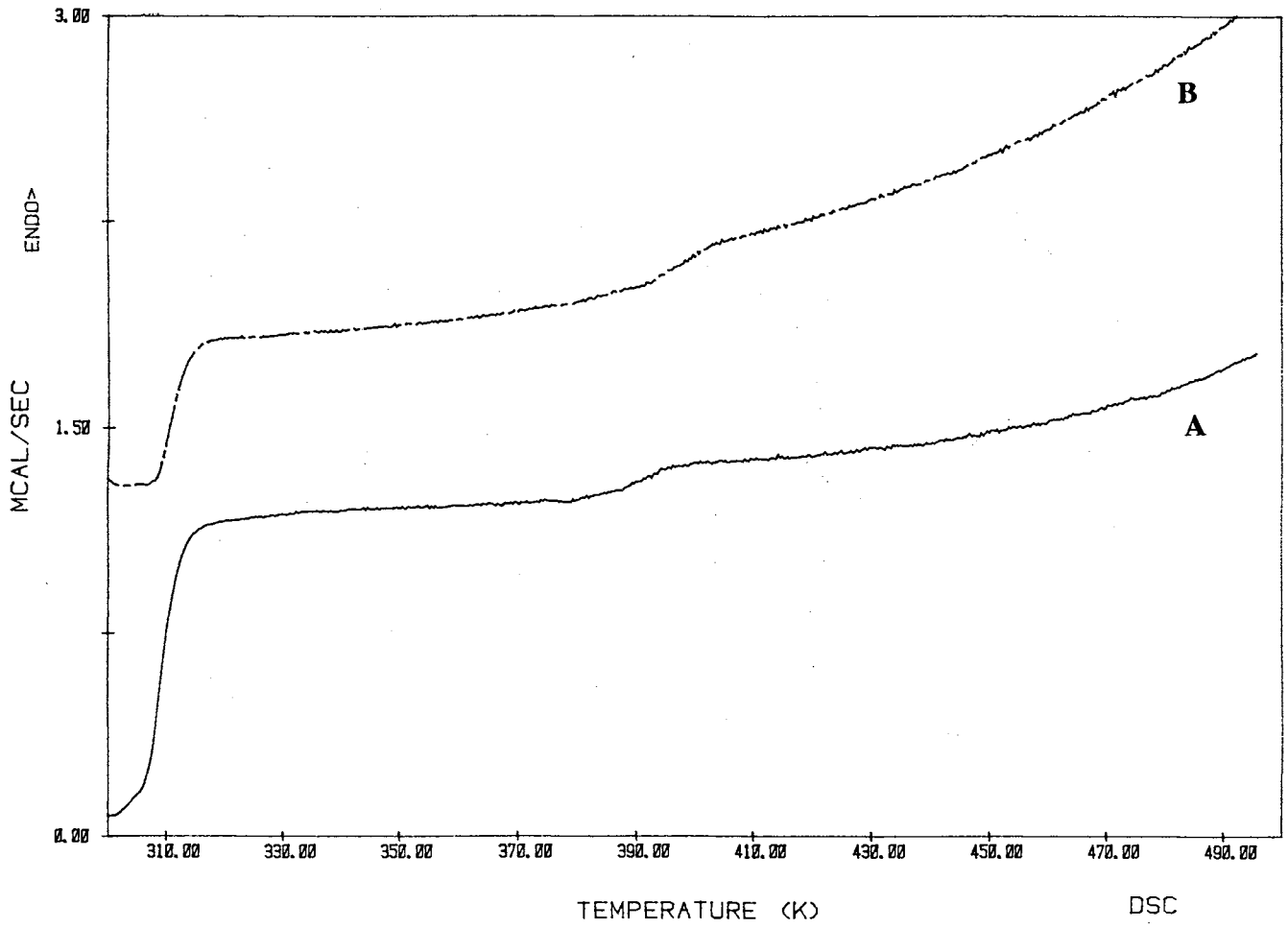

Figure 2. DSC thermograms of 35 wt % 152 nm TPM-silica-PMMA composite films A) without colloidal crystals and B) with colloidal crystals at a scan rate of 10 K/min (sample weights = 20 mg and 19 mg, respectively).

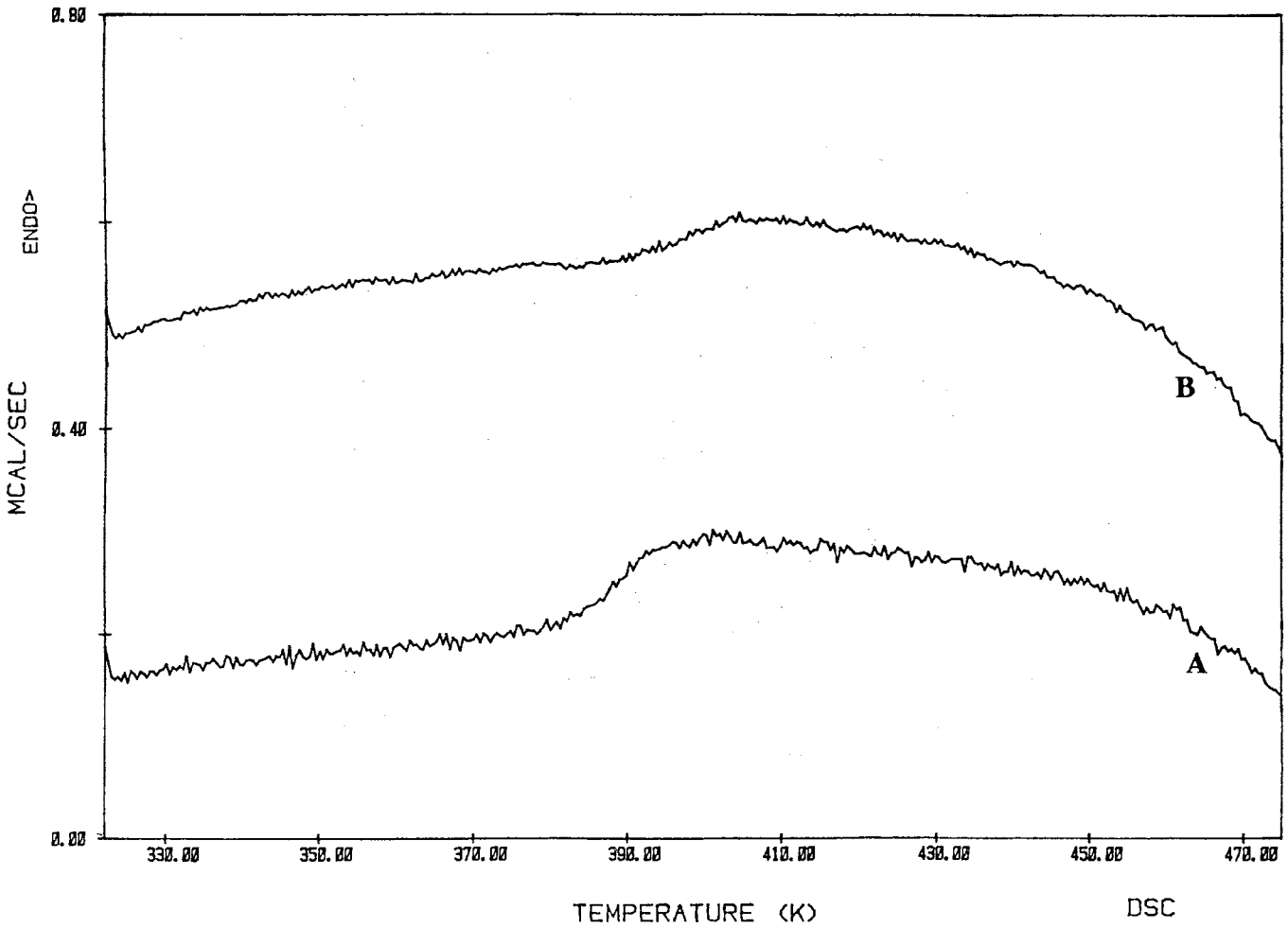

Figure 3. DSC thermograms of 40 wt % 153 nm TPM-silica-PMMA composite films A) without colloidal crystals and B) with colloidal crystals at a scan rate of 10 K/min (sample weight = 20 mg).

TGA

We have analyzed the decomposition behavior of 153 nm TPM-silica-PMA films by TGA. The silica particles were first ordered in MA and on polymerization formed the silica-PMA composites. Colloidal crystals spontaneously form which show good diffraction between 35 and 45 wt % TPM-silica particles in MA dispersions, and polymerization of MA dispersions trap the crystal order in the PMA matrices. PMA films with randomly dispersed silica particles were made by photopolymerization of the MA dispersion before the nucleation and crystallization occurred, while PMA composite with aggregated silica particles was made by polymerization of MA with redispersed dried silica particles. Figures 4, 5 and 6 show the TGA thermograms of the 35, 40 and 45 wt % 153 nm TPM-silica PMA films with particles that were randomly distributed, ordered and aggregated, respectively. In all cases, the composite films undergo initial loss between 90 and 100 °C and further weight loss between 375 and 410 °C. The amounts of residue left after the analyses are compared with the theoretical amounts of silica based on elemental compositions of TPM-silica in PMA composites in Table II. Similar results have been observed for polyimide-silica hybrids where the amount of silica residue is proportional to the initial amount of TEOS incorporated.[8] The amounts of silica left and those calculated are close in agreement, which suggests that the polymer matrix and the TPM groups are decomposed leaving silica particles as residue.

Table II. Analysis of Silica Content in PMA Composites

sample	TGA residue (%)	theoretical residue (%)[a]
34.4 wt %	31.2	31.1
39.2 wt %	32.2	35.4
44.4 wt %	37.0	40.1

[a] From Chapter II, Table II: elemental analysis, 7.76 % C, 1.92 % H and 90.32 % (Si+O).

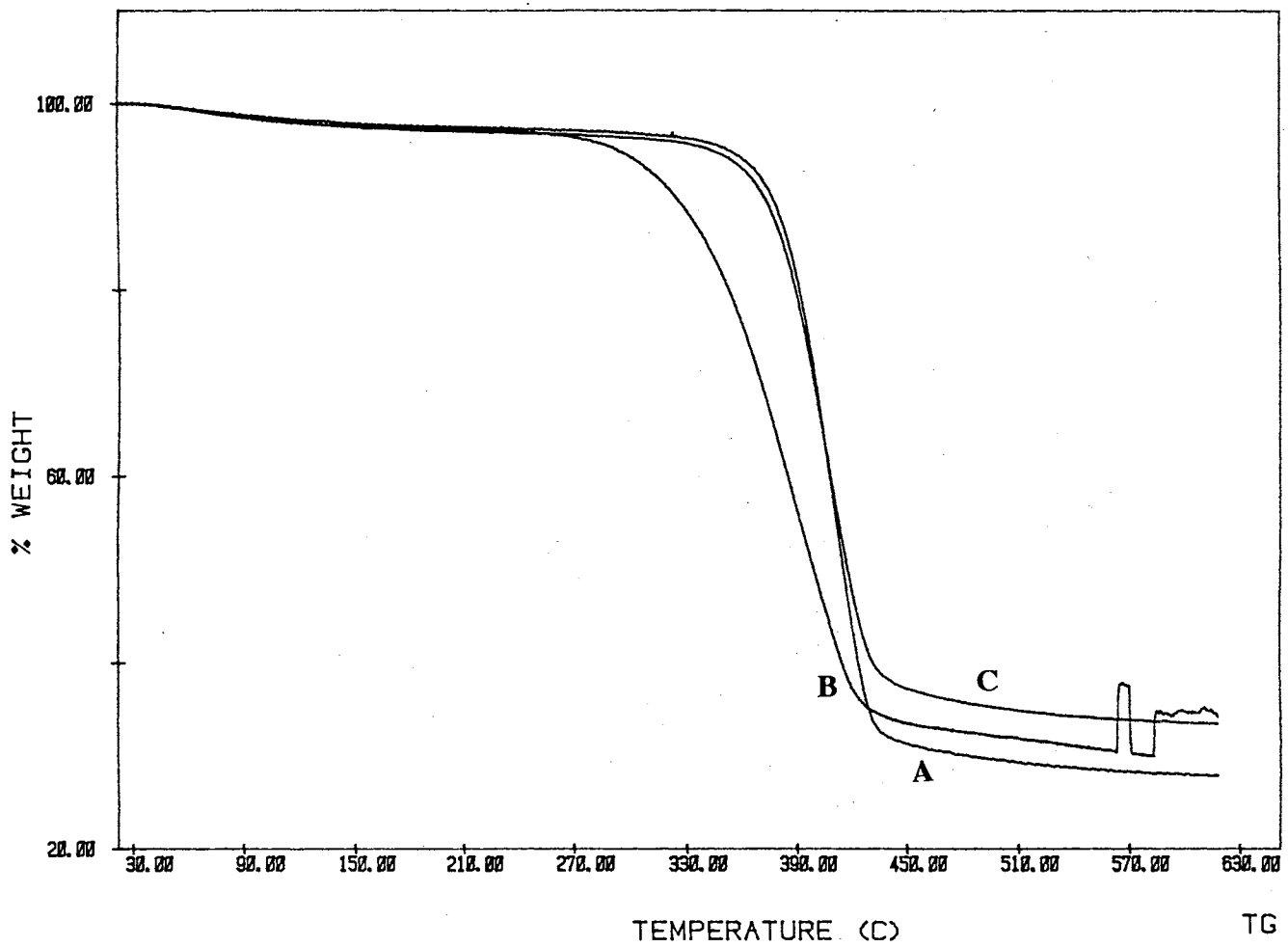

Figure 4. TGA thermograms for 153 nm randomly distributed TPM-silica-PMA composite films A) 35 wt %, B) 40 wt %, and C) 45 wt % at a scan rate of 10 °C/min.

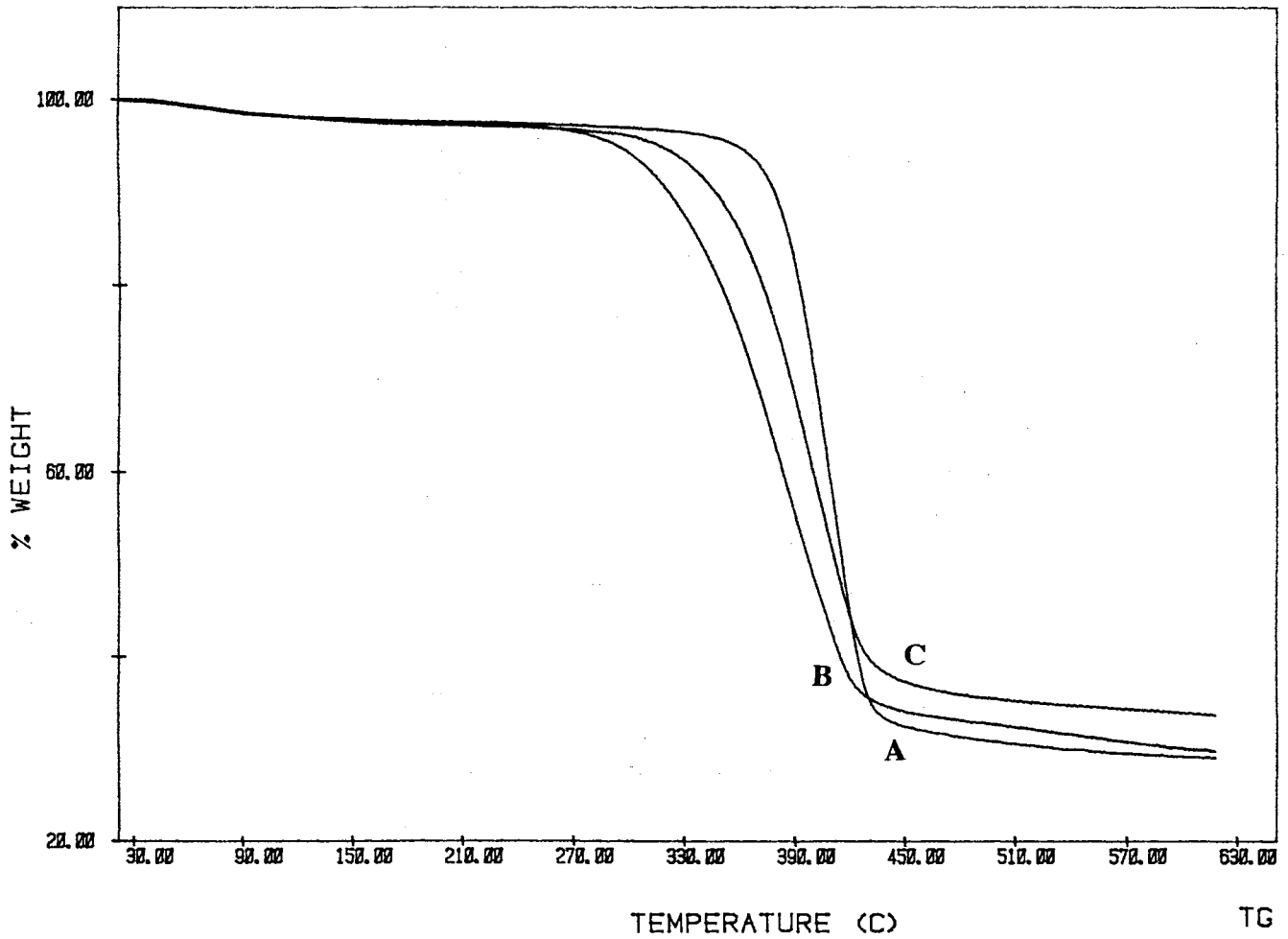

Figure 5. TGA thermograms for 153 nm ordered TPM-silica-PMA composite films A) 35 wt %, B) 40 wt %, and C) 45 wt % at a scan rate of 10 °C/min.

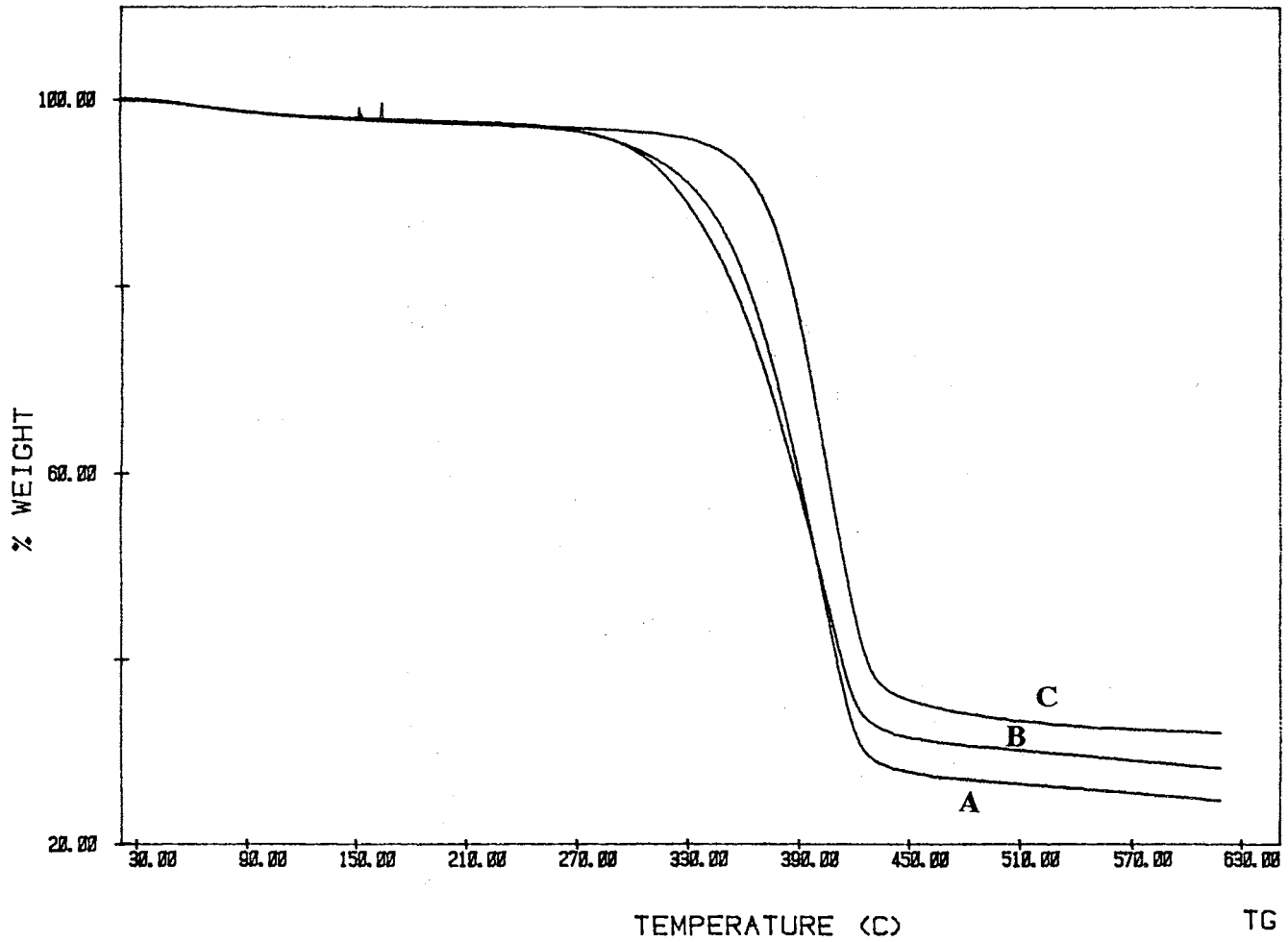

Figure 6. TGA thermograms for 153 nm aggregated silica TPM-silica-PMA composite films A) 35 wt %, B) 40 wt % and C) 45 wt % at a scan rate of 10 °C/min.

CONCLUSIONS

We have made novel composites which contain randomly distributed, ordered, and aggregated monodisperse 153 nm TPM-silica particles in PMMA and PMA matrices. The thermal properties of these composites were analyzed by DSC and TGA techniques. The T_g value was high for the ordered silica-PMMA composite film as compared with the randomly distributed silica-PMMA composite. The composite film decomposes between 375 and 410 °C leaving behind silica residue.

REFERENCES

1. Mark, J. E.; Lee, C. Y.-C.; Biancone, P. A., Eds. *Hybrid Organic-Inorganic Composites*; ACS Symposium Series 585; American Chemical Society; Washington, DC, 1995.
2. Landry, C. J. T.; Coltrain, B. K.; Brady, B. K. *Polymer* **1992**, *33*, 1486.
3. Sanchez, C.; Ribot, F. *New J. Chem.* **1994**, *18*, 1007.
4. Barbin, W. W.; Rodgers, M. B. In "Science and Technology of Rubber", Eds. Mark, J. E.; Erman, B.; Eirich, F. R. Academic Press: San Diego, CA, 1994, pp. 419-468.
5. Nishiyama, N.; Horie, K.; Schick, R.; Ishida, H. *Polym. Commun.* **1990**, *31*, 380.
6. Nishiyama, N.; Ishizaki, T.; Horie, K.; Tomari, M.; Someya, M. *J. Biomed. Mater. Res.*, **1991**, *25*, 213.
7. Nishiyama, N.; Komatsu, K.; Fukai, K.; Nemoto, K.; Kumagai, M. *Composites*, **1995**, *26*, 309.
8. Wang, S.; Ahmad, Z.; Mark, J. E. *Chem. Mater.* **1994**, *6*, 943.
9. Morikawa, A.; Yamaguchi, H.; Kakimoto, M.; Imai, Y. *Chem. Mater.* **1994**, *6*, 913.
10. Brennan, A. B.; Wilkes, G. L. *Polymer* **1991**, *32*, 733.
11. Wei, Y.; Yang, D.; Tang, L. *Makromol. Chem. Rapid Commun.* **1993**, *14*, 273.
12. Coltrain, B. K.; Landry, C. J. T.; O'Reilly, J. M.; Chamberlain, A. M.; Rakes, G. A.; Sedita, J. S.; Kelts, L. W.; Landry, M. R.; Long, V. K. *Chem. Mater.* **1993**, *5*, 1445.
13. Karasz, F. E.; MacKnight, W. J. *Macromolecules*, **1968**, *1*, 537.
14. Ute, K.; Miyatake, N.; Hatada, K. *Polymer*, **1995**, *36*, 1415.
15. Sunkara, H. B.; Jethmalani, J. M.; Ford, W. T. *Chem. Mater.* **1994**, *6*, 362.
16. Sunkara H. B.; Jethmalani J. M.; Ford, W. T. *ACS Symp. Ser.* **1995**, *585*, 181-191.
17. Jethmalani, J.; Ford, W. T. *Chem.. Mater.*, **1996**, *8*, 000.
18. Brandrup, J.; Immergut, E. H., Eds. *Polymer Handbook*, Third Ed; John Wiley and Sons, New York, 1989, pp. V78.

VITA

Jagdish Maghanmal Jethmalani

Candidate for the Degree of

Doctor of Philosophy

Thesis: COLLOIDAL CRYSTALS OF MONODISPERSE SILICA IN POLYMER COMPOSITES

Major Field: Chemistry

Biographical:

Personal Data: Born in Bombay, India, November 1964, son of Maghanmal R. Jethmalani and Vimla.

Education: Received Bachelor of Science Degree in Chemistry from University of Bombay in May, 1986; Master of Science Degree in Organic Chemistry from University of Bombay in May, 1988; Diploma in Industrial Analytical Chemistry, Ramnaian Ruia College, Bombay, June, 1990; Master of Science Degree in Chemistry from University of Arkansas at Little Rock, May 1992; completed requirements for the Doctor of Philosophy Degree at Oklahoma State University in July, 1996.

Professional Experience: Lecturer at R. D. National College, Bombay, June, 1989 to June, 1990; Teaching Assistant, Department of Chemistry, University of Arkansas at Little Rock, August, 1990 to May, 1992; Research Assistant, Department of Chemistry, Oklahoma State University, June, 1992 to August, 1992; Teaching Assistant, Department of Chemistry, Oklahoma State University, August, 1992 to May, 1993; Research Assistant, Department of Chemistry, Oklahoma State University, June, 1993 to June, 1996.

Professional memberships: American Chemical Society, Phi Lambda Upsilon.